Physical Oceanographic Conditions in the Gulf of St. Lawrence during 2023

Peter S. Galbraith, Joël Chassé, Jean-Luc Shaw, Jacqueline Dumas, Marie-Noëlle Bourassa

Fisheries and Oceans Canada,
Québec Region,
Maurice Lamontagne Institute,
P.O. Box 1000,
Mont-Joli, QC,
G5H 3Z4

2024

Canadian Technical Report of Hydrography and Ocean Sciences 378

Fisheries and Oceans Canada

Pêches et Océans Canada

Canada

Canadian Technical Report of Hydrography and Ocean Sciences

Technical reports contain scientific and technical information of a type that represents a contribution to existing knowledge but which is not normally found in the primary literature. The subject matter is generally related to programs and interests of the Oceans and Science sectors of Fisheries and Oceans Canada.

Technical reports may be cited as full publications. The correct citation appears above the abstract of each report. Each report is abstracted in the data base *Aquatic Sciences and Fisheries Abstracts.*

Technical reports are produced regionally but are numbered nationally. Requests for individual reports will be filled by the issuing establishment listed on the front cover and title page.

Regional and headquarters establishments of Ocean Science and Surveys ceased publication of their various report series as of December 1981. A complete listing of these publications and the last number issued under each title are published in the *Canadian Journal of Fisheries and Aquatic Sciences*, Volume 38: Index to Publications 1981. The current series began with Report Number 1 in January 1982.

Rapport technique canadien sur l'hydrographie et les sciences océaniques

Les rapports techniques contiennent des renseignements scientifiques et techniques qui constituent une contribution aux connaissances actuelles mais que l'on ne trouve pas normalement dans les revues scientifiques. Le sujet est généralement rattaché aux programmes et intérêts des secteurs des Océans et des Sciences de Pêches et Océans Canada.

Les rapports techniques peuvent être cités comme des publications à part entière. Le titre exact figure au-dessus du résumé de chaque rapport. Les rapports techniques sont résumés dans la base de données *Résumés des sciences aquatiques et halieutiques*.

Les rapports techniques sont produits à l'échelon régional, mais numérotés à l'échelon national. Les demandes de rapports seront satisfaites par l'établissement auteur dont le nom figure sur la couverture et la page de titre.

Les établissements de l'ancien secteur des Sciences et Levés océaniques dans les régions et à l'administration centrale ont cessé de publier leurs diverses séries de rapports en décembre 1981. Vous trouverez dans l'index des publications du volume 38 du *Journal canadien des sciences halieutiques et aquatiques*, la liste de ces publications ainsi que le dernier numéro paru dans chaque catégorie. La nouvelle série a commencé avec la publication du rapport numéro 1 en janvier 1982.

Canadian Technical Report of Hydrography and Ocean Sciences 378

2024

Physical Oceanographic Conditions in the Gulf of St. Lawrence during 2023

Peter S. Galbraith[1], Joël Chassé[2], Jean-Luc Shaw[1],
Jacqueline Dumas[1], Marie-Noëlle Bourassa[1]

[1]Fisheries and Oceans Canada
Maurice Lamontagne Institute
P.O. Box 1000
Mont-Joli, QC
G5H 3Z4

[2]Fisheries and Oceans Canada
Gulf Fisheries Centre
P.O. Box 5030
Moncton, NB
E1C 9B6

Correct citation for this publication:

Galbraith, P.S., Chassé, J., Shaw, J.-L., Dumas, J. and Bourassa, M.-N. 2024. Physical Oceanographic Conditions in the Gulf of St. Lawrence during 2023. Can. Tech. Rep. Hydrogr. Ocean Sci. 378 : v + 91 p.

TABLE OF CONTENTS

ABSTRACT

Galbraith, P.S., Chassé, J., Shaw, J.-L., Dumas, J. and Bourassa, M.-N. 2024. Physical Oceanographic Conditions in the Gulf of St. Lawrence during 2023. Can. Tech. Rep. Hydrogr. Ocean Sci. 378 : v + 91 p.

An overview of physical oceanographic conditions in the Gulf of St. Lawrence in 2023 is presented as part of the Atlantic Zone Monitoring Program. Annual runoff was above normal for the St. Lawrence River and for the RIVSUM II index. Sea ice seasonal maximum volume and January-April average volume were below normal. The winter surface mixed cold layer (< -1 °C and < 0 °C) volume was below normal. The August cold intermediate layer average minimum temperature was the fourth highest since 1985 and the seasonally averaged minimum temperature index was above normal. On the Magdalen Shallows, the areas covered by water with low temperatures were smaller than normal at all threshold temperatures from < -1 °C to < 3 °C during both periods of June and August/September. Sea surface temperatures (SST) averaged monthly over the Gulf were the highest of the satellite record (1981) in July and October. The May-November average SST for the Gulf was second highest of the time series. Deep water temperatures increased overall in the Gulf between 2009 and 2022, with inward advection from Cabot Strait, but decreased in 2023 from the 2022 record high. The Gulf-wide average of the deep temperature maximum has increased from 5.2 °C in 2009 to a record high of 7.0 °C in 2022, dropping slightly back down to 6.9 °C in 2023 which is the same value as in 2021. This is an indication that deep water temperatures are stabilizing in the Gulf.

RÉSUMÉ

Le présent document donne un aperçu des conditions d'océanographie physique qui ont prévalu dans le golfe du Saint-Laurent en 2023 et est un produit du Programme de monitorage de la zone atlantique (PMZA). Le débit d'eau douce était supérieur à la normale pour le fleuve Saint-Laurent et pour l'indice RIVSUM II. Le volume maximal saisonnier de glace de mer et la moyenne de janvier à avril étaient inférieurs à la normale. Le volume de la couche de mélange hivernale (< -1 °C et < 0 °C) était près de la normale. La température minimale moyenne de la couche intermédiaire froide d'août était la quatrième plus élevée depuis 1985 et l'indice de température minimale moyenne saisonnière était au-dessus de la normale. Sur le Plateau madelinien, la superficie du fond recouverte par des eaux froides était sous la normale pour tous les seuils de température de < -1 °C à < 3 °C en juin ainsi qu'en août/septembre. Les températures de surface de la mer enregistrées par satellite (SST) moyennées mensuellement sur l'étendue du golfe étaient les plus élevées de la série (1981) en juillet et octobre. La SST moyenne de mai à novembre pour le golfe était la seconde plus élevée de la série chronologique. Les températures des eaux profondes ont augmenté dans l'ensemble du golfe entre 2009 et 2022, avec une advection vers l'intérieur à partir du détroit de Cabot, mais ont baissé en 2023 depuis le record de 2022. La moyenne des températures maximales en profondeur dans l'ensemble du Golfe est passée de 5,2 °C en 2009 à un niveau record de 7,0 °C en 2022, retombant légèrement à 6,9 °C en 2023, soit la même valeur qu'en 2021. Ceci est une indication que les températures des eaux profondes se stabilisent dans le Golfe.

1.   INTRODUCTION

This document presents the physical oceanographic conditions and related atmospheric forcing in the Gulf of St. Lawrence in 2023 (Fig. 1). It complements similar reviews of the environmental conditions on the Newfoundland and Labrador Shelf and the Scotian Shelf and Gulf of Maine as part of the Department of Fisheries and Oceans' (DFO) Atlantic Zone Monitoring Program (AZMP; see Therriault et al. 1998 for background information on the program, as well as Cyr et al. 2024 and Hebert et al. 2023 for examples of past reviews of physical conditions in other AZMP regions, and Blais et al. 2023 for chemical and biological oceanographic conditions in the Estuary and Gulf of St. Lawrence) in support of the zonal state of the ocean report provided as a Scientific Advisory Report (DFO 2023). The last detailed report of physical oceanographic conditions in the Gulf of St. Lawrence was produced for the year 2022 (Galbraith et al. 2023).

Some of the variables presented are spatially averaged over distinct regions of the Gulf (Fig. 2) into what will be termed "regional averages". These regions were developed for the Ecosystem approach to fisheries management and differ from those used in reports on conditions prior to those of 2020. The report uses data obtained from the AZMP, other DFO surveys, and other sources. Environmental variables are usually expressed as anomalies, i.e., deviations from their long-term mean. The long-term mean or normal conditions are calculated for the standard 1991–2020 reference period when possible. Furthermore, because these series have different units (°C, m^3, m^2, etc.), each anomaly time series is normalized by dividing by its standard deviation (SD), also calculated for the same reference period. This allows a more direct comparison of the various series. Missing data are represented by grey cells in the tables, values within ±0.5 SD of the average are considered to be near normal and are shown as white cells, and conditions corresponding to warmer than normal (higher temperatures, reduced ice volumes, reduced cold-water volumes or areas) by more than 0.5 SD as red cells, with more intense reds corresponding to increasingly warmer conditions. Similarly, blue represents colder than normal conditions. Higher than normal freshwater inflow is shown as red, but does not necessarily correspond to warmer-than-normal conditions. Salinity values are shown as practical salinity (PSU) but written without units throughout the text and figures.

The summertime water column in the Gulf of St. Lawrence consists of three distinct layers: the surface layer, the cold intermediate layer (CIL), and the deeper water layer (Fig. 3). Surface temperatures typically reach maximum values in early to mid-August (Galbraith et al. 2012). Gradual cooling occurs thereafter, and wind forced mixing during the fall leads to a progressively deeper and cooler mixed layer, eventually encompassing the CIL. During winter, the surface layer thickens partly because of buoyancy losses (cooling and reduced runoff) and brine rejection associated with sea-ice formation, but mostly from wind-driven mixing prior to ice formation (Galbraith 2006). The surface winter layer extends to an average depth of 75 m, but may reach > 150 m in places such as the Mécatina Trough where near freezing waters (-1.8 to 0 ºC) from the Labrador shelf entering through the Strait of Belle Isle may extend from the surface to the bottom in depths > 200 m (Galbraith 2006). During spring, surface warming, sea-ice melt waters, and continental runoff produce a lower-salinity and higher-temperature surface layer. Underneath this surface layer, cold waters from the previous winter are partly isolated from the atmosphere and form the summer CIL. This layer will persist until the next winter, gradually warming up and deepening during summer (Gilbert and Pettigrew 1997; Cyr et al. 2011) and more rapidly during the fall as vertical mixing intensifies.

This report considers air temperature and freshwater runoff, both significant drivers of the surface layer which are discussed next. Winter sea ice conditions and the winter mixed layer are then presented. The latter is the precursor to the summer CIL, which affects bottom temperatures on the Magdalen Shallows. The deeper waters, mostly isolated from exchanges with the surface, are presented last along with a summary of major oceanographic surveys, modelling results on currents and transports, and details of observations at high frequency sampling stations.

2.   AIR TEMPERATURE

The source of air temperature data is the third generation of homogenized surface air temperature data, part of the Adjusted and Homogenized Canadian Climate Data (AHCCD), which accounts for shifts due to the relocation of stations, changes in observing practices and automation (Vincent et al. 2020). The monthly air temperature anomalies for several stations around the Gulf are shown in Fig. 4 for 2022 and 2023, as well as the average of all station anomalies. There were multiple monthly records set at stations around the Gulf in 2023: the warmest July on record at Sept-Îles, Natashquan, Daniel's Harbour, Stephenville, Charlottetown and Port aux Basques; the warmest September and October on record at Sept-Îles, Baie Comeau and Port aux Basques, and also the warmest October at Mont-Joli. Averaged over all stations, only two months were below normal and July was the warmest on record (+2.5 °C, +2.4 SD).

Fig. 5 shows the annual, winter (December-March), and April-November mean air temperature anomalies averaged over all available stations shown in Fig. 4 since 1873. Record-high annual and winter temperatures occurred in 2010 and record-high April-November temperatures in 2021. Galbraith et al. (2012) found the average April-November air temperature over the Gulf from Environment Canada's National Climate Data and Information Archive (NCDIA) to be a good proxy for May-November sea-surface temperature over the Gulf (but excluding the estuary) and found within the former a warming trend of 0.9 °C per century between 1873 and 2011; a slightly higher trend of 1.2 °C per century is found here over the selected AHCCD stations between 1873 and 2023 (Fig. 5). The NCDIA December-March air temperatures in the western Gulf were found to be highly correlated ($R^2 = 0.67$) with sea-ice properties, as well as with winter mixed layer volumes (Galbraith et al. 2010). Galbraith et al. (2013) found slightly higher correlations ($R^2 = 0.72$) with sea-ice using December-February AHCCD averages, possibly because March temperatures are of less importance during low sea-ice cover since much of the sea-ice cover decrease has occurred much earlier in February.

The December-March air temperature average was above normal (+1.9 °C, +1.2 SD; 7th warmest). The April-November average was above normal (+1.0 °C, +1.6 SD; 5th warmest) and so was the annual average (+1.4 °C, +1.6 SD; 5th warmest).

3.   PRECIPITATION AND FRESHWATER RUNOFF

A freshwater runoff hindcast for the St. Lawrence River is updated using the model and methods described in Lefaivre et al. (2016). Observations of water levels at the Saint-Joseph-de-la-Rive station were used at the downstream boundary of the model. The runoff at the upstream boundary of the model was calculated using the stage-discharge relationships at the

outlets of Lake Deux-Montagnes and Lake Saint-Louis; runoff at both of these outlets were updated, slightly altering values from those previously published. In addition, a correction was made to minimize the difference between modeled and observed water levels at the Varennes station; this station is directly influenced by the outflow from both lakes and allows the validation of the upstream flow of the St. Lawrence River. The runoff at Québec City is extracted from the model at 3-minute intervals, filtered to remove the tidal signal and sub-sampled at noon local time (EST) every day (Fig. 6). The dataset is available <u>on-line</u> (Fisheries and Oceans Canada, 2023). To combine it with runoffs downstream and recreate the runoff that feeds the Estuary, the time series is then lagged by 21 days to approximate the time taken to reach the Estuary at the height of the Saguenay mouth[1], and new monthly means are computed (Fig. 7, lower curve).

A hydrological watershed model was used to estimate the monthly runoff since 1948 for all other major rivers flowing into the Gulf of St. Lawrence, with discharge locations as shown in Fig. 8. The precipitation data (NCEP reanalysis, six hourly intervals) used as input in the model were obtained from the NOAA-CIRES Climate Diagnostics Center (Boulder, Colorado, USA; Kalnay et al. 1996). The data were interpolated to a ¼° resolution grid and the water routed to river mouths using a simple algorithm described here. When air temperatures were below freezing, the water was accumulated as snow in the watershed and later melted as a function of warming temperatures. Water regulation is modelled for three rivers that flow into the estuary (Saguenay, Manicouagan, Outardes) for which the annual runoff is redistributed following the climatology of the true regulated runoffs for 12 months thereafter. Runoffs were summed for each region shown and the climatology established for the 1991–2020 period. The waters that flow into the Estuary (Fig. 8) were added to the lagged St. Lawrence River runoff (above) to produce the RIVSUM II index (Fig. 7, upper curve). In 2023, the RIVSUM II spring freshet was above normal and peaked during the usual period of May.

Monthly anomalies of the summed runoffs for 2022 and 2023 are shown in Fig. 9. Rivers other than the St. Lawrence contribute about 5 000 $m^3 s^{-1}$ runoff to the Estuary, the equivalent of 40% of the St. Lawrence River, while the other tributaries distributed along the border of the GSL provide an additional 4 000 $m^3 s^{-1}$ in freshwater runoff to the system. River regulation has a strong impact on the relative contributions of sources. For example, in May 2022 the lower-than-average river runoff into the Estuary (an effect of the previous low precipitation and river regulation) compensated the above normal runoff of the St. Lawrence River to yield a near normal RIVSUM II. The long-term time series are shown, summed by large basins, in Fig. 10. The annual average runoff of the St. Lawrence River at Québec City and RIVSUM II both show a general downward trend from the mid-1970s until 2001, an upwards trend between 2001 and 2009 followed by another between 2012 and 2019 (Fig. 10). In 2023, the annual runoff was above normal at 13 700 $m^3 s^{-1}$ (+1.0 SD) for the St. Lawrence River and at 18 800 $m^3 s^{-1}$ (+1.0 SD) for the RIVSUM II index.

4.   SEA SURFACE TEMPERATURE AND SALINITY

The seasonal cycle of weekly averaged sea surface temperature over the Gulf of St. Lawrence is illustrated in Fig. 11 using data streams that are described below. Galbraith et al. (2012) have

---

[1] Senneville and Lefaivre 2010, unpublished manuscript

shown that Gulf-averaged monthly air temperature and SST climatologies matchup quite well with SST lagging air temperature by half a month, and this is shown to remain true with climatologies updated to 1991–2020 in Fig. 11. The climatological maximum sea-surface temperatures are reached during the first and second week of August but that can vary by a few weeks from year to year. The maximum surface temperature averages to 16.1ºC over the Gulf during the first and second week of August (1991–2020), but there are spatial differences: temperatures in the Northumberland Strait region are the warmest in the Gulf, averaging 18.8 ºC over that area, and the coolest are at the head of the St. Lawrence Estuary (7.0 °C) and in upwelling areas along the lower north shore. The annual observations will be explored below.

4.1 SHIPBOARD THERMOLISANOGRAPH

The surface layer temperature and salinity conditions of the Gulf are monitored by various complementary methods. The first is the shipboard thermosalinograph network (Galbraith et al. 2002), which consists of temperature-salinity sensors (SBE-21; Sea-Bird Electronics Inc., Bellevue, WA) that have been installed on various ships starting with the commercial ship Cicero of Oceanex Inc. in 1999 (retired in 2006) and on the (Oceanex) Cabot from 2006 to fall 2013. The (Oceanex) Connaigra, was outfitted with a thermosalinograph in early 2015. Fig. 12 shows a mean annual cycle of water temperature at a depth of 8 m along the Montréal to St. John's shipping route based on thermosalinograph data collected from 2000 to 2023. The data were averaged for each day of the year at intervals of 0.1 degrees of longitude to create a climatological composite along the ship track. The most striking climatological feature is the area at the head of the Laurentian Trough (69.5°W), where strong vertical mixing leads to cold summer water temperatures (around 5 °C to 6 °C and sometimes lower) and winter temperatures that are always above freezing (see also Fig. 11). The climatological cycle shows the progression to winter conditions, first reaching near-freezing temperatures in the Estuary and then progressing eastward with time, usually reaching Cabot Strait by the end of the winter (but no further).

4.2 THERMOGRAPH NETWORK

The second data source is the Maurice Lamontagne Institute thermograph network (Pettigrew et al. 2016, 2017), which consists of a number of stations with moored instruments recording water temperature every 5 to 30 minutes (Fig. 13). Most instruments are installed on Coast Guard buoys that are deployed in the ice-free season, but a few stations are monitored year-round. The data are typically only available after the instruments are recovered except for oceanographic buoys that transmit data in real-time.

Thermograph network observations are examined as anomalies relative to daily average temperatures (or salinities) calculated using all available years of data for each day of the year at each station and depth (Fig. 14 to Fig. 17). The seasonal cycle of near-surface temperature is measured by shallow instruments, while the cold intermediate layer warming from spring to fall is captured by instruments moored between 30 m and 120 m depth. Monthly averages are also shown, with the magnitude of their anomaly colour-coded. Monthly shallow-water anomalies were fairly consistent across all stations of each of the regions.

The Saguenay Sill 1 station is located just inside the first sill connecting the Saguenay Fjord to the St. Lawrence Estuary. The salinity of the water (hence its density) determines the type of circulation that renews basin waters. These time series extend those first presented in Belzile et

al. (2016) and Galbraith et al. (2018). A second mooring was deployed just inside the inner and deepest basin of the Fjord (Saguenay Sill 3). The sharp changes in temperature (

Fig. 14) as well as the increases in salinity in February and April 2023 (Fig. 17) correspond to deep renewal events. The slow decrease of salinity after sudden increases is indicative of vertical mixing occurring in the deep basin, which reduces water density and preconditions the fjord to subsequent deep renewal events.

The Île Shag (10 m) station shows bottom temperatures close to Îles-de-la-Madeleine that are important to the lobster fishery. April and May temperatures were above normal at this station in 2023 (

Fig. 16). The Île Shag panel shows with a red line spanning historical dates when spring temperature last increased over 1.5 °C, a temperature associated with increased lobster mobility, as well as the mean date (April 25th) plus and minus 0.5 SD (5 days). In 2023, this crossing occurred very early, on April 12th, the second earliest date since 1994. It can then take up to two more weeks for waters to warm at 30 m starting from the time recorded at 10 m.

4.3 SST FROM SATELLITE REMOTE SENSING BLEND

The satellite-based sea surface temperature product blends data from Pathfinder version 5.3 (4 km resolution for 1982–2020; Casey et al. 2010), Maurice Lamontagne Institute (MLI; 1.1 km resolution for 1985–2013) with the NOAA/STAR L3S-LEO-Daily "super-collated" product (0.02 degree resolution for 2007 to current; NOAA/STAR 2021). The process selects the products with the best percent coverage for every averaging area and period (week or month). Monthly (and weekly) temperature composites are calculated from averaged available daily anomalies to which monthly (or weekly) climatological average temperatures are added (Galbraith et al. 2021). Daily composites for the NOAA/STAR product are created from downloaded day and night composites as the average of both values if available for a pixel, or using the available day or night pixel value minus or plus half of the average diurnal variation in the Atlantic Zone (0.22 °C). Daily pixel values from 2007 to 2022 were then compared against the daily range of observations at four offshore thermograph stations (Mont-Louis, Havre-Saint-Pierre, Beaugé, La Romaine) as well as all oceanographic Viking buoys. This initially consisted of 10165 days of observations. We then excluded from the comparison all thermograph and buoy daily data that had diurnal temperature variations greater than the mean diurnal range, leaving 6691 days of observations. A linear regression was performed of the average daily temperature at thermographs against the NOAA/LEO daily composite values at corresponding pixels and used as a calibration (SST = 1.01 LEO – 0.41). This calibration cools the NOAA/LEO daily composite values by 0.41 °C at 0 °C and by 0.19 °C at 20 °C. Before calibration, 69% of NOAA/LEO observations up to 2022 were within the thermograph/buoy diurnal ranges for days when diurnal range was less than half of the 1.8 °C average diurnal range. After calibration, this increased to 95.4%.

Monthly mean sea-surface temperatures from AVHRR imagery are presented as maps (Fig. 18), temperature anomaly maps against the 1985–2010 climatology (Fig. 19), and spatial averages and anomalies against the 1991–2020 climatology (Fig. 20 and Fig. 21). To convert Fig. 19 to using a 1991–2020 climatology, new pixel-level monthly climatologies will need to be rebuilt that combine two AVHRR products. Sea-surface temperature monthly climatologies and time series were also extracted for more specific regions of the Gulf. The region of the

Magdalen Shallows, excluding Northumberland Strait, is divided into western and eastern areas as shown in Fig. 22. Since the NOAA/LEO data alter previously published regional monthly averages, we also include the monthly time series since 1982 for Gulf regions (Fig. 23 and Fig. 24).

Seasonal trends in relation to air temperature are examined by first displaying weekly averaged AVHRR SST in the GSL for all years between 1982 and 2023 (Fig. 25) with years on the x-axis and weeks of the year on the y-axis (See Galbraith and Larouche 2013 for a full description). Isotherms show the first and last occurrences of temperature averages of 12 °C over the years, chosen to be representative of spring (and fall) transitions to (and from) typical summer temperatures. Although the selected temperature is arbitrary, the results that follow are not particularly sensitive to the exact temperature chosen because the surface mixed layer tends to warm and cool linearly in spring and fall (e.g., Fig. 11) and a 10 °C threshold is also used to demonstrate this. However in some recent years sudden surface fall cooling has occurred from post-tropical storms mixing the water column, introducing more variability. The interannual variability in the time of year when the 12 °C threshold is cross-correlated with June-July average air temperature for the summer onset (0.8 weeks sooner per 1 °C increase; $R^2 = 0.63$) and with September average air temperature for the fall (0.8 weeks later per 1 °C increase; $R^2 = 0.57$). These air temperature averages, shown in Fig. 25, can be used as proxies prior to 1982 and for climate change predictions. The implication is that the duration of the Gulf of St. Lawrence warm season has increased and will increase by about 2 weeks for each 1 °C of seasonal warming (e.g., associated with anthropogenic climate change).

4.4   SEA SURFACE TEMPERATURE IN 2023

Thermosalinograph data show above average temperatures in the later half of December 2022 and into winter 2023, with near-freezing surface layer conditions first appearing later than normal (Fig. 12), driving late onset of sea ice. Temperature anomalies were generally positive all year except in June and reached values of +5 to +6 °C in October.

The summer pattern of sea surface temperature observed by the thermosalinograph is in agreement with remote sensing data (Fig. 19 and Fig. 20), with most regions experiencing above normal temperatures averaged over the Gulf except in June. Warming to summer temperatures (12 °C, Fig. 25) was near normal compared to the climatological average time. The seasonal Gulf maximum was reached early, in late July (Fig. 20), coincident with a zonal marine heatwave; that month's average was at a record high (16.5 °C, +2.5 °C, +2.6 SD; Fig. 21). From August, temperatures remained fairly stable through mid-September, then decreased slowly with increasing anomalies into October when another record high was observed (+2.8 °C, +4.8 SD).

Regional monthly average temperature records occurred for the warmest months of July, September and October in many regions (Fig. 20). The September and October records had highest anomalies in the Estuary and northwest Gulf. In the Estuary, temperatures in late September were higher than the climatological seasonal maximum expected in early August (12.1 °C versus 11.8 °C); anomalies remained high up to the last week of October when it was still of +5 °C.

The seasonal May-November average was at record highs in the Upper Estuary, Estuary, northwest Gulf and Baie des Chaleurs (Fig. 23, Fig. 24). For the Gulf, the seasonal May-November average was second highest, tied with 2021 (11.2 °C,+1.4 °C, +2.6 SD).

4.5   MARINE HEATWAVES

Marine heatwaves (MHWs) are defined as prolonged discrete anomalously warm water events or, quantitatively, by temperatures exceeding the 90th percentile of temperatures for that day of year during at least 5 consecutive days (Hobday et al., 2016; Oliver et al., 2021). It is recommended that the 90th percentile thresholds be calculated over a full 30 year climatology, but similar results can be obtained using as few as 10 years (Schlegel et al., 2019). Here, a 30 year reference period (1991-2020) is used despite some time series starting as late as 2005. MHW metrics obtained for these time series using the 1991-2020 and 2005-2020 reference periods are similar (not shown), which suggests that having temporal coverage of differing lengths during the reference period does not introduce a bias between metrics calculated for different stations.

Common metrics of MHWs are duration (D), average (I_{mean}), maximum (I_{max}), and integrated (I_{cum}) temperatures above the climatology. These metrics were calculated for thermograph time series using the Python implementation of Hobday et al. (2016) written by Eric Oliver (https://github.com/ecjoliver/marineHeatWaves), and further aggregated to annual metrics (Sum of durations, ΣD; duration-weighted mean of the averages, $\bar{I}_{mean}$; annual maximum, $\hat{I}_{max}$; annually integrated temperatures above the climatology, ΣI_{cum}). Following Hobday et al. (2018), MHWs with I_{max} values greater than 1, 2, 3, and 4 times the difference between the 90th percentile and the climatology are respectively referred to as moderate, strong, severe and extreme events. Strong, severe and extreme MHWs occurred in respectively 0.8%, 0.2% and 0.05% of our data.

The most intense MHW event of 2023 peaked in the Fall and was recorded at several stations in the Estuary and northwest Gulf, reaching extreme levels at Tadoussac, Bic and Rimouski Station (Fig. 14). Starting in August, it lasted until the instruments were recovered (up to 66 days later) making it the 2nd longest MHW event detected in these time series (the longest was 71 days at Borden in 2010). It was most cumulatively intense at Sept-îles station (I_{cum} = 361 °C days), breaking the previous record by 166°C days. Although similar in seasonal timing, this event was more intense than the MHW recorded in the Estuary in the Fall of 2021, which was previously considered exceptional.

In summary, 2023 was an active MHW year with ΣD more than twice the interannual average in almost all regions, and a total MHW count twice the interannual average (Fig. 26). Contrary to 2022, ΣI_{cum} was higher in the Estuary and northwest Gulf and lower in the rest of the Gulf. A record number of 6 stations cumulated more than 300 °C days in ΣI_{cum}.

5.   SEA ICE

Ice cover area, duration and volume are estimated from ice cover products obtained from the Canadian Ice Service (CIS), then converted into regular grids that are used in analyses. These are weekly Geographic Information System (GIS) charts covering the period 1969–2023 and daily charts covering the period 2009–2023. All charts were gridded on a 0.01° latitude by 0.015° longitude grid (approximately 1 km resolution). Thickness (and therefore volume) are estimated from stages of ice growth from new ice and nilas (5 cm), grey ice (12.5 cm), grey-white ice (22.5 cm), thin first year ice (50 cm), medium first year ice (95 cm) and thick first year

ice (160 cm). Prior to 1983, the CIS reported ice categories into fewer classifications using a single category of first year ice (≥ 30 cm) with a suggested average thickness of 65 cm. We have found this value to lead to underestimates of the seasonal maximum thickness and volume based on high interannual correlations obtained between the estimated volume and area of the weekly seasonal maximums. The comparison pre- and post-1983 provided an estimate of 85 cm in the Gulf of St. Lawrence and of 95 cm on the Newfoundland and Labrador Shelf. To avoid a spatial discontinuity and preferring slightly underestimating ice volume in the northeast Gulf rather than over-estimating it everywhere else, we choose to set it at 85 cm.

Several products were computed to describe the sea-ice cover interannual variability: day of first and last occurrence and duration maps (Fig. 27) and regional extreme values (Fig. 28); distribution of ice thickness during the week of maximum volume (Fig. 29, upper panels) and maximum thickness reached at any week during the season (Fig. 29, lower panels); daily evolution of the estimated sea-ice volume in relation to the climatology and historical extremes (Fig. 30); estimated seasonal maximum ice volumes within the Gulf as well as on the Scotian Shelf (Fig. 31); time series of seasonal maximum ice volume, area (excluding thin new ice) and ice season duration in relation with December-to-March air temperature anomaly (Fig. 32). The durations shown in Fig. 28 and Fig. 32 are different products. The first corresponds to the number of weeks where the volume of ice anywhere within the region exceeded 5% of the climatological maximum, while the second is the average duration at every pixel of Fig. 27, which is much shorter than the first.

There has been a declining trend in ice cover metrics since 1990 with rebounds in 2003 and 2014 (Fig. 32). The correlation between annual maximum ice volume (including the cover present on the Scotian Shelf) and the December-February air temperature averaged over five western Gulf stations (Sept-Îles, Mont-Joli, Gaspé, Charlottetown and Îles-de-la-Madeleine) accounted for 72% of the variance using the 1969–2012 time series (Galbraith et al. 2013). Fig. 32 shows a similar comparison using ice volume and the ACCHD December-to-March air temperature anomaly from Fig. 5 yielding an R^2 of 0.75. The correlations between air temperature and the ice parameters season duration and area are also very high (R^2 = 0.81–0.83). Correlation coefficients are slightly higher when using January to February air temperatures, perhaps because March air temperatures have no effect on ice cover that has almost disappeared by then during very mild winters. Sensitivity of the ice cover to air temperature increase (e.g., through climate change) can be estimated using 1969–2023 co-variations between winter air temperature and sea-ice parameters, which indicate losses of 18 km^3, 31 000 km^2 and 14 days of sea-ice season for each 1 °C increase in winter air temperature.

Only 5 winters on record have had December-March air temperature anomalies of +2.4 °C or greater: 1958, 1969, 2010, 2011 and 2021. Averaging the normalized anomalies of sea ice duration, seasonal maximum area and volume from Fig. 32, the four years with weakest sea ice conditions since 1969 could be classified as nearly ice-free. They were, in order, 2010, 2021, 2011 and 1969 and matching all winters with air temperature anomalies of +2.4 °C or greater. In the 14-year span since 2010, 9 of the 14 lowest seasonal maximum ice volumes of the time series have occurred (Fig. 32), including 2023 ranking 6th lowest. Almost no ice (0.1 km^3, -0.9 SD) made it past Cabot Strait onto the Scotian Shelf (Fig. 29 to Fig. 31).

Ice typically forms first in December on the coast of the St. Lawrence Estuary (in the recent 1991–2020 climatology versus the entire estuary in the previous 1981–2010 climatology) and in shallow waters along New Brunswick, Prince Edward Island and the lower north shore, and melts last in the northeast Gulf where the ice season duration tends to be longest apart from shallow bays elsewhere (Fig. 27). Offshore sea ice is typically produced in the northern parts of the Gulf and drifts towards Îles-de-la-Madeleine and Cabot Strait during the ice season.

In 2023, the sea-ice cover formed several weeks later than usual in most areas, and did not form at all off most of the west coast of Newfoundland out to Anticosti Island and Îles-de-la-Madeleine (Fig. 27). First occurrence was later than normal and last occurrence earlier than normal except for the Strait of Belle Isle area, where late inflow from the Labrador Shelf occurred (Fig. 27). Ice volume progressed well below normal, reaching historical daily record lows during 6 days at the end of January (Fig. 30). It was briefly above normal at the end of the season because of the late inflow from the Labrador Shelf.

The below-normal seasonal maximum ice volume of 20 km³ (-1.1 SD; Fig. 29) and seasonal maximum area of 106 000 km^2 (-0.9 SD; Fig. 32) occurred the week of February 27th; they ranked 6th and 9th lowest since 1969. Other metrics were below normal: the area-weighted ice season duration of 25 days (-1.5 SD; Fig. 32) ranked 5th lowest and the January-April average volume (reported in the AZMP zonal report) of 7.8 km³ (-1.1 SD; Fig. 31) ranked 6th lowest. Ice metrics were consistent with the mild winter air temperatures (+1.8 °C, +1.1 SD) that also ranked 6th warmest since 1969 and 7th warmest since 1873. Winter 2023 missed being the 6th occurrence of nearly ice-free conditions in the Gulf due to a week-long cold air temperature outbreak at the end of February that pushed the waters on the Magdalen Shallows to ice formation.

6.   WINTER WATER MASSES

A wintertime survey of the Gulf of St. Lawrence waters (typically 0–200 m) has been undertaken in early March since 1996, typically using a Canadian Coast Guard helicopter but using Canadian Coast Guard ships in 2016 and 2017. The survey, sampling methods, and results of the cold-water volume analysis in the Gulf and the estimate of the water volume advected into the Gulf via the Strait of Belle Isle over the winter are described in Galbraith (2006) and in Galbraith et al. (2006). Fig. 33 and Fig. 34 show gridded interpolations of near-surface temperature, temperature difference above freezing, salinity, cold layer thickness and bottom contacts, and thickness of the Labrador Shelf water intrusion (detailed below) for 2023 as well as climatological means.

The March surface mixed layer is usually very close (within 0.1 °C) to the freezing point in most regions of the Gulf but thickness of the surface layer varies, resulting in variability in the cold-water volume between mild and severe winters rather than in temperature. One exception was 2010 when, for the first time since the inception of the winter survey, the mixed layer was on average 1 °C above freezing. During typical winters, surface waters in the temperature range of ~ 0 °C to -1 °C are only found from the northeast side of Cabot Strait spreading into the Gulf. Some of these warm waters presumably enter the Gulf during winter and flow northward along the west coast of Newfoundland. However it is also possible that local waters could have simply not cooled close to freezing; this is likely to have been the case in 2023. The mixed layer in March 2023 was near-freezing only around Prince Edward Island, the mouth of Baie des

Chaleurs, north of Anticosti Island and in Mécatina Trough (Fig. 33). These areas corresponded to those where sea ice was found at the peak cover a week earlier (Fig. 29). Most of the Gulf mixed layer was >0.7 °C above freezing with some areas up to >2 °C above freezing.

Near-freezing waters with salinities of around 32 are responsible for the (local) formation of the CIL since that is roughly the salinity at the temperature minimum during summer. These are coded in green-blue in the salinity panel of Fig. 33 and are typically found to the north and east of Anticosti Island. Surface salinities were lower than the climatology during the winter of 2023.

Near-freezing waters with salinity > 32.35 (colour-coded in violet) are considered to be too saline to have been formed from waters originating within the Gulf (Galbraith 2006) and are presumed to have been advected as an intrusion from the Labrador Shelf through the Strait of Belle Isle. These cold high-salinity waters were not present at the surface in March 2023 in Mécatina Trough (Fig. 33). However, Labrador Shelf waters can have lower salinity than this threshold. A second criterion based on temperature-salinity (T-S) signatures of water (Galbraith 2006, revisited in Shaw & Galbraith 2023) is used to identify intruding Labrador Shelf waters that have exhibited no evidence of mixing with warm and saline deep Gulf water. In March 2023, a fixed salinity of > 32.0 was used to identify Labrador Shelf Waters.

This identified a subsurface layer from about 30 m to the bottom at >200 m in Mécatina Trough (top-right panel of Fig. 34). The recent history of Labrador Shelf water intrusions is shown in Fig. 35, where its volume is shown as well as the fraction it represents of all the cold-water volume in the Gulf. See Shaw and Galbraith (2023) for a comparison to measured transports in the Strait of Belle Isle, updated in Fig. 35 (blue and red lines). This volume was near normal in March 2023 at 1045 km³ (-0.4 SD), and represented 14% (+0.2 SD) of the cold water (T < -1 °C) in the Gulf. The near-bottom thermograph in the Strait of Belle Isle (Fig. 15) showed that water temperature increased above -1 °C on May 28th 2023, later than the 2008-2023 average by only 2 days (+0.1 SD) and indicating near-normal end of the inflow of Labrador Shelf Water after the March survey.

The cold mixed layer depth typically reaches about 75 m in the Gulf and is usually delimited by the -1 °C isotherm because the mixed layer is typically near-freezing and deeper waters are much warmer (Galbraith 2006). In March 2010 and 2011, much of the mixed layer was warmer than -1 °C such that the criterion of T < 0 °C was also introduced (see middle panels of Fig. 34). The cold surface layer is the product of local formation as well as cold waters advected from the Labrador Shelf, and can consist either of a single water mass or of layers of increasing salinity with depth. This layer reaches the bottom in many regions of the Gulf, with interannual variability of the deepest parts of the Magdalen Shallows or of Mécatina Trough being reached (see bottom panels of Fig. 34). The thickness of the winter layer is usually greatest north and northeast of Anticosti Island, and the doming of the Anticosti Gyre isopycnals appears in the climatology as a thinner centre part. There is some interannual variability in the extent of the warm area centered on Port Aux Basques, expressed as thinning in the climatology. In 2023, this area that never reached near-freezing by the end of winter was very large in the southeast portion of the Gulf, with no waters of T < -1 °C even as far into the Gulf as Îles-de-la-Madeleine and Anticosti Island. A large area of the mixed layer was even warmer, with T > 0 °C; this previously rare observation has occurred in the last three winters and may play a role in warming cold intermediate layer conditions.

Integrating the cold layer (< -1 °C) depth over the area of the Gulf (excluding the Estuary and the Strait of Belle Isle) yields a below normal (-1.5 SD) volume of 7 600 km³ in 2023. The interannual variability of winter volumes of water colder than 0 °C and 1 °C are shown in Fig. 36. The mixed layer volume increases to 13 400 km³ (-1.5 SD) when water temperatures < 0 °C are considered, which is well below normal because of the large area of zero thickness (warmer than 0 °C) off of Port aux Basques. This volume of cold water corresponds to 40% of the total water volume of the Gulf (33 500 km³, excluding the Estuary), compared to the 1996–2020 average of 44%.

7.   COLD INTERMEDIATE LAYER

7.1   FORECAST FROM THE MARCH 2023 SURVEY

The summer CIL minimum temperature index (Gilbert and Pettigrew 1997) has been found to be highly correlated with the Gulf (excluding the estuary) volume of cold water (< -1 °C) measured the previous March when much of the mixed layer is near-freezing (Galbraith 2006). This is expected because the CIL is the remnant of the winter cold surface layer. A measurement of the volume of cold water present in March is therefore a valuable tool for forecasting the coming summer CIL conditions (Fig. 36, right panel). In the outlook for 2023 section of Galbraith et al. (2023), we forecasted a CIL index of 0.33 °C similar to that of summer 2022, which was 3rd warmest since the early 1980s. A new relation between the winter volume of water colder than 0 °C and the following summer CIL temperature minimum predicted a slightly cooler index of 0.21 °C. The actual outcome is described next.

7.2   AUGUST–SEPTEMBER CIL

The CIL minimum temperature, thickness and volume for T < 0 °C and < 1 °C were estimated using temperature profiles from all sources for August and September. Most data are from the multi-species surveys in September for the Magdalen Shallows and August for the rest of the Gulf. Using all available temperature profiles, spatial temperature interpolations of the Gulf were done for each 1 m depth increment, with the interpolated field bound between the minimum and maximum values observed within each of the different regions of the Gulf (Fig. 2) to avoid spurious extrapolations. The CIL thickness at each grid point is simply the sum of depth bins below the threshold temperature, and the CIL minimum temperature is only defined at grid points where temperature rises by at least 0.5 °C at depths greater than that of the minimum, or if the grid point minimum temperature is below the CIL spatial average of the Gulf.

Fig. 37 shows the gridded interpolation of the CIL thickness < 1 °C and < 0 °C and the CIL minimum temperature for August–September 2023 as well their 1991–2020 climatology (1994–2020 for Mécatina Trough). Similar maps were produced for all years back to 1971 (although some years have no data in some regions), allowing the calculation of volumes for each region for each year as well as the climatologies shown on the left side of Fig. 37. Fig. 38 shows the volume of CIL water (< 0 °C and < 1 °C) and the average CIL minimum core temperature from the yearly August–September interpolated grids (e.g., Fig. 37). The CIL areal minimum temperature average and volume shown in Fig. 38 exclude data from Mécatina Trough which has very different water masses from the rest of the Gulf; it is influenced by inflow through the Strait of Belle Isle and is therefore not indicative of the climate in the rest of the Gulf. The time series of the regional August–September CIL volumes are shown in Fig. 39 (for < 0 °C and < 1 °C) and CIL regional average minimum core temperatures in Fig. 40.

Most regions showed only small increases in August CIL volumes and decreases in core temperature in 2023 relative to 2022 (Fig. 39 and Fig. 40). Overall, volumes defined by T < 0 °C and < 1 °C increased weakly from 2022, with still barely any recorded volume of CIL colder than 0 °C and fourth lowest volume colder than 1 °C (Fig. 38). The 2023 average temperature minimum (excluding Mécatina Trough, the Strait of Belle Isle and the Magdalen Shallows) decreased to 0.54 °C (Fig. 38 bottom panel, green line), still fourth highest. The climatological difference between this CIL index and the Gilbert and Pettigrew (1997) index (described below) is 0.26 °C because of the warming between mid-June and the August survey. After adjusting for timing, this 2023 index would correspond to a Gilbert and Pettigrew (1997) seasonal index of 0.28 °C.

7.3 NOVEMBER CIL CONDITIONS IN THE ST. LAWRENCE ESTUARY

Since 2006, the AZMP November survey usually provides a good number of conductivity-temperature-depth (CTD) casts in the St. Lawrence, allowing a good estimation of CIL properties in the Estuary. The data show the temporal warming (Fig. 40) and thinning (Fig. 39) of the CIL since the August survey. Fig. 40 shows that the fairly rapid increase of the CIL minimum temperature occurring between August and November is fairly constant interannually in spite of the differences in August temperature. Results indicate no CIL colder than 1 °C in the fall of 2023.

7.4 SEASONAL MEAN CIL INDEX

The Gilbert and Pettigrew (1997) CIL index is defined as the mean of the CIL core temperatures observed between 1 May and 30 September of each year, adjusted to 15 July with a region-dependent warming rate. It was updated using all available temperature profiles measured within the Gulf between May and September inclusively since 1947 (black line of the bottom panel of Fig. 38). As expected, the CIL minimum core temperature interpolated to 15 July is almost always colder than the estimate based on August and September data for which no temporal corrections were made. This is because the CIL is eroded over the summer and therefore its minimum core warms over time.

This CIL index for summer 2023 was +0.24 °C, the 6th highest value since (and including) 1981. Thus the seasonal CIL index for 2023 was consistent with predictions from the March cold layer volumes and with the August CIL.

The highest CIL index in recent years of 2021 is still far below the record highs observed in the 1960s and in 1980. These earlier CIL temperature minimums will need to be re-examined to confirm that they were calculated using data with sufficient vertical resolution to correctly resolve the core minimum temperature.

7.5 SUMMARY OF CIL CONDITIONS

As a summary, Fig. 41 shows selected time series of winter and summertime CIL conditions (June and September bottom temperatures also related to the CIL are outlined below) and highlights the strong correlations between these various time series. Conditions related to the 2023 CIL were warmer than normal.

8. BOTTOM WATER TEMPERATURES ON THE MAGDALEN SHALLOWS

A long-standing assessment survey covering the Magdalen Shallows has taken place in June for mackerel assessments and was since merged with the June AZMP survey. This survey provides good coverage of the temperature conditions that are greatly influenced by the cold intermediate layer that reaches the bottom at roughly half of the surface area at this time of the year.

Near-surface waters warm quickly in June, midway between the winter minimum and the annual maximum in early August. This can introduce a bias if the survey dates are not the same each year. To account for this, the seasonal warming observed at the Shediac Valley AZMP monitoring station was evaluated by Galbraith and Grégoire (2015). A linear regression was performed of temperature versus time for each meter of the water column for each year with monitoring data at Shediac Valley between May and July. Visual inspection showed that the depth-dependent warming rate was fairly constant for all years and an average was computed for every depth. Warming is maximal at the surface at 18 °C per 100 days and, in spite of some uncertainties between 30 m and 55 m, decreases almost proportionally with depth to reach 2 °C per 100 days at 40 m, followed by a further linear decrease to reach 1 °C per 100 days at 82 m.

All available temperature profiles taken in June from a given year are binned at 1 m depth intervals (or interpolated if the resolution is too coarse) and then adjusted according to the sampling date to offset them to June 15th according to the depth-dependent warming rate extracted from Shediac Valley monitoring data. An interpolation scheme is used to estimate temperature at each 1 m depth layer on a 2 km resolution grid. Fig. 42 shows temperatures and anomaly maps at depths of 20 m, 30 m, 40 m and 50 m. Fig. 43 shows averages over the grids at 10 m, 20 m, 30 m, 50 m and 75 m for all years when interpolation was possible, as well as SST June averages since 1982, for both western and eastern regions of the Magdalen Shallows (Fig. 22). In 2023, temperatures were on average below normal to normal down to 10 m, then normal at mid-depths, and finally above normal from 30 m on the western Shelf and at 75 m on the eastern Shelf (Fig. 42 and Fig. 43).

Bottom temperature is then estimated at each point of the grids constructed from the June survey by looking up the interpolated temperature at the depth level corresponding to a bathymetry grid provided by the Canadian Hydrographic Service with some corrections applied (Dutil et al. 2012). The method is fully described in Tamdrari et al. (2012). A climatology was constructed by averaging all available temperature grids between 1991 and 2020, and anomaly grids were then computed for each year based on that climatology. The June bottom temperature climatology as well as the 2023 reconstructed temperature and anomaly fields are shown in Fig. 43. The same method just described was applied using the available CTD data from August and September, mostly from the multispecies surveys for the northern Gulf in August and for the Magdalen Shallows in September. Bottom temperatures were from near normal to above the climatological mean on the Magdalen Shallows in June and August/September 2023. The pattern shifted slightly between the two periods with waters north of Prince Edward Island and the eastern Shelf exchanging near-normal and above-normal conditions, but remaining above normal on the western Shelf (Fig. 44).

Time series of the bottom area covered by water in various temperature intervals were estimated from the gridded data for the June surveys as well as for the September multispecies survey on the Magdalen Shallows (Fig. 45). The time series of areas of the Magdalen Shallows covered by water colder than 0, 1, 2, and 3 °C in June and September are also shown in Fig. 41 as part of the CIL summary. In 2023, areas were smaller than normal at all threshold temperatures from < -1 °C to < 3°C during both periods.

9.   DEEP WATERS (> 150 M)

The deeper water layer (> 150 m) below the CIL originates at the entrance of the Laurentian Channel at the continental shelf break and circulates towards the heads of the Laurentian, Anticosti, and Esquiman channels without much exchange with the upper layers. The layer from 150 m to 540 m is characterized by temperatures between 1 and > 7 °C and salinities between 32.5 and 35 (except for Mécatina Trough where near-freezing waters may fill the basin to 235 m in winter and usually persist throughout the summer). Decadal changes in temperature, salinity, and dissolved oxygen of the deep waters entering the Gulf at the continental shelf are related to the varying proportion of the source cold—fresh and oxygen-rich Labrador Current water and warm—salty and oxygen-poor slope water (McLellan 1957, Lauzier and Trites 1958, Gilbert et al. 2005, Jutras et al. 2020). The deeper waters travel from the mouth of the Laurentian Channel to the Estuary in roughly three to four years (Gilbert 2004), decreasing in dissolved oxygen from in situ respiration and oxidation of organic material as they progress to the channel heads. The lowest levels of dissolved oxygen (below 12% saturation in 2022; Blais et al 2023) are therefore found in the deep waters at the head of the Laurentian Channel in the Estuary.

9.1   BOTTOM WATER TEMPERATURES IN DEEP WATERS

As described above, bottom water temperature was computed for entire Gulf using all available CTD data from August and September, mostly from the multispecies surveys for the northern Gulf in August and for the Magdalen Shallows in September (Fig. 46). We also included selected temperature casts from a trawl mounted SBE19plus that yields data at a vertical resolution of 5 m for 2019 to 2023. All of the Gulf deep bottom water temperatures were above normal in 2023, with most areas of Central Gulf, Anticosti and Esquiman Channels, and northwest Gulf above 6 °C, with some areas of Anticosti and Esquiman Channels above 7 °C but decreased from August 2021.

As done for the Magdalen Shallows (Fig. 45), time series of the bottom area covered by water in various temperature intervals were also estimated for the other regions of the Gulf based on August-September temperature profile data (Fig. 47). The figures show compression of the bottom habitat area in the temperature range of 5–6 °C in 1992, offset by the larger colder 4–5 °C habitat. In 2012, a return of > 6 °C temperatures to the sea floor began. By 2015, there was a large decrease of the 5–6 °C habitat in the northeast Gulf, this time replaced by a warmer 6–7 °C habitat. The 6–7 °C area then increased sharply in Central and northwest Gulf in 2017, and increased sharply again in northwest Gulf in 2018 and again in 2019. Some 7–8 °C habitat appeared for the first time in the northeast Gulf in 2020 and increased in 2021. In 2021, the 6–7 °C area increased dramatically in the Estuary. In 2022, the 6–7 °C area increased slightly in the combined Estuary and northwest Gulf area, but the 7–8 °C area decreased slightly in the northeast Gulf in favour of increased 6–7 °C area. In 2023, the 6–7 °C and 7–8 °C areas

14

reverted to conditions very similar to those of 2021; this is the first indication that deep water temperatures are stabilizing in the Gulf.

9.2   DEEP TEMPERATURE MAXIMUM

The warm waters found at the bottom of the Laurentian Channel and elsewhere are associated with the deep temperature maximum evident in the temperature profiles in these areas (e.g., the temperature maximum observed at spatially and interannually variable depth between 200 and 300 m on Fig. 3). The recent interannual progression to current conditions of the deep temperature maximum is shown on Fig. 48. Temperatures above 7 °C have been recorded since 2012 in the Gulf near Cabot Strait and occupied a large area in the northeast Gulf for the first time in 2020, extending further towards the heads of Esquiman and Anticosti channels. The Gulf-wide average and regional areal averages of the deep temperature maximum are shown in Fig. 49. The Gulf-wide average of the deep temperature maximum has increased from 5.2 °C in 2009 to a record high of 7.0 °C in 2022, dropping slightly back down to 6.9 °C in 2023 which is the same value as in 2021. This is again an indication that deep water temperatures are stabilizing in the Gulf.

9.3   TEMPERATURE AND SALINITY ANNUAL MEANS

Monthly temperature and salinity averages were constructed for various depths using a method used by Petrie et al. (1996) but for the geographical regions shown in Fig. 2. In this method, all available data obtained during the same month within a region and close to each depth bin are first averaged together for each year. Monthly averages from all available years from 1991 to 2020 and their standard deviations are then computed for climatologies. This two-fold averaging process reduces the bias that occurs when the numbers of profiles in any given year are different. These monthly averages were further averaged into regional yearly time series that are presented in Fig. 49 (temperature) and Fig. 50 (salinity) for 200 m and 300 m. The 300 m observations suggest that temperature anomalies are advected up-channel from Cabot Strait to the Estuary in two to three years, consistent with the findings of Gilbert (2004), while variability at 200 m often appears or disappears in all regions at the same time, suggesting vertical changes. The regional averages are weighted into a Gulf-wide average in accordance to the surface area of each region at the specified depth. These Gulf-wide averages are shown for 150 m, 200 m and 300 m in Fig. 49, Fig. 50 and Fig. 51. Linear trends (calculated over 1915–2022) in temperature and salinity at 300 m of 2.5 °C and 0.3 per century, respectively, are shown in Fig. 51 (see also Galbraith et al. 2013 for other long-term trends), although the temperature increase has been of 1.3 °C per decade since 2009 (5.3 times the long-term rate of change).

In 2023, Gulf-wide average temperatures decreased from 2022 series record highs to 3.7 °C at 150 m (+1.5 SD), 5.7 °C (+1.9 SD) at 200 m, 6.7 °C (+2.6 SD) at 250 m and to 6.9 °C (+2.8 SD) at 300 m. The 300 m average temperature is similar to that of 2021 whereas the 150 and 200 m average temperatures are similar to those of 2020 (Fig. 49 and Fig. 51). Gulf-wide average salinities also decreased considerably to 34.80 at 300 m (a value similar to that of 2020), to 34.10 at 200 m (midway between values of 2018 and 2019) and to 33.31 at 150 m similar to 2019 (Fig. 50 and Fig. 51).

Most of the sudden changes from 2022 temperatures at 150 and 200 m are likely attributed to halocline vertical downward motion rather than by a change in water mass properties. Looking at August surveys, the mean temperature of waters at a salinity of 34 (generally found close to

200 m depth) decreased slightly in 2023 to 5.4 °C from the 2022 peak of 5.5 °C (Fig. 51), the 0.1 °C difference in water mass characteristics is much less than the decrease of 0.5 °C observed at 200 m. The mean depth of waters at the salinity of 34 was shallowest since 1985 in 2022 (167 m) and increased by 16 m in 2023 (to 183 m, line green in Fig. 51); thus most of the 0.5 °C decrease is associated with a deepening of the thermocline/halocline. This implies a change in estuarine circulation or perhaps the inflow of thicker mid-depth intrusions that must be compensated for by either outflow or reduced inflow at greater depths.

On the other hand, the decrease of the mean temperature at 300 m from the 2022 maximum does appear to be associated with water mass changes. The average temperature of salinity 34.7 waters tracks the average temperature at 300 m well (black line overlying temperature at 300 m in Fig. 51). In recent years the salinity at 300 m has increased to 34.8 and the average temperature at that salinity has decreased from a maximum value of 7.2 °C in 2022 to 7.0 °C in 2023 (red line in Fig. 51).

In 2023 , temperatures at 200 m, 250 m (not shown) and 300 m decreased from regional record highs in all deep regions of the Gulf (Fig. 49). The values at 300 m were: Estuary (6.1 °C, +2.8 SD), northwest Gulf (6.6 °C, +3.4 SD), Central Gulf (6.9 °C, +2.9 SD). Temperature at 300 m in the Laurentian Mouth region outside the Gulf decreased below 7 °C for the first time since 2013, as the salinity decreased to near-normal, and was near normal at 200 m (7.6 °C) for the first time since 2010. Deep temperatures in the Gulf may have begun a slight decrease that should propagate further into the Gulf during next few years, or at least have reached a plateau.

10. SEASONAL AND REGIONAL AVERAGE TEMPERATURE STRUCTURE

In order to show the seasonal progression of the vertical temperature structure, regional averages are shown in Fig. 52 to Fig. 55 based on the profiles collected during the March helicopter survey, the June AZMP and mackerel survey, the August multi-species survey (September survey for the Magdalen Shallows), and the October AZMP survey. All additional archived CTD data for those months were also used. This was particularly useful in August because the multi-species survey exceptionally did not include the Estuary in 2023. The temperature scale was adjusted to highlight the CIL and deep-water features; the display of surface temperature variability is best suited to other tools such as remote sensing and thermographs. Average discrete depth layer conditions are summarized for the surveyed months of 2022 and 2023 in Fig. 56 for temperature and in Fig. 57 for salinity and 0–50 m stratification. The anomalies were computed relative to monthly temperature and salinity 1991–2020 climatologies calculated for each region, shown in grey as the mean value ± 0.5 SD in Fig. 52 to Fig. 55.

Caution is needed in interpreting mean profiles. Indeed, regional averaging of winter profiles does not work very well in the northeast Gulf because very different water masses are present in the area such as the cold Labrador Shelf intrusion with saltier and warmer deeper waters of Anticosti Channel or Esquiman Channel. Similarly, the deeper portions of the Magdalen Shallows averaging region consists of two widely separated zones to the north and southeast.

The highlights of March 2023 water temperatures shown in Fig. 52 include the previously discussed cold layer volumes which were well below normal, as evidenced here by mixed layers

warmer than the -1 °C or 0 °C thresholds in many regions. The March survey was also the first to indicate a cooling of deep waters induced by a shift in halocline depth. This was particularly evident in the estuary and northeast Gulf where the 2023 thermocline was observed 20 to 30 m deeper than in 2022, with temperatures returning to near normal values in the northeast. This thermocline shift in the northeast Gulf was not as evident by June (Fig. 53) and disappeared by August when temperature at 200 m was similar between the two years (Fig. 54). It was however present in Centre Gulf and Cabot Strait in June, August and October.

11.   CURRENTS AND TRANSPORTS

Currents and transports are derived from a NEMO (Nucleus for European Modelling of the Ocean) numerical model of the Gulf of St. Lawrence, Scotian Shelf, and Gulf of Maine. The model is prognostic, i.e., it allows for evolving temperature and salinity fields. It has a spatial resolution of 1/12° with 46 depth-levels in the vertical axis. The atmospheric forcing is taken from the Global Environmental Multiscale (GEM) model running at the Canadian Meteorological Center (CMC). Freshwater runoff is obtained from observed data and the hydrological model, as discussed in the freshwater runoff section, but does not use the new daily calculation of runoff at Québec City. The spring freshet may therefore differ from what was described in an earlier section of this document. A simulation was run for 2006–2023 from which transports were calculated. The reader is reminded that the results outlined below are not measurements but simulations and improvements in the model may lead to changes in the transport values.

Fig. 58 to Fig. 60 show seasonal depth-averaged currents for 0–20 m, 20–100 m, and 100 m to the bottom for 2022. Currents are strongest in the surface mixed layer, generally 0–20 m, except in winter months when the 20–100 m averages are almost as high, and the 100 m to bottom averages are still much higher than during other seasons (note the different scale for this depth). Currents are also strongest along the slopes of the deep channels. The Anticosti Gyre (Fig. 1) is usually evident but strongest during winter months, when it even extends strongly into the bottom-average currents (Fig. 60). The Gaspé Current usually flows along the Gaspé Peninsula but may meander in the Estuary, sometimes hugging the north shore and forming gyres. In 2023, the Gaspé Current was strongest along the north shore of the Estuary in winter and extended across the Estuary for most of the year, with no indication of upstream flow along the north shore.

Monthly averaged transports across seven sections of the Gulf of St. Lawrence are shown in Fig. 61 for sections with estuarine circulation, and in Fig. 62 for sections where only net transports are relevant. In Fig. 61, the net transport integrates both up and downstream circulation and, for example, corresponds to freshwater runoff at the Pointe-des-Monts section. The outflow transport integrates all (eastward) currents heading towards the ocean, while the estuarine ratio corresponds to the outflow divided by the net transports. Note that the only section where estuarine circulation is dominant is at Pointe-des-Monts. The net transport at Honguedo is on average 15 times higher than at Pointe-des-Monts, consisting mostly of circulation around Anticosti Island first observed at the Jacques-Cartier section. Similarly, the net transport at Cabot Strait is outflow that is mostly balanced by inflow from the Strait of Belle Isle, such that an estuarine ratio is perhaps a misleading description. Transports through sections under the direct estuarine influence of the St. Lawrence River (e.g., Pointe-des-Monts) have a more direct response to change in freshwater runoff while others (e.g., Cabot Strait,

Bradelle Bank) have a different response, presumably due to redistribution of circulation in the GSL under varying runoff. The estuarine circulation ratio is determined by the mixing intensities within the estuary and is greatly influenced by stratification, but also includes horizontal estuarine-like circulation that occurs when waters flow from the Anticosti Gyre and into the Estuary at Pointe-des-Monts. It is on average greatest during winter months and weakest during the spring freshet. In fact, it is sufficiently reduced in spring that the climatological outflow transport at Pointe-des-Monts reaches its minimum value in June even though this month corresponds to the third highest net transport of the year, i.e., the estuary becomes sufficiently stratified that freshwater runoff tends to slip on top of the denser salty waters underneath. This occurred in 2019 when the exceptionally high May-June freshet led to decreased modelled estuarine circulation and decreased outflow transport by entrainment at the Pointe-des-Monts section. In contrast, the weak freshet of 2021 coincided not only with increased estuarine circulation but also with increased outflow transport. The estuarine circulation ratio at the Pointe-des-Monts section was generally above normal in 2023 except in winter, reaching a record high in June; this continues a pattern of above normal conditions since 2020 (Fig. 61). Transports were very high across the Bradelle and Northumberland sections (Fig. 62).

11.1   TRANSPORT THROUGH THE STRAIT OF BELLE ISLE

Transport through the Strait of Belle Isle is estimated using data from an acoustic Doppler current profiler (ADCP) moored off of the northern coast in the Strait (Fig. 13). Studies have shown that although low-frequency currents through the strait are sheared, they are towards the GSL over most of the cross section and coherent across the strait (Garrett and Petrie 1981; Petrie et al 1988); they are driven by large-scale meteorological forcing. Transports are therefore computed here by assuming velocity at the mooring to be representative of the whole cross-section, although it may underestimate transport towards the Labrador Shelf. The methodological details can be found in Shaw and Galbraith (2023).

Transport through the Strait is largely towards the GSL, with monthly values ranging up to 8.1 (deci-Sverdrups, dSv; Fig. 63). On average, transport switches between low values (0.5-1 dSv) from April to July and stronger values (3-5 dSv) from September to February. Monthly-averaged transport is occasionally towards the Labrador Shelf during the spring and early summer and has been measured up to 1.1 dSv (May 2011). Strong transport towards the GSL was measured during November 2022, matching the previous time series record of -8.1 dSv, and also during June and September 2023 (-4.2 and -5.6 dSv, respectively). The strong June transport was the second largest of the time series for any months from April to August. It coincided with lower-than-normal surface temperatures (Fig. 18 and Fig. 19) and the late-season transport of sea ice into the GSL from the Labrador Shelf.

12.   HIGH FREQUENCY SAMPLING AZMP STATIONS

Sampling by the Maurice Lamontagne Institute began in 1991 at a station offshore of Rimouski (48° 40' N 68° 35' W, 320 m depth; Plourde et al. 2009), typically once a week during summer and less often during spring and fall and almost never in winter (Fig. 64). In 2013, following several analyses that identified good correlations and correspondences between the prior AZMP Anticosti Gyre and Gaspé Current stations with the Rimouski station, it was decided to drop sampling efforts at these logistically difficult stations and officially integrate the Rimouski station into the AZMP program, and begin winter sampling there when opportunities arose. The

AZMP station in the Shediac Valley (47° 46.8' N, 64° 01.8' W, 84 m depth) is usually sampled by the Bedford Institute of Oceanography, by DFO Gulf Region and by the Maurice Lamontagne Institute (Fig. 64). This station has been sampled irregularly since 1947, nearly every year since 1957, and more regularly during the summer months since 1999 when the AZMP program began.

Oceanographic moorings have been deployed on rotation since the summer of 2015 at these two AZMP stations, providing data to fill sampling gaps in winter or during other times of the year. Unfortunately most of the Shediac Valley mooring was lost to fishing gear in the 2023 deployment. In 2023, Viking oceanographic buoys equipped with an automatic temperature and salinity profiler carried out 138 full-depth casts at Shediac Valley station, and 333 casts to 300 m at Rimouski station.

Isotherms and isohalines as well as monthly averages of layer temperature and salinity, stratification, and CIL minimum core temperature and thickness at < 1 °C are shown for 2021–2023 for the Rimouski station in Fig. 65 and for the Shediac Valley station in Fig. 66. As for most metrics in this report the scorecard climatologies are calculated from 1991 to 2020 data, but there are few data prior to 1999 for Shediac Valley. Mooring data are also used to fill winter gaps in the isotherms and isohalines, and are used throughout the tables of monthly averages when available at the corresponding depths. Fig. 67 shows the interannual variability of some seasonal layer averages from May to October for the two stations.

At the Rimouski station, the gradual shift of cold-fresh deep anomalies at 200–300 m present in 2010 to warmer-saltier waters advected from Cabot Strait led to a shift to warm anomalies by summer 2014 (not shown). A slow but persistent warming has been observed at 320 m at the station. A monthly average record high of 6.41 °C was recorded in October 2023 (Fig. 65). The CIL was warmer and thinner than normal for all recorded months (Fig. 67). Salinity was below normal down to 150 m beginning in June, indicating a deeper than normal halocline and consistent with the average August-September temperature profile observed in the estuary (Fig. 54). May to October 0-50 m and 0-100 m average temperatures were at near record values. While temperature at 320 m was at a record high in 2023 (Fig. 65), temperature at 290 m decreased slightly in 2023 from the 2022 record high (Fig. 67).

Conditions at the Shediac Valley station show normal to above-normal temperatures and normal to below-normal salinities (Fig. 66). Temperatures averaged May to October from 0 to 50 m and to the bottom (0-84 m) were at record highs.

13. SUMMARY

Fig. 68 summarizes SST, summertime CIL and deep-water average temperatures. The August SST was above normal (+0.9 SD) and the May-November average tied for second highest. The average temperature at 150 m, 200 m, 250 m and 300 m decreased from the 100+ year series record highs of 2022 but remained very high. The seasonal CIL core temperature was above normal, the 5th highest value after 1981.

Another summary of the temperature state of the Gulf of St. Lawrence over a shorter time span (since 1971) allows the inclusion of more datasets, and three sets of four time series are chosen to represent surface, intermediate and deep conditions (Fig. 69). The SST summer and fall timing are from Fig. 25 (12 °C threshold) with air temperature proxies used prior to 1982. Sea-

ice is grouped as an intermediate feature since all are associated with winter formation. Fig. 69 shows the sums of these three sets of anomalies representing the state of different parts of the system and is reproduced on Fig. 70 with each time series contribution shown as stacked bars (Petrie et al. 2007). These composite indices measure the overall state of the climate system with positive values representing warm conditions and negative representing cold conditions. The plot also indicates the degree of correlation between the various measures of the environment.

The index of surface anomalies was above normal (+2.4 SD) and second highest of the time series in 2023, with record late timing of the fall cooling. Only the summer timing was near normal. The index of intermediate layer anomalies was above normal (+1.7 SD). The index of deep temperature anomalies decreased from the 2022 series record high to the 3rd highest value (+2.3 SD).

14.   KEY FINDINGS

- The annual runoff was above normal at 13 700 m^3 s^{-1} (+1.0 SD) for the St. Lawrence River and at 18 800 m^{3}s^{-1} (+1.0 SD) for the RIVSUM II index.

- The seasonal maximum ice volume of 20 km³ (-1.1 SD) was below normal, ranking 6th lowest since 1969, as did the January-April average (-1.1 SD). In the 14-year span since 2010, 9 of the 14 lowest seasonal maximum ice volumes of the time series have occurred.

- The winter surface mixed cold layer (< -1 °C) volume of 7 600 km³ was below normal (-1.5 SD). The mixed layer volume increases to 13 400 km³ (-1.5 SD) when water temperatures < 0 °C are considered, which is also below normal. The Labrador Shelf water intrusion volume into Mécatina Trough of 1045 km³ (-0.4 SD) was near normal.

- The August cold intermediate layer (CIL) average minimum temperature was above normal at 0.54 °C (+1.6 SD), 4th highest since 1985. The Gilbert & Pettigrew (1997) minimum temperature index, which includes data over a longer season, was above normal at 0.24 °C (+1.6 SD). These metrics are consistent with each other.

- On the Magdalen Shallows, the areas covered by water with low temperatures were smaller than normal at all threshold temperatures from < -1 °C to < 3 °C during both periods of June and August/September.

- The timing of summer onset of the surface layer at 12 °C was near normal but the post-season cooling was much later than normal following a severe to extreme marine heatwave in the estuary (+3.3 weeks, +3.6 SD).

- Surface temperatures averaged over the Gulf were highest of the satellite record (since 1981) for the months of July (16.5 °C, +2.5 °C, +2.6 SD) and October (11.5 °C, +2.8 °C, +4.8 SD). The Estuary experienced a severe to extreme marine heatwave in the fall, leading to monthly records in September (12.7 °C, +4.8 °C, +5.1 SD) and October (9.9 °C, +5.0 °C, +6.4 SD).

- Marine heatwaves were numerous and intense, with a record number of 6 stations cumulating more than 300 °C days in cumulative intensity (ΣI_{cum}).

- The overall seasonal average May-November SST for the Gulf was second highest of the time series (since 1982, +1.4 °C, +2.6 SD), and the seasonal August maximum was above normal (+0.8 °C, +0.9 SD).

- Gulf-wide average temperatures decreased from 2022 series record highs (since 1915) at depths of 150 m (3.7 °C, +1.5 SD), 200 m (5.7 °C, +1.9 SD), 250 m (6.7 °C, +2.6 SD) and 300 m (6.9 °C, +2.8 SD). Most of the 2022 to 2023 decreases at 150 and 200 m are attributed to halocline vertical downward motion rather than by a change in water mass properties.

- The Gulf-wide average of the deep temperature maximum has increased from 5.2 °C in 2009 to a record high of 7.0 °C in 2022, dropping slightly back down to 6.9 °C in 2023 which is the same value as in 2021. This is an indication that deep water temperatures are stabilizing in the Gulf.

OUTLOOK FOR 2024

Air temperatures were 3.1 °C, 2.0 °C and 3.7 °C above normal over the Gulf in December 2023, January and February 2024, leading to very late first occurrence of sea ice and a nearly ice free season with the lowest recorded seasonal maximum volume. This was the setting for the March 2024 survey, which provides an outlook for CIL conditions expected for the remainder of 2024. Fig. 71 shows the March 2024 surface mixed layer temperature, salinity, and thickness (at T < -1 °C and T < 0 °C), as well as the thickness and extent of the cold and saline layer that has intruded into the Gulf from the Labrador shelf.

The often-observed pattern of warmer waters off the southern part of Newfoundland's west coast was present in March 2024, with temperatures above 0 °C in Cabot Strait and offshore of the Port au Port Peninsula, which occurs only rarely. The predictive relation between the winter volume of water colder than -1 °C and the following summer CIL minimum temperature index (Fig. 33) forecasts a CIL index of +0.57 °C because of the very low volume of waters colder than -1 °C, however this relation failed to adequately predict the CIL using a similarly low volume in 2010. A new relation between the winter volume of water colder than 0 °C and the following summer CIL temperature minimum would predict a slightly cooler index of +0.16 °C. It is likely that the outcome will lie between these two extremes and resemble conditions of 2022 and 2023.

Waters at 150 and 200 m have cooled in 2023 from records observed in 2022. In March 2024, the gulf average temperature at 200 m was 5.6 °C, a slight increase from 5.4 °C observed in March 2023 but below the 2023 annual average of 5.7 °C. While we usually look at the temperature of waters flowing into the Gulf on the eastern side of Cabot Strait as in indicator of warm water inflows, in March 2024 cold waters were outflowing on that side while waters reaching 7.3 °C were inflowing on the western side. It is likely that gyre recirculation was at play during the survey.

15. ACKNOWLEDGEMENTS

REFERENCES CITED

Belzile, M., Galbraith, P.S., and Bourgault, D. 2016. Water renewals in the Saguenay Fjord. J. Geophys. Res. Oceans. 121: 638–657. doi:10.1002/ 2015JC011085.

Benoît, H.P., Savenkoff, C., Ouellet, P., Galbraith, P.S., Chassé, J. and Fréchet, A. 2012. Impacts of fishing and climate-driven changes in exploited marine populations and communities with implications for management. In State-of-the-Ocean Report for the Gulf of St. Lawrence Integrated Management (GOSLIM) Area. Edited by H.P. Benoît, J.A. Gagné, C. Savenkoff, P. Ouellet and M.-N. Bourassa. Can. Manuscr. Rep. Fish. Aquat. Sci. 2986: viii + 73 p.

Blais, M., Galbraith, P.S., Plourde, S. and Lehoux, C. 2023. Chemical and Biological Oceanographic Conditions in the Estuary and Gulf of St. Lawrence during 2022. Can. Tech. Rep. Hydrogr. Ocean Sci. 357 : v + 70 p.

Casey, K.S., Brandon, T.B., Cornillon, P., and Evans, R. 2010. The Past, Present and Future of the AVHRR Pathfinder SST Program. In Oceanography from Space: Revisited. Edited by V. Barale, J.F.R. Gower, and L. Alberotanza. Springer. pp. 273–287.

Cyr, F., Bourgault, D. and Galbraith, P.S. 2011. Interior versus boundary mixing of a cold intermediate layer. J. Geophys. Res. (Oceans). 116: C12029. doi:10.1029/2011JC007359.

Cyr, F., Coyne, J., Snook, S., Bishop, C., Galbraith, P.S., Chen, N., Han, G. 2024. Physical Oceanographic Conditions on the Newfoundland and Labrador Shelf during 2022. Can. Tech. Rep. Hydrogr. Ocean Sci. 354: vi + 52 p.

DFO. 2023. Oceanographic Conditions in the Atlantic Zone in 2022. DFO Can. Sci. Advis. Sec. Sci. Advis. Rep. 2023/019.

Dutil, J.-D., Proulx, S., Galbraith, P.S., Chassé, J., Lambert, N. and Laurian, C. 2012. Coastal and epipelagic habitats of the estuary and Gulf of St. Lawrence. Can. Tech. Rep. Fish. Aquat. Sci. 3009: ix + 87 p.

Fisheries and Oceans Canada. 2023. Daily Freshwater Runoffs of the St. Lawrence at the Height of Quebec City [Data set]. https://catalogue.ogsl.ca/dataset/ca-cioos_27913e4c-975c-4cab-9fc7-5ff556d82e68

Galbraith, P.S. 2006. Winter water masses in the Gulf of St. Lawrence. J. Geophys. Res. Oceans 111: C06022. doi:10.1029/2005JC003159.

Galbraith, P.S. and Grégoire, F. 2015. Habitat thermique du maquereau bleu; profondeur de l'isotherme de 8 °C dans le sud du golfe du Saint-Laurent entre 1960 et 2014. Secr. can. de consult. sci. du MPO. Doc. de rech. 2014/116. v + 13 p.

Galbraith, P.S. and Larouche, P. 2013. Trends and variability in eastern Canada sea-surface temperatures. Ch. 1 (pp. 1–18). In Aspects of climate change in the Northwest Atlantic off Canada. Edited by Loder, J.W., G. Han, P.S. Galbraith, J. Chassé and A. van der Baaren. Can. Tech. Rep. Fish. Aquat. Sci. 3045: x + 190 p.

Galbraith, P.S., Saucier, F.J., Michaud, N., Lefaivre, D., Corriveau, R., Roy, F., Pigeon, R. and Cantin, S. 2002. Shipborne monitoring of near-surface temperature and salinity in the Estuary and Gulf of St. Lawrence. Atlantic Zone Monitoring Program Bulletin, Dept. of Fisheries and Oceans Canada. No. 2: 26–30.

Galbraith, P.S., Desmarais, R., Pigeon, R. and Cantin, S. 2006. Ten years of monitoring winter water masses in the Gulf of St. Lawrence by helicopter. Atlantic Zone Monitoring Program Bulletin, Dept. of Fisheries and Oceans Canada. No. 5: 32–35.

Galbraith, P.S., Larouche, P., Gilbert, D., Chassé, J. and Petrie, B. 2010. Trends in sea-surface and CIL temperatures in the Gulf of St. Lawrence in relation to air temperature. Atlantic Zone Monitoring Program Bulletin. No. 9: 20–23.

Galbraith P.S., Larouche, P., Chassé, J. and Petrie, B. 2012. Sea-surface temperature in relation to air temperature in the Gulf of St. Lawrence: interdecadal variability and long term trends. Deep Sea Res. II. V77–80: 10–20.

Galbraith. P.S., Hebert, D., Colbourne, E. and Pettipas, R. 2013. Trends and variability in eastern Canada sub-surface ocean temperatures and implications for sea ice. Ch.5. In: Aspects of climate change in the Northwest Atlantic off Canada. Edited by: Loder, J.W., G. Han, P.S. Galbraith, J. Chassé and A. van der Baaren. Can. Tech. Rep. Fish. Aquat. Sci. 3045: x + 192 p.

Galbraith, P.S., Bourgault, D. and Belzile, M. 2018. Circulation et renouvellement des masses d'eau du fjord du Saguenay. Naturaliste Canadien. 142(2): 36–46. doi:10.7202/1047147ar

Galbraith, P.S., Chassé, J., Shaw, J.-L., Dumas, J. Lefaivre, D. and Bourassa, M.-N. 2023. Physical oceanographic conditions in the Gulf of St. Lawrence during 2022. Can. Tech. Rep. Hydrogr. Ocean Sci. 354 : v + 88 p.

Galbraith, P.S., Larouche P., and Caverhill, C. 2021. A sea-surface temperature homogenization blend for the Northwest Atlantic. Can. J. Remote Sens. 47(4): 554–568. doi: 10.1080/07038992.2021.1924645

Garrett, C.J.R and B. Petrie. 1981. Dynamical Aspects of the Flow Through the Strait of Belle Isle. J. Phys. Ocean. 11: 376-393. DOI: 10.1175/1520-0485(1981)011<0376:DAOTFT>2.0.CO;2

Gilbert, D. 2004. Propagation of temperature signals from the northwest Atlantic continental shelf edge into the Laurentian Channel. ICES CM. 2004/N: 7. 12 p.

Gilbert, D. and Pettigrew, B. 1997. Interannual variability (1948–1994) of the CIL core temperature in the Gulf of St. Lawrence. Can. J. Fish. Aquat. Sci. 54 (Suppl. 1): 57–67.

Gilbert, D., Sundby, B., Gobeil, C., Mucci, A. and Tremblay, G.-H. 2005. A seventy-two-year record of diminishing deep-water oxygen in the St. Lawrence estuary: The northwest Atlantic connection. Limnol. Oceanogr. 50(5): 1654–1666.

Hammill, M.O. and Galbraith, P.S. 2012. Changes in seasonal sea-ice cover and its effect on marine mammals. In State-of-the-Ocean Report for the Gulf of St. Lawrence Integrated Management (GOSLIM) Area. Edited by H.P. Benoît, J.A. Gagné, C. Savenkoff, P. Ouellet and M.-N. Bourassa, Eds. Can. Manuscr. Rep. Fish. Aquat. Sci. 2986: viii + 73 p.

Hebert, D., Layton, C., Brickman, D., and Galbraith, P.S. 2023. Physical Oceanographic Conditions on the Scotian Shelf and in the Gulf of Maine during 2022. Can. Tech. Rep. Hydrogr. Ocean Sci. 359: vi + 81 p

Hobday, A. J., Alexander, L. V., Perkins, S. E., Smale, D. A., Straub, S. C., Oliver, E. C. J., Benthuysen, J. A., Burrows, M. T., Donat, M. G., Feng, M., Holbrook, N. J., Moore, P. J., Scannell, H. A., Sen Gupta, A., & Wernberg, T. 2016. A hierarchical approach to defining marine heatwaves. *Progress in Oceanography*, *141*, 227–238. https://doi.org/10.1016/j.pocean.2015.12.014

Hobday, A. J., Oliver, E. C. J., Sen Gupta, A., Benthuysen, J. A., Burrows, M. T., Donat, M. G., Holbrook, N. J., Moore, P. J., Thomsen, M. S., Wernberg, T., & Smale, D. A. 2018. Categorizing and naming marine heatwaves. *Oceanography*, *31*(2), 162–173.

Kalnay, E., Kanamitsu, M., Kistler, R., Collins, W., Deaven, D., Gandin, L., Iredell, M., Saha, S., White, G., Woollen, J., Zhu, Y., Chelliah, M., Ebisuzaki, W., Higgins, W., Janowiak, J., Mo, K., Ropelewski, C., Wang, J., Leetmaa, A., Reynolds, R., Jenne, R. and Josephé, D. 1996. The NCEP/NCAR 40-year reanalysis project. Bull. Am. Meteorol. Soc. 77 : 437–470.

Jutras, M., Dufour, C. O., Mucci, A., Cyr, F., & Gilbert, D. 2020. Temporal changes in the causes of the observed oxygen decline in the St. Lawrence Estuary. Journal of Geophysical Research: Oceans, 125, e2020JC016577. https://doi.org/10.1029/2020JC016577

Kelley, D.E. and Galbraith, P.S. 2000. Gri: A language for scientific illustration. Linux J. 75: 92–101.

Lauzier, L.M. and Trites, R.W. 1958. The Deep Waters in the Laurentian Channel. J. Fish. Res. Board Can. 15: 1247–1257.

Lefaivre, D., D'Astous, A. and Matte, P. 2016. Hindcast of Water Level and Flow in the St. Lawrence River over the 2005–2012 period. Atmosphere-Ocean. 54 (3): 264–277.

McLellan, H.J. 1957. On the distinctness and origin of the slope water off the Scotian Shelf and its easterly flow south of the Grand Banks. J. Fish. Res. Board. Can. 14: 213–239.

NOAA/STAR. 2021. GHRSST NOAA/STAR ACSPO v2.80 0.02 degree L3S Dataset from Afternoon LEO Satellites (GDS v2). Ver. v2.80. PO.DAAC, CA, USA. https://doi.org/10.5067/GHLPM-3SS28

Oliver, E. C. J., Benthuysen, J. A., Darmaraki, S., Donat, M. G., Hobday, A. J., Holbrook, N. J., Schlegel, R. W., & Sen Gupta, A. 2021. Marine Heatwaves. *Annual Review of Marine Science*, *13*, 313–342. https://doi.org/10.1146/annurev-marine-032720-095144

Petrie, B., Drinkwater, K., Sandström, A., Pettipas, R., Gregory, D., Gilbert, D. and Sekhon, P. 1996. Temperature, salinity and sigma-t atlas for the Gulf of St. Lawrence. Can. Tech. Rep. Hydrogr. Ocean Sci. 178: v + 256 p.

Petrie, B., Pettipas, R.G. and Petrie, W.M. 2007. An overview of meteorological, sea ice and sea surface temperature conditions off eastern Canada during 2006. DFO Can. Sci. Advis. Sec. Res. Doc. 2007/022. iv + 38 p.

Petrie, B., Toulany, B. and Garrett, C. 1988. The transport of water, heat and salt through the Strait of Belle Isle, Atmosphere-Ocean, 26(2): 234–251. doi:10.1080/07055900.1988.9649301.

Pettigrew, B., Gilbert, D. and Desmarais R. 2016. Thermograph network in the Gulf of St. Lawrence. Can. Tech. Rep. Hydrogr. Ocean Sci. 311: vi + 77 p.

Pettigrew, B., Gilbert, D. and Desmarais R. 2017. Thermograph network in the Gulf of St. Lawrence: 2014–2016 update. Can. Tech. Rep. Hydrogr. Ocean Sci. 317: vii + 54 p.

Plourde, S., Joly, P., St-Amand, L. and Starr, M. 2009. La station de monitorage de Rimouski : plus de 400 visites et 18 ans de monitorage et de recherche. Atlantic Zone Monitoring Program Bulletin, Dept. of Fisheries and Oceans Canada. No. 8: 51–55.

Schlegel, R. W., Oliver, E. C. J., Hobday, A. J., & Smit, A. J. 2019. Detecting Marine Heatwaves With Sub-Optimal Data. *Frontiers in Marine Science*, *6*(November), 1–14. https://doi.org/10.3389/fmars.2019.00737

Shaw, J.-L. and P.S. Galbraith. 2023. Climatology of transport in the Strait of Belle Isle. J. Geophys. Res. Oceans, 128, e2022JC019084. https://doi.org/10.1029/2022JC019084.

Tamdrari, H., Castonguay, M., Brêthes, J.-C., Galbraith, P.S. and Duplisea, D.E. 2012. The dispersal pattern and behaviour of Atlantic cod in the northern Gulf of St. Lawrence: results from tagging experiments. Can. J. Fish. Aquat. Sci. 69: 112–121.

Therriault, J.-C., Petrie, B., Pépin, P., Gagnon, J., Gregory, D., Helbig, J., Herman, A., Lefaivre, D., Mitchell, M., Pelchat, B., Runge, J. and Sameoto, D. 1998. Proposal for a Northwest Atlantic zonal monitoring program. Can. Tech. Rep. Hydrogr. Ocean Sci., 194: vii + 57 p.

Vincent, L. A., Hartwell, M. M., & Wang, X. L. 2020. A third generation of homogenized temperature for trend analysis and monitoring changes in Canada's climate. Atmosphere-Ocean, 58:3 , 173-191. doi:10.1080/ 750 07055900.2020.1765728
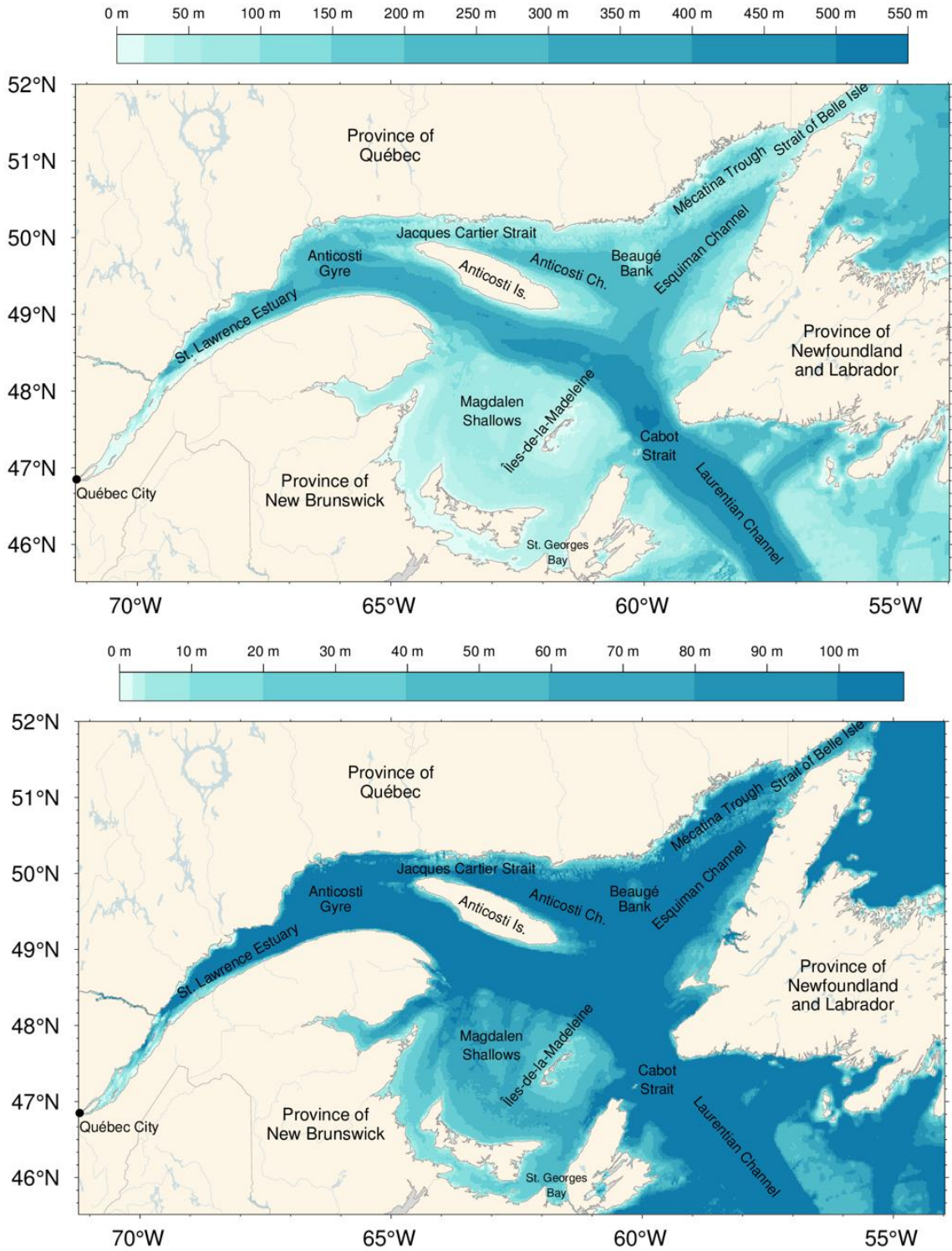
FIGURES

Fig. 1. The Gulf of St. Lawrence. Locations discussed in the text are indicated. Bathymetry datasets used are from the Canadian Hydrographic Service to the west of 56°47' W (with some corrections applied to the Baie des Chaleurs and Magdalen Shallows) and TOPEX data to the east. Bottom panel shows detail for 0–100 m bathymetry.
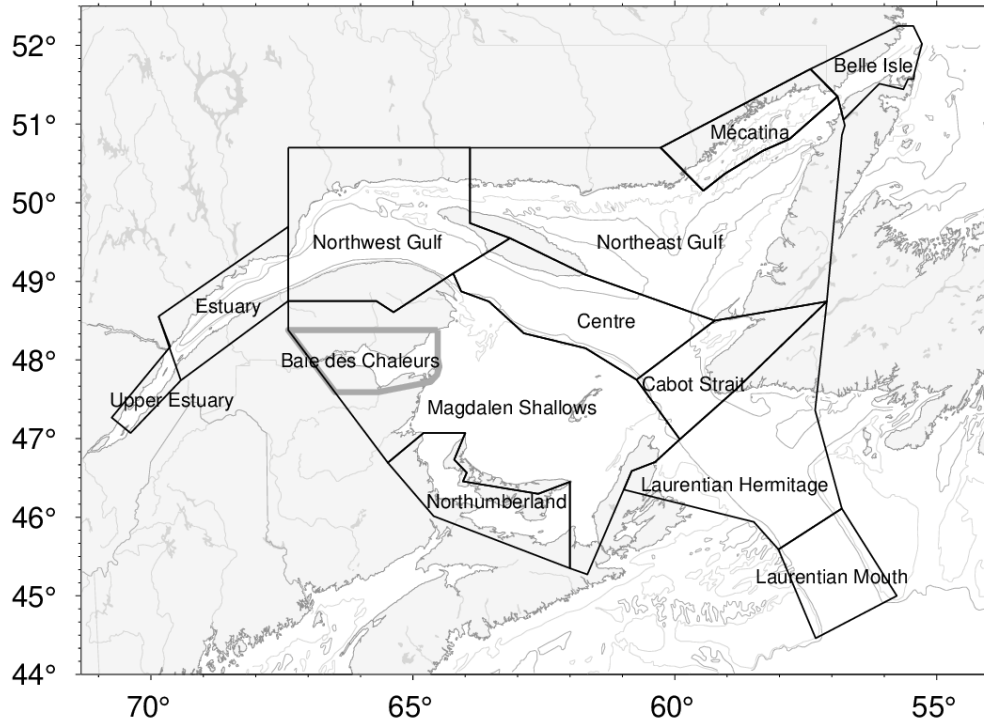
Fig. 2. Gulf of St. Lawrence divided into oceanographic regions used in spatial averaging. Baie des Chaleurs is sometimes reported separately but is always included in the Magdalen Shallows.
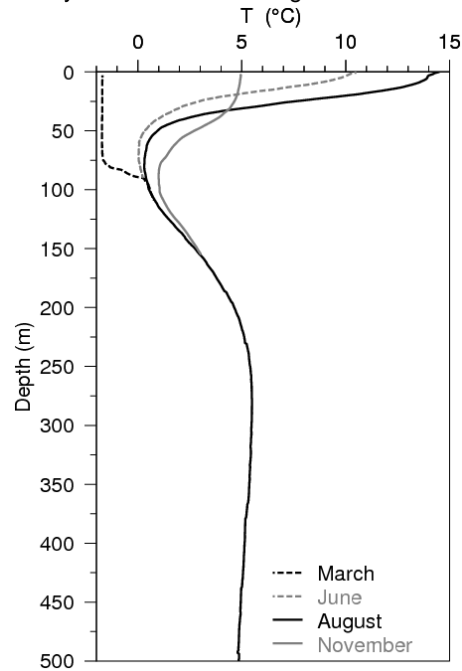

Fig. 3. Typical seasonal progression of the depth profile of temperature observed in the Gulf of St. Lawrence. Profiles are averages of observations in August, June and November 2007 in the northern Gulf. The dashed line at left shows a single winter temperature profile (March 2008), with near freezing temperatures in the top 75 m. The cold intermediate layer (CIL) is defined as the part of the water column that is colder than 1 °C, although some authors use a different temperature threshold. Figure from Galbraith et al. (2012).
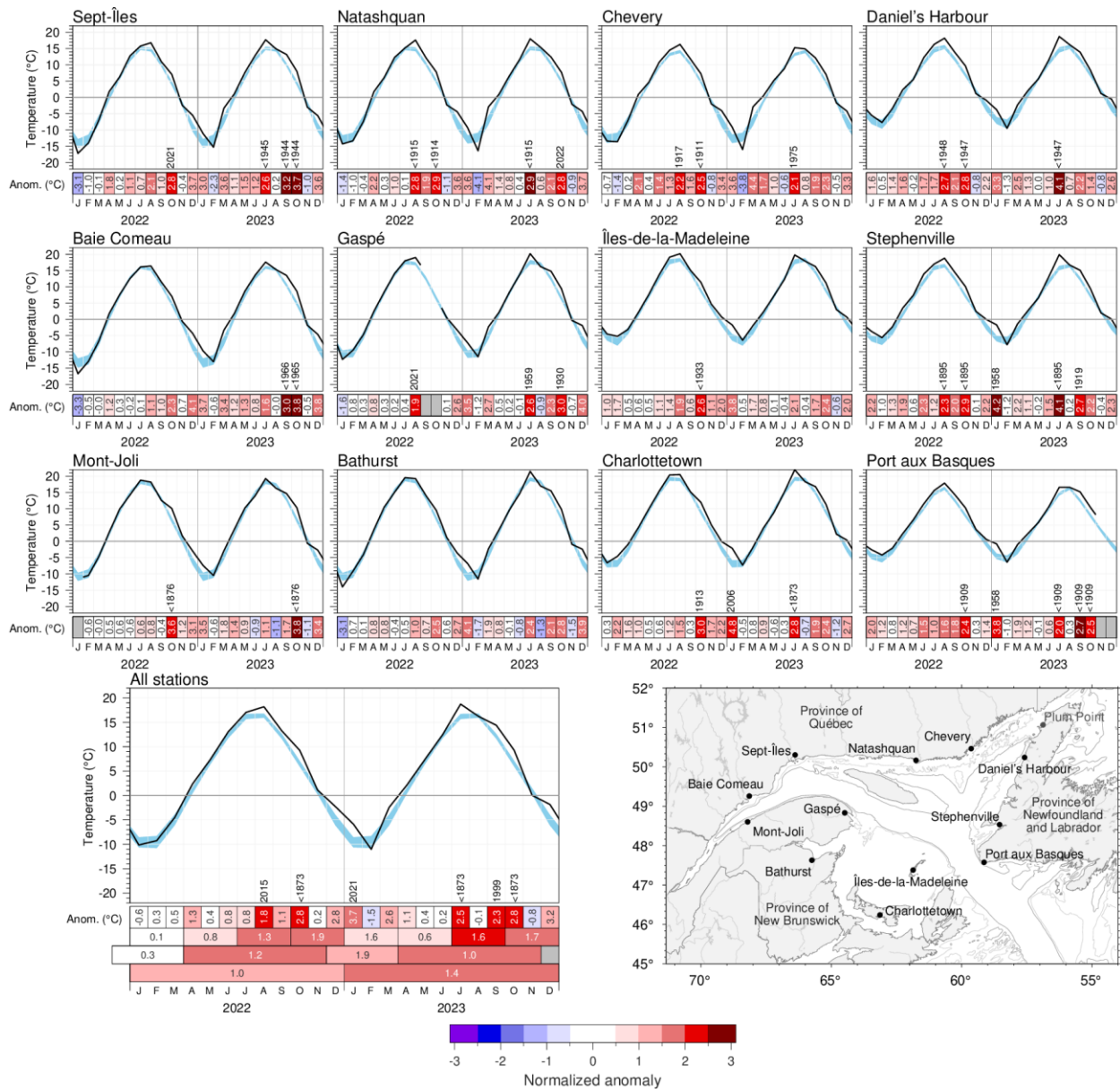
Fig. 4. Monthly air temperatures and anomalies for 2022 and 2023 at selected meteorological stations around the Gulf as well as the average for all stations. The blue area represents the 1991–2020 climatological monthly mean ± 0.5 SD. Months with 4 or more days of missing data are omitted. The bottom scorecards are colour-coded according to the monthly normalized anomalies based on the 1991–2020 climatologies for each month (colour palette at bottom), but the numbers are the monthly anomalies in ℃. For anomalies greater than 2 SD from normal, the prior year with a greater anomaly is indicated, with < used to indicate a series record. Seasonal, December-March, April-November and annual anomalies are included for the all-station average. Observations at Plum Point (not shown) had been interrupted between 2016 and 2019 and are included in the all-station average.
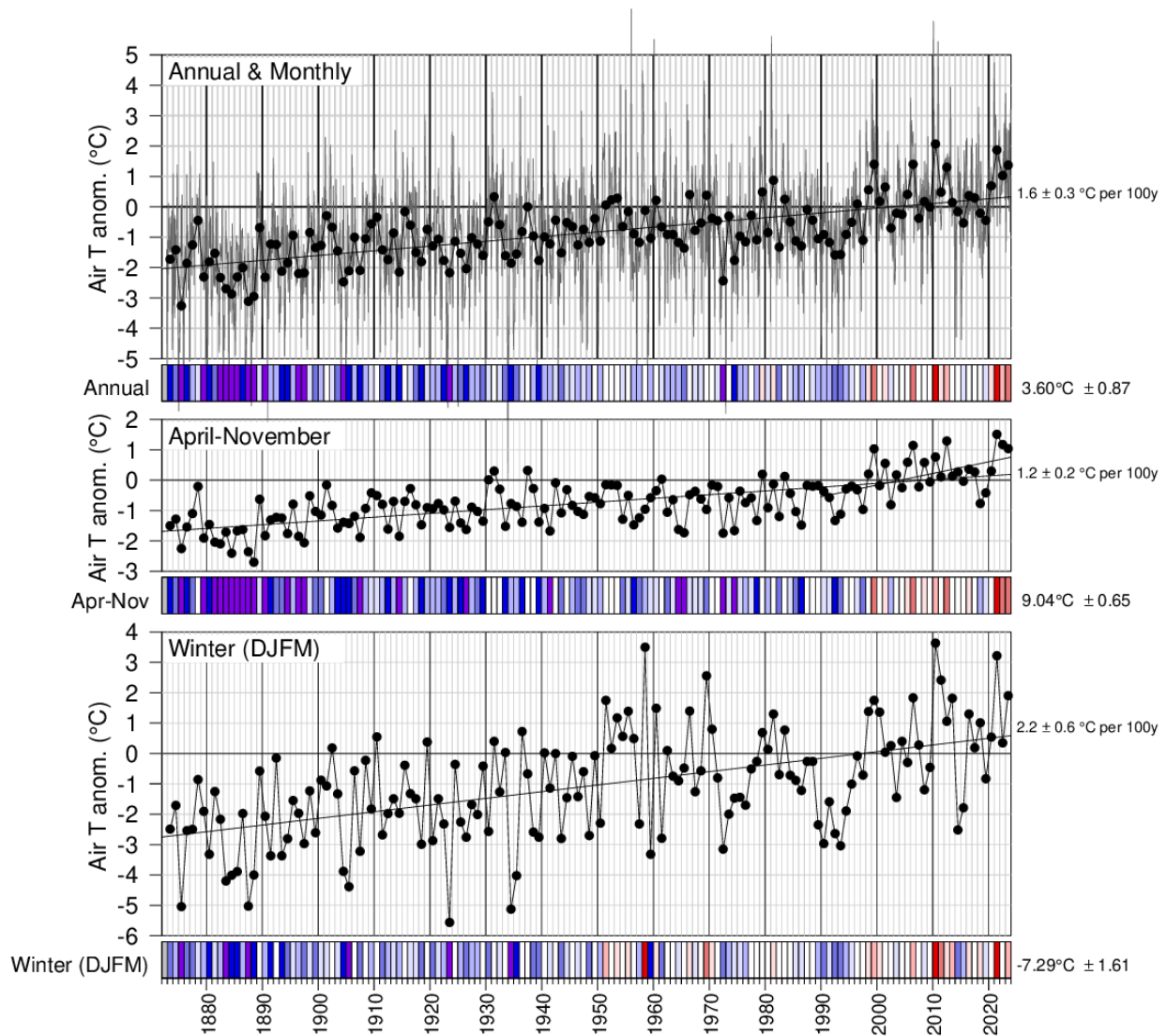
Fig. 5. Annual, April-November December-March mean air temperature anomalies averaged for the selected stations around the Gulf from Fig. 4. The grey line in the top panel shows monthly values and the thicker black line and dots show annual averages. The bottom scorecards are colour-coded according to the normalized anomalies based on the 1991–2020 climatology. Trends plus and minus their 95% confidence intervals are shown. April-November air temperature anomalies tend to be highly-correlated with May-November sea-surface temperature anomalies (Galbraith et al. 2012; Galbraith and Larouche 2013; Galbraith et al. 2021) whereas winter air temperature anomalies correlate highly with sea-ice cover parameters and winter mixed-layer volume (Galbraith et al. 2010; Galbraith et al. 2013).
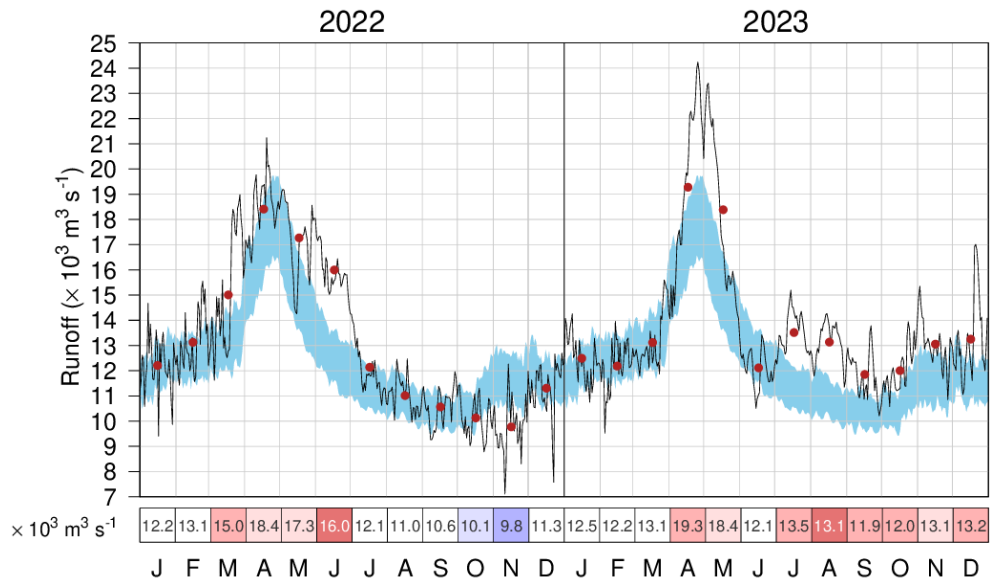
31

Fig. 6. Daily mean freshwater flow of the St. Lawrence River at Québec City. The 1991–2020 climatological mean (± 0.5 SD) is shown (blue shading). Monthly means are shown by red dots and displayed in the scorecard. It is colour-coded according to the monthly anomalies normalized for each month of the year, but the numbers are the actual monthly anomalies in 10^3 m^3s^{-1}.

Fig. 7. Monthly mean freshwater flow of RIVSUM II (upper curve), which is the sum of the St. Lawrence River at Québec City lagged by 21 days (middle curve) and rivers flowing into the St. Lawrence Estuary (lower curve). The 1991–2020 climatological means (± 0.5 SD) are shown (blue shading). The scorecards are colour-coded according to the monthly anomalies normalized for each month of the year, but the numbers are the actual monthly anomalies in 10^3 m^3s^{-1}.

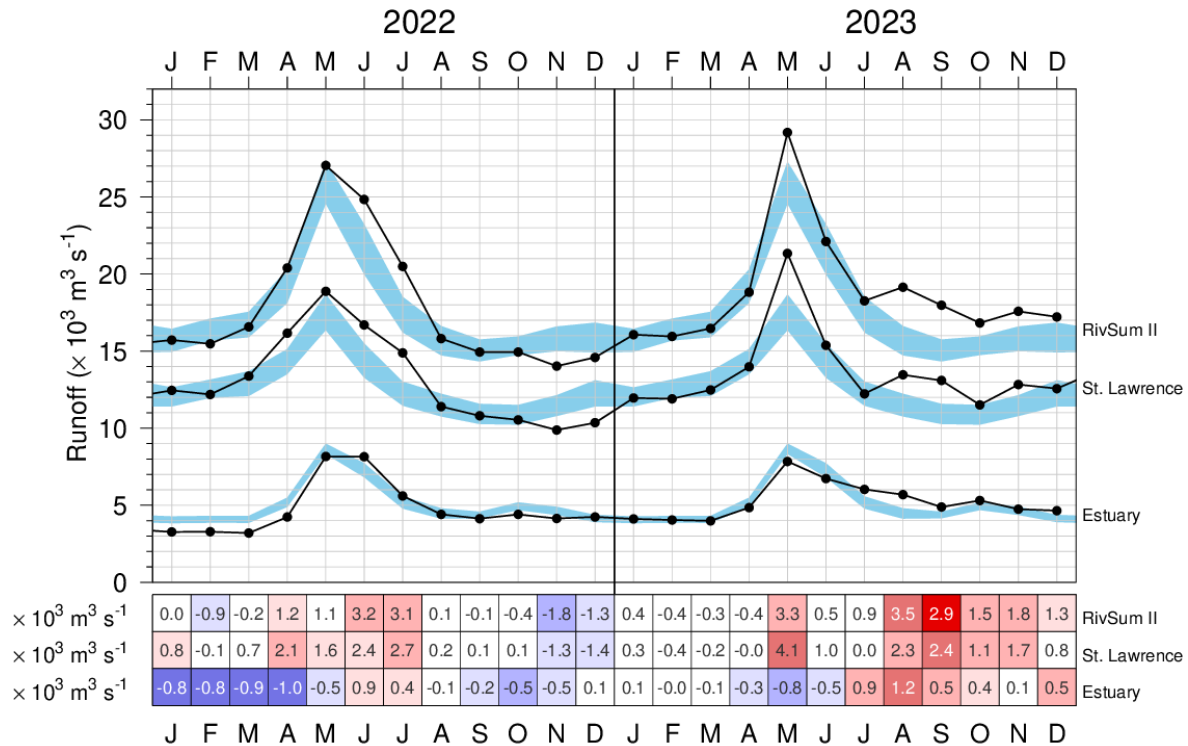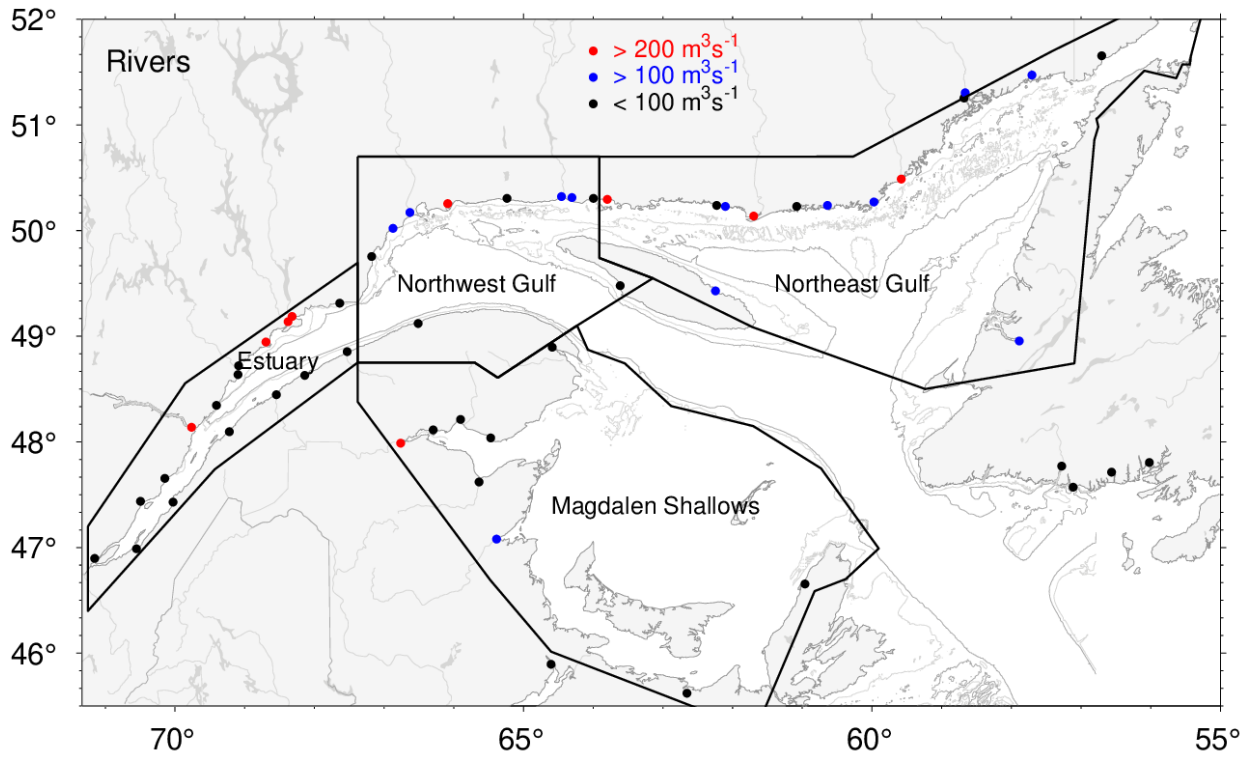Fig. 8. River discharge locations for the regional sums of runoffs listed in Fig. 9 and Fig. 10. Red and blue dots indicate rivers that have climatological mean runoff greater than 200 m³s⁻¹ and between 100 and 200 m³s⁻¹, respectively.

	J	F	M	A	M	J	J	A	S	O	N	D	J	F	M	A	M	J	J	A	S	O	N	D	
RIVSUM II	15718	15469	16570	20400	27040	24834	20494	15810	14936	14942	14023	14591	16067	15950	16469	18822	29182	22102	18261	19147	17972	16824	17575	17221	17555 m³ s⁻¹
St. Lawrence River	12453	12187	13374	16168	18880	16689	14889	11401	10804	10539	9883	10348	11956	11907	12480	13977	21338	15375	12230	13461	13091	11513	12828	12569	12746 m³ s⁻¹
Estuary	3265	3282	3196	4232	8160	8145	5605	4409	4132	4403	4140	4243	4111	4043	3989	4845	7844	6727	6031	5686	4881	5311	4747	4652	5090 m³ s⁻¹
Northwest Gulf	48	15	60	596	2473	4424	2420	905	1192	812	425	624	268	83	165	511	1835	3387	2802	2346	1678	1048	572	635	1177 m³ s⁻¹
Northeast Gulf	704	363	279	1071	4260	8984	6288	2172	1452	705	702	1423	938	369	274	769	3340	6034	3580	3512	3678	2544	1879	1692	2228 m³ s⁻¹
Magdalen Shallows	513	563	601	1410	2131	829	259	268	323	189	671	1244	953	375	286	971	1879	1194	886	1144	957	756	767	788	735 m³ s⁻¹

2022	2023

Fig. 9. Monthly anomalies of the RIVSUM II, the 21-day lagged St. Lawrence River runoff and sums of all other major rivers draining into separate Gulf regions for 2022 and 2023 as delimited in Fig. 8. The scorecards are colour-coded according to the monthly normalized anomalies based on the 1991–2020 climatologies for each month, but the numbers are the monthly average runoffs in m³ s⁻¹. Numbers on the right side are annual climatological means. Runoff regulation is simulated for three rivers that flow into the Estuary (Saguenay, Manicouagan, Outardes).

Fig. 10. Annual mean freshwater runoff. (Top panel) Sum of all rivers flowing into the Estuary, the St. Lawrence River at Québec City and their sum, the RIVSUM II. (Bottom panel) Sums of all rivers flowing into three regions of the Gulf. The 1991–2020 climatological means are shown as horizontal lines and indicated on the right side of the scorecards. Numbers in scorecards are normalized anomalies.
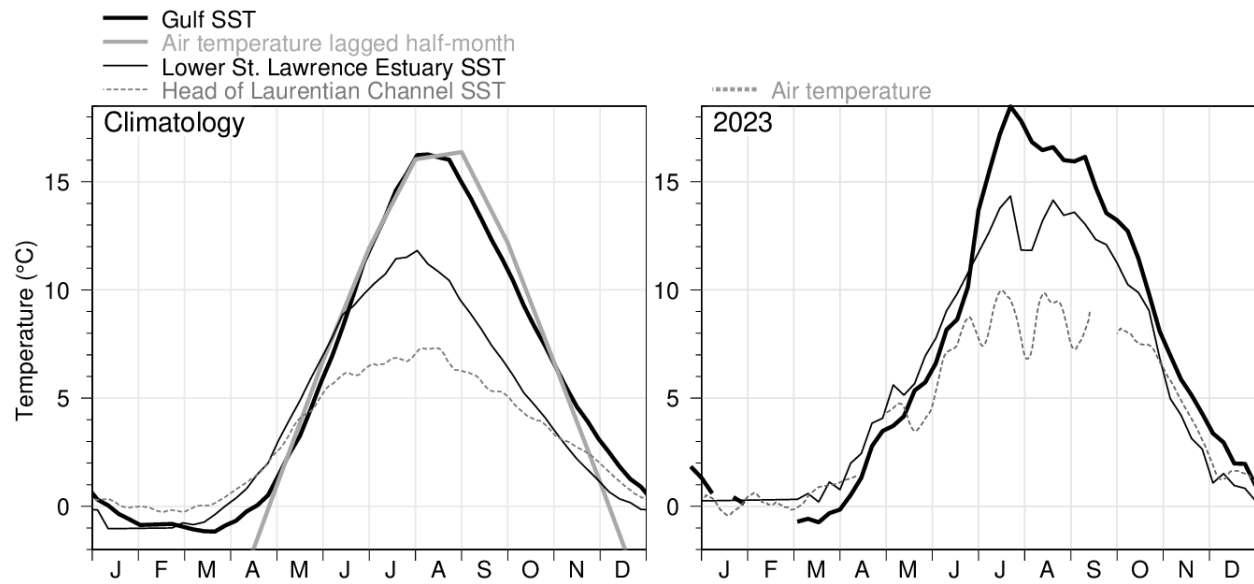
Fig. 11. Sea-surface temperature climatological (1991-2020) and 2023 seasonal cycle in the Gulf of St. Lawrence. AVHRR temperature weekly averages are shown for the Gulf (thick black line) and the cooler Lower St. Lawrence Estuary (thin black line). Thermosalinograph data averages are shown for the head of the Laurentian Channel (at 69°30'W, thin grey dashed line). Monthly air temperature averaged over stations in the Gulf of St. Lawrence (excluding the Estuary) are shown offset by 2 weeks into the future (thick grey line; winter months not shown) and also not offset in the annual panel (thick grey dashed line). Figure adapted from Galbraith et al. (2012).
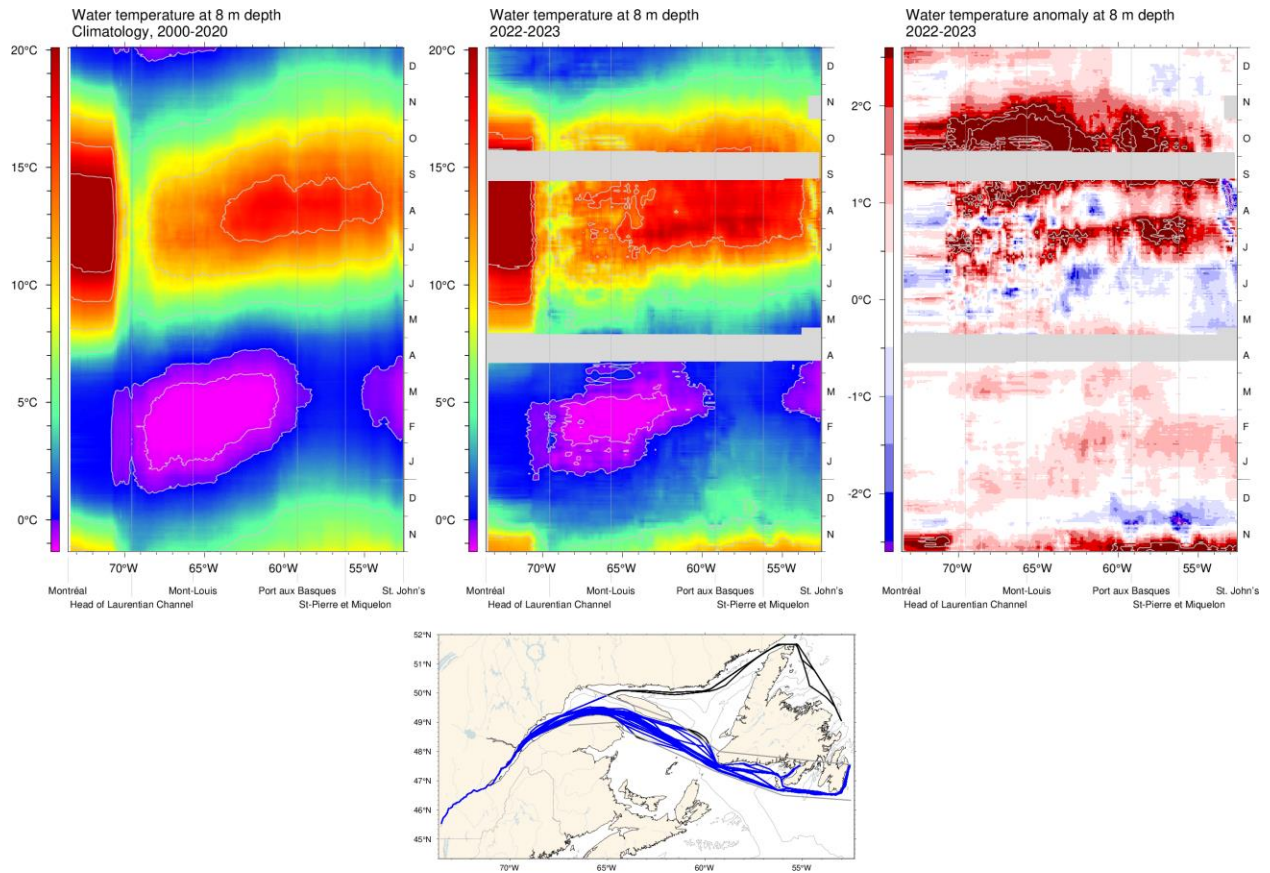
Fig. 12. Hovmöller diagram of thermosalinograph data at 8 m depth along the Montréal to St. John's shipping route: composite mean annual cycle of the water temperature for the 2000–2020 period (top left panel), composite annual cycle of the water temperature for the end of 2022 and 2023 (top middle panel), and water temperature anomaly relative to the 2000–2020 composite (top right panel). The map indicates all ship tracks in 2023, with those in blue used in the analysis.

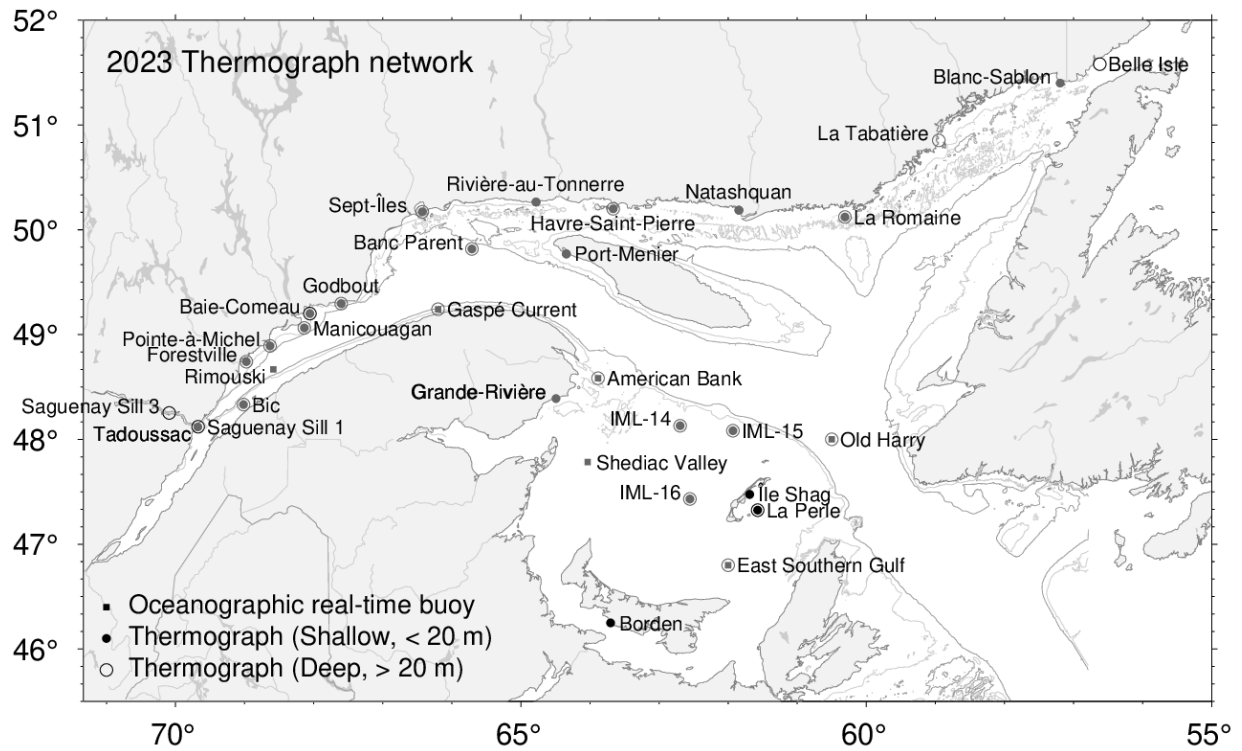Fig. 13. Maurice Lamontagne Institute thermograph network stations in 2023, including oceanographic buoys that transmit data in real time (squares). Deep and shallow instruments are denoted by open circles and dots, while seasonal and year-round deployments are denoted by grey and black symbols. Belle Isle station includes an upward-looking current profiler (ADCP) to estimate transports through the Strait.
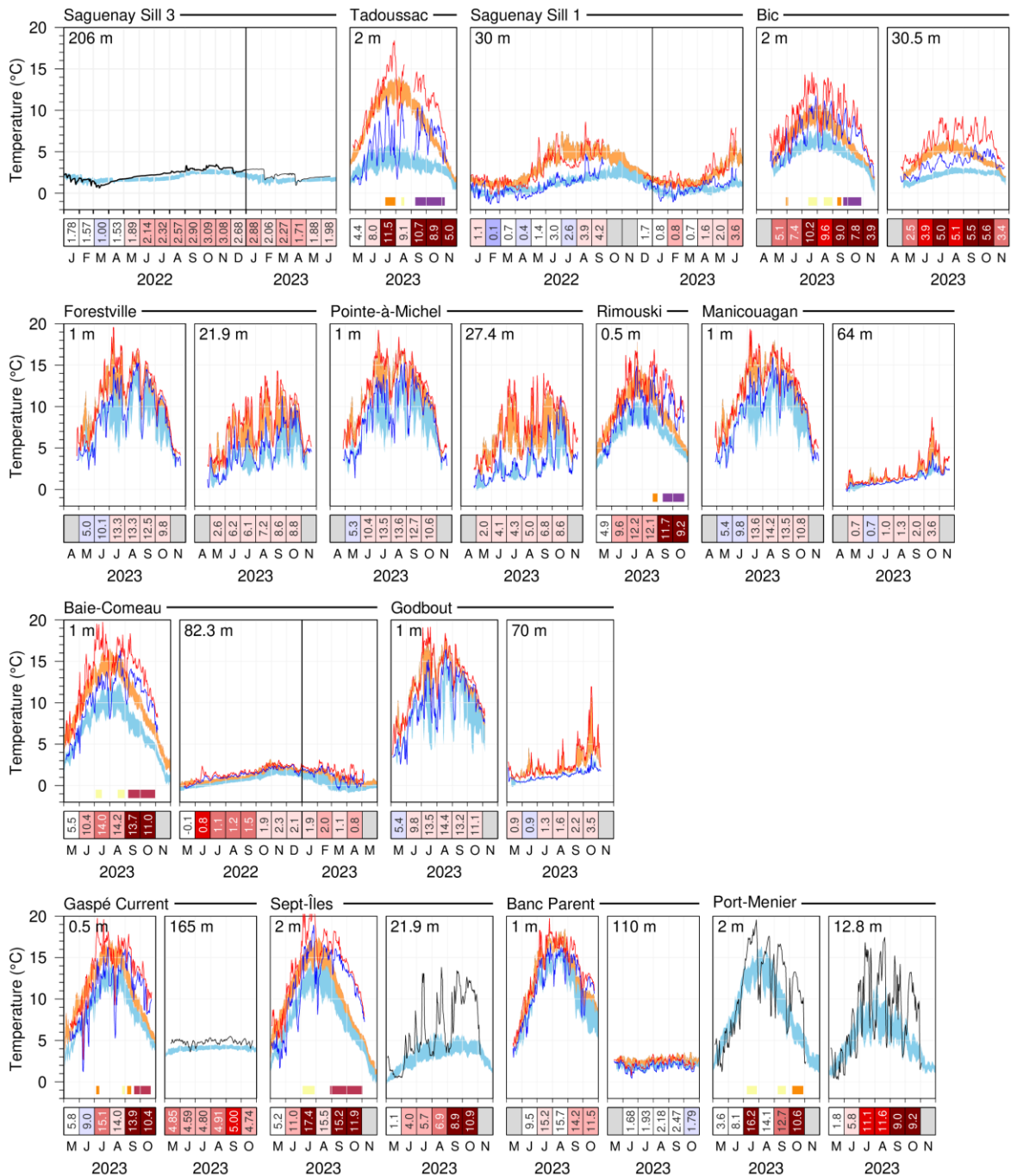
Estuary and NW Gulf / Estuaire et NO du Golfe

Fig. 14. Thermograph network daily mean temperatures (black line) compared with the daily climatology (blue areas are daily climatological averages ± 0.5 SD) for stations in the Estuary and northwestern Gulf. Stations that exhibit large tidal variations are displayed showing daily minimum (blue) and maximum (red) values, overlying daily climatological averages ± 0.5 SD of the minimum (blue shaded area) and maximum (orange shaded areas) values. Data from 2022 are included for stations collecting data year-round. The scorecards show monthly average temperatures in ºC colour-coded according to the monthly normalized anomalies based on the climatologies for each month. Stations without scorecards are new and have no climatology. Periods of marine heatwave conditions are shown by yellow (moderate), orange (strong), burgundy (severe) or purple (extreme) rectangular patches.
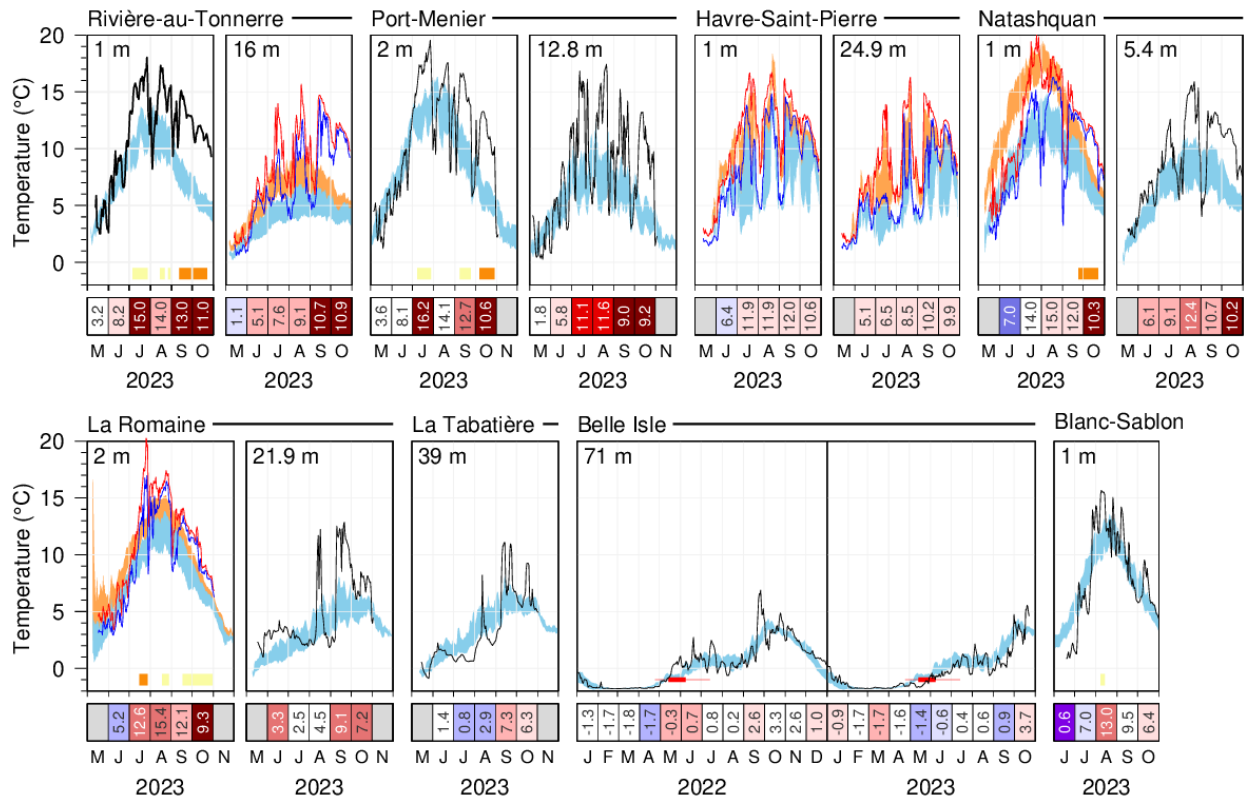
38

Fig. 15. Thermograph network data. Daily mean temperatures in 2023 (black line) compared with the daily climatology (blue areas are daily climatological averages ± 0.5 SD) for stations of the lower north shore. Stations that exhibit large tidal variations are displayed showing daily minimum (blue) and maximum (red) values, overlying daily climatological averages ± 0.5 SD of the minimum (blue shaded area) and maximum (orange shaded areas) values. Data from 2022 are included for stations collecting data year-round. Thin red lines in the Belle Isle panel span the historical dates when spring temperature increased over -1 °C, a temperature associated with inflow of winter Labrador Shelf Water into the Gulf. Thick red line indicates mean date plus and minus 0.5 SD. The scorecards show monthly average temperatures in °C colour-coded according to the normalized anomalies based on the climatologies for each month. Stations without scorecards are new and have no climatology. Periods of marine heatwave conditions are shown by yellow (moderate), orange (strong), burgundy (severe) or purple (extreme) rectangular patches.

Southern Gulf / Sud du Golfe

Fig. 16. Thermograph network data. Daily mean 2023 temperatures compared with the daily climatology (daily averages ± 0.5 SD; blue area) for stations of the southern Gulf. Data from 2022 are included for stations collecting data year-round. Thin red lines in the Île Shag panel span the historical dates when spring temperature increased over 1.5 °C, a temperature associated with increased lobster mobility. Thick red line indicates mean date plus and minus 0.5 SD. Stations without scorecards are new and have no climatology. Periods of marine heatwave conditions are shown by yellow (moderate), orange (strong), burgundy (severe) or purple (extreme) rectangular patches.
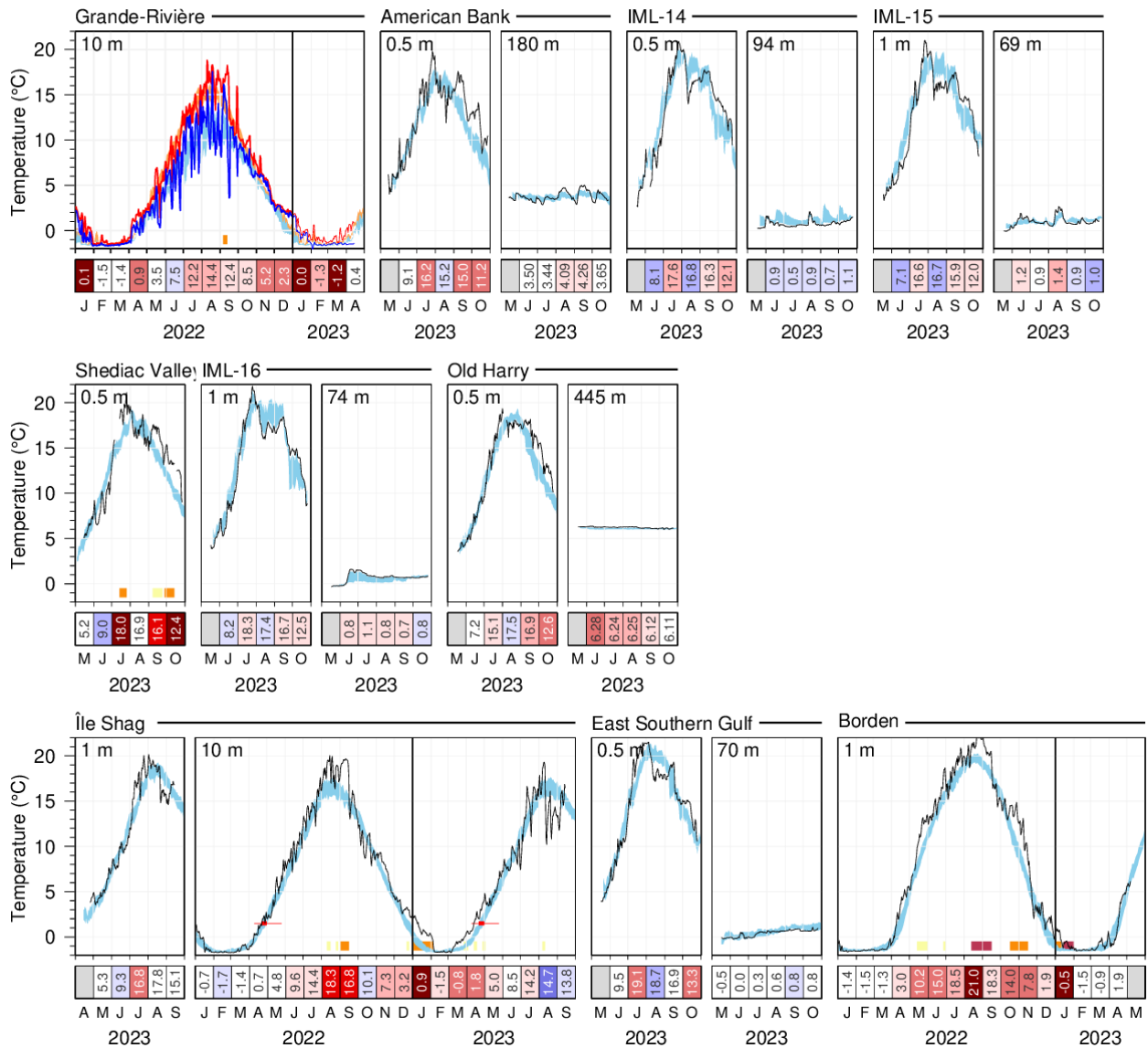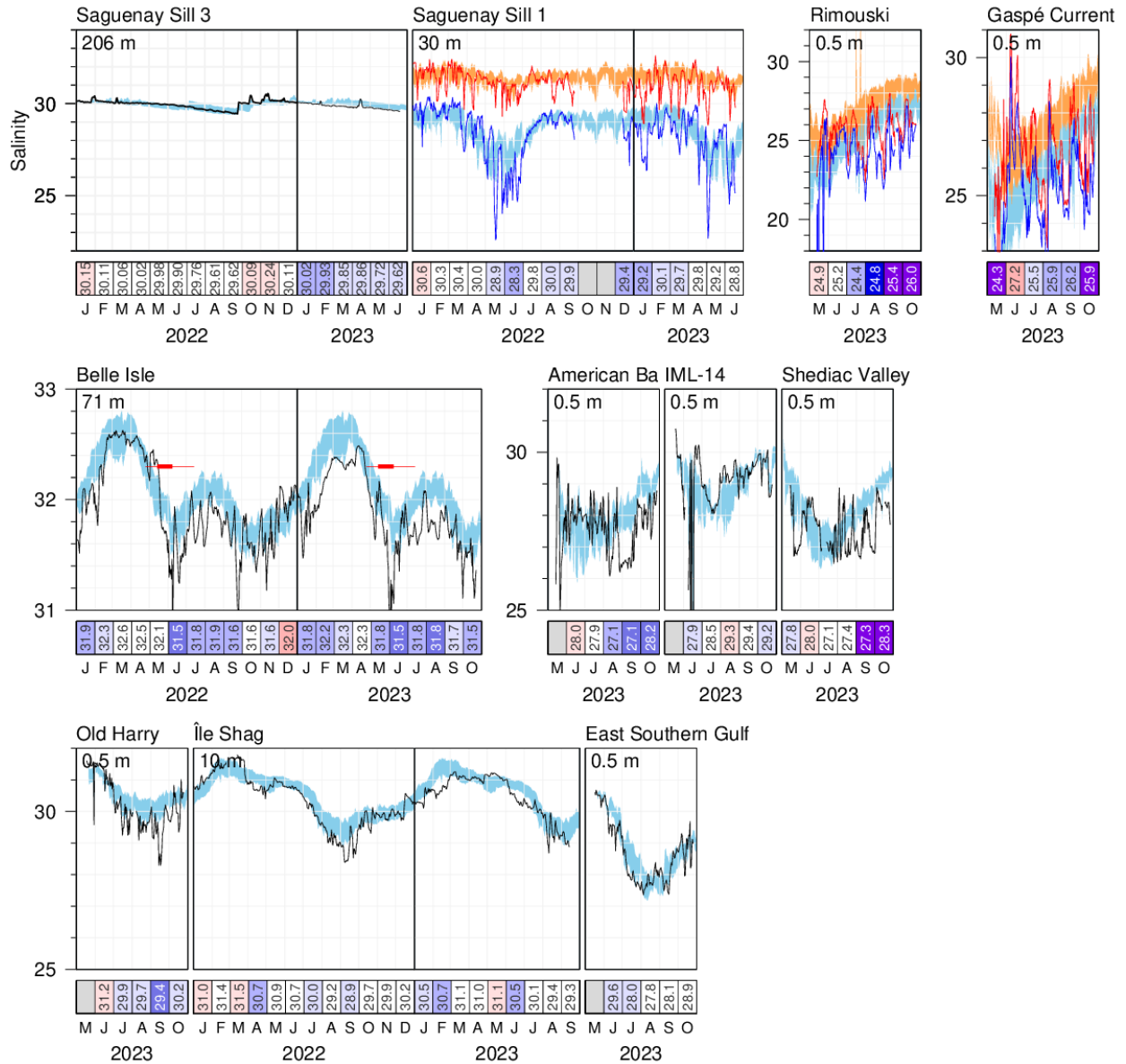
Fig. 17. Thermograph network data. Daily mean 2023 salinities (black lines) compared with the daily climatology (daily averages ± 0.5 SD; blue area) computed from all available stations. Stations that exhibit large tidal variations are displayed showing daily minimum (blue) and maximum (red) values, overlying daily climatological averages ± 0.5 SD of the minimum (blue shaded area) and maximum (orange shaded areas) values. Data from 2022 are included for stations collecting data year-round. The scorecards show monthly average salinities colour-coded according to the normalized anomalies based on the climatologies for each month.

41

Fig. 18. Sea-surface temperature monthly averages for 2023 as observed with AVHRR remote sensing. Grey areas have no data for the period due to ice cover or clouds.
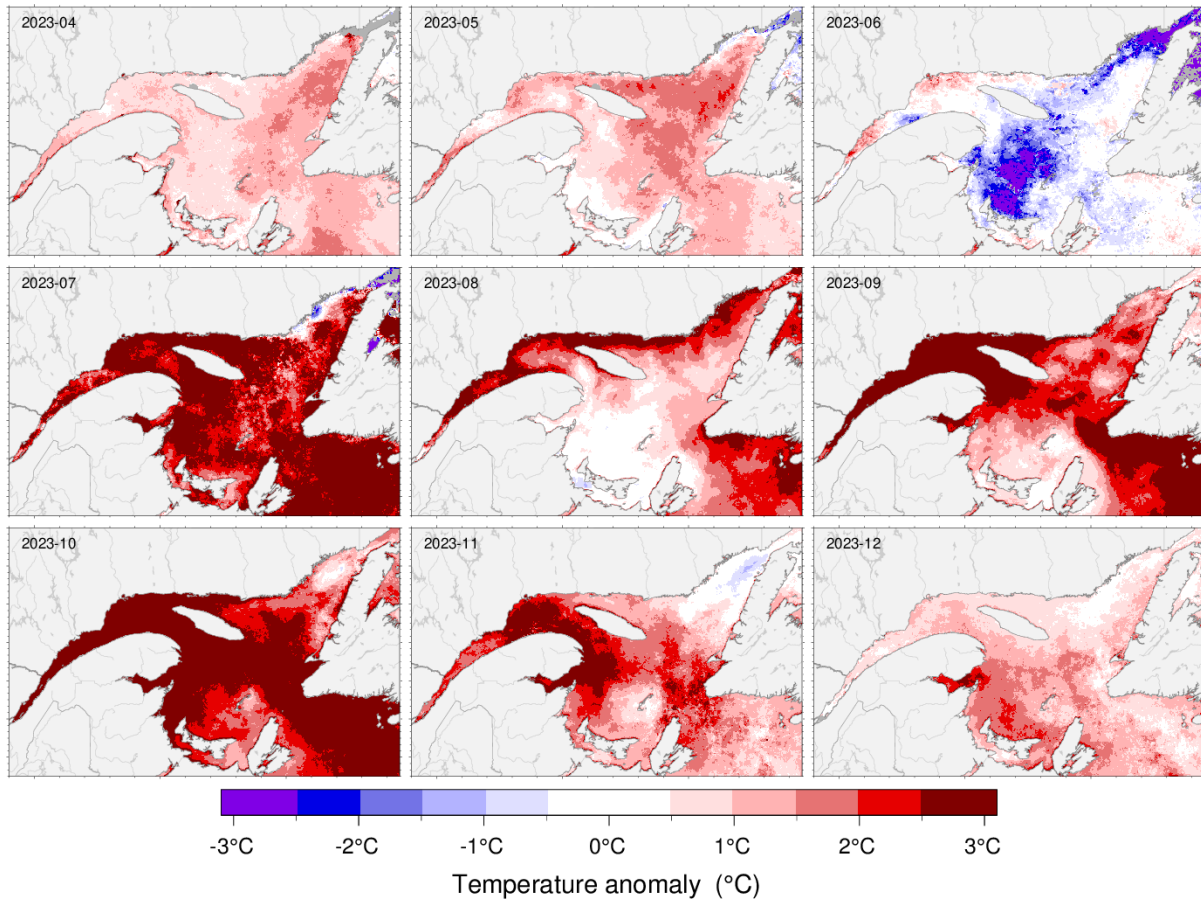
Fig. 19. Sea-surface temperature monthly anomalies for April-December 2023 based on monthly climatologies calculated for the 1985–2010 period observed with AVHRR remote sensing. This is the only product in this report that has not been updated to a 1991–2020 climatology.

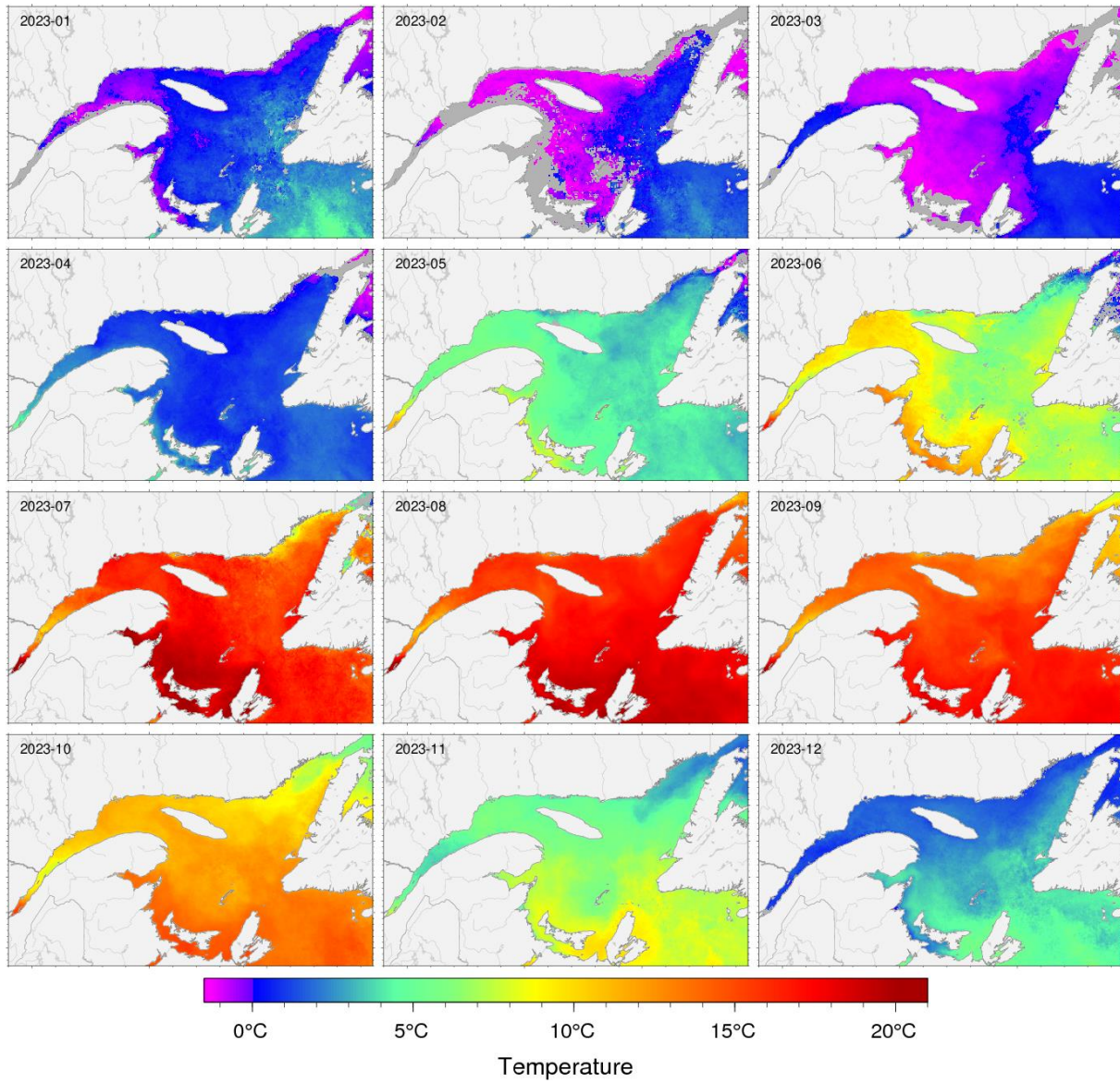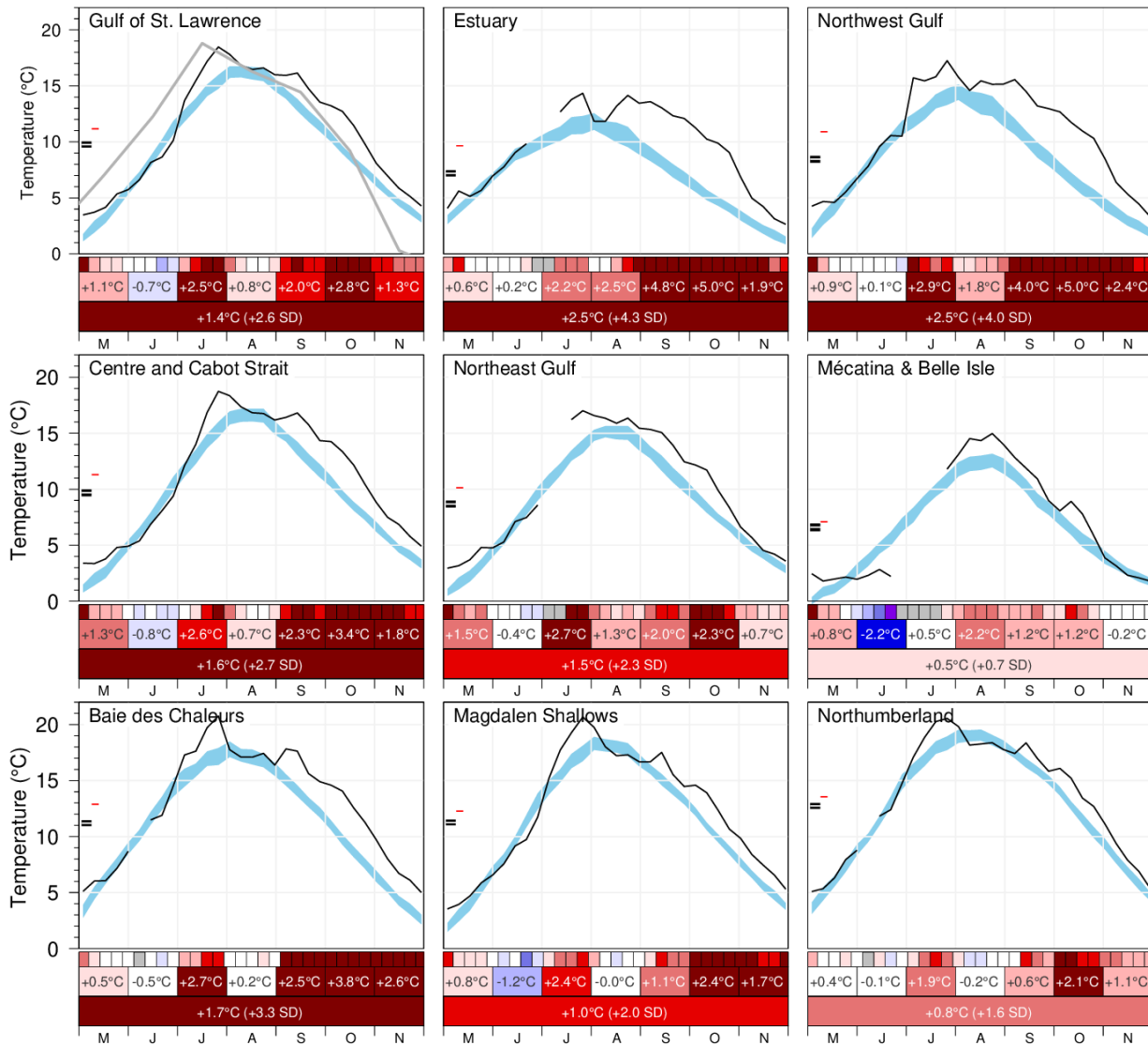Fig. 20. AVHRR SST May to November 2023 weekly, monthly and seasonal averages over the Gulf and over eight regions of the Gulf. The blue area represents the 1991–2020 climatological weekly mean ± 0.5 SD. The climatological average plus and minus half the standard deviation of the seasonal mean temperature are indicated by the black double bars on the left side of panels, while the year's seasonal mean is indicated by the red line. For anomalies greater than 2 SD from normal, the prior year with a greater anomaly is indicated, with the less-than symbol (<) indicating a series record since that first year of observations. The thick grey line in the Gulf panel is the monthly average air temperature (Fig. 4). The scorecards are colour-coded according to the normalized anomalies based on the 1991–2020 climatologies for each week (top row), month (middle row) or for the May-November period (bottom row), but the monthly numbers are average temperature anomalies.

44

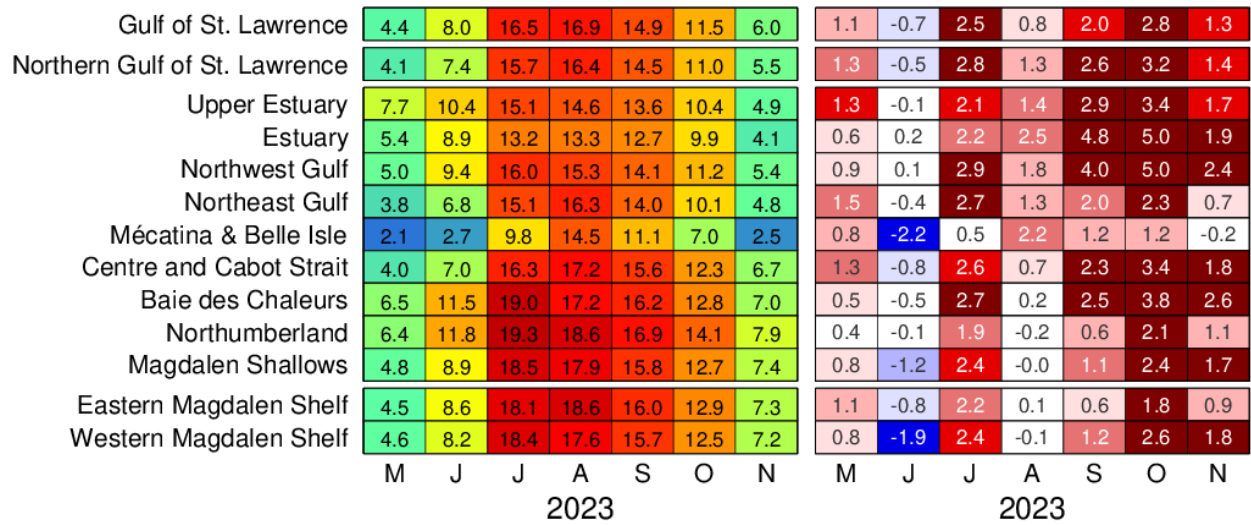|	M	J	J	A	S	O	N		M	J	J	A	S	O	N
Gulf of St. Lawrence	4.4	8.0	16.5	16.9	14.9	11.5	6.0		1.1	-0.7	2.5	0.8	2.0	2.8	1.3
Northern Gulf of St. Lawrence	4.1	7.4	15.7	16.4	14.5	11.0	5.5		1.3	-0.5	2.8	1.3	2.6	3.2	1.4
Upper Estuary	7.7	10.4	15.1	14.6	13.6	10.4	4.9		1.3	-0.1	2.1	1.4	2.9	3.4	1.7
Estuary	5.4	8.9	13.2	13.3	12.7	9.9	4.1		0.6	0.2	2.2	2.5	4.8	5.0	1.9
Northwest Gulf	5.0	9.4	16.0	15.3	14.1	11.2	5.4		0.9	0.1	2.9	1.8	4.0	5.0	2.4
Northeast Gulf	3.8	6.8	15.1	16.3	14.0	10.1	4.8		1.5	-0.4	2.7	1.3	2.0	2.3	0.7
Mécatina & Belle Isle	2.1	2.7	9.8	14.5	11.1	7.0	2.5		0.8	-2.2	0.5	2.2	1.2	1.2	-0.2
Centre and Cabot Strait	4.0	7.0	16.3	17.2	15.6	12.3	6.7		1.3	-0.8	2.6	0.7	2.3	3.4	1.8
Baie des Chaleurs	6.5	11.5	19.0	17.2	16.2	12.8	7.0		0.5	-0.5	2.7	0.2	2.5	3.8	2.6
Northumberland	6.4	11.8	19.3	18.6	16.9	14.1	7.9		0.4	-0.1	1.9	-0.2	0.6	2.1	1.1
Magdalen Shallows	4.8	8.9	18.5	17.9	15.8	12.7	7.4		0.8	-1.2	2.4	-0.0	1.1	2.4	1.7
Eastern Magdalen Shelf	4.5	8.6	18.1	18.6	16.0	12.9	7.3		1.1	-0.8	2.2	0.1	0.6	1.8	0.9
Western Magdalen Shelf	4.6	8.2	18.4	17.6	15.7	12.5	7.2		0.8	-1.9	2.4	-0.1	1.2	2.6	1.8
	M	J	J	A	S	O	N		M	J	J	A	S	O	N
				2023								2023			

Fig. 21. AVHRR SST May to November monthly temperatures and anomalies, averaged over the Gulf and over regions of the Gulf for 2023. The numbers on the left-hand panel are area average temperatures and are colour-coded accordingly. The right-hand scorecards are colour-coded according to the monthly normalized anomalies based on the 1991–2020 climatologies for each month, but the numbers are the monthly average temperature anomalies expressed in °C. The northern Gulf of St. Lawrence region corresponds to northwest Gulf, northeast Gulf, Centre and Cabot Strait and is reported in the AZMP Science Advisory Report.
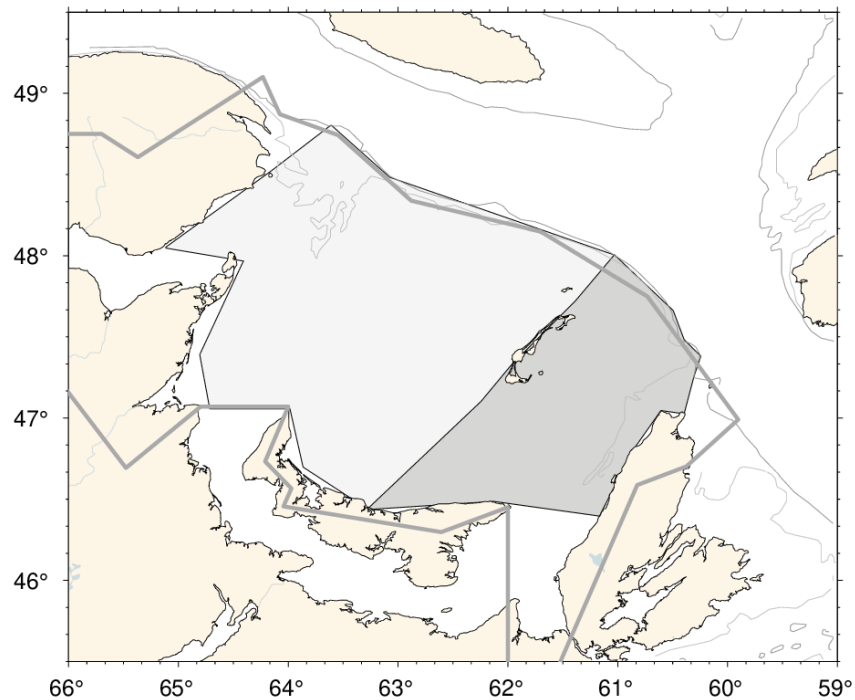

Fig. 22. Areas defined as the western and eastern Magdalen Shelf. The thick grey line shows the outline of the Ecosystem Approach region for the Magdalen Shallows (Fig. 2).

Fig. 23. AVHRR SST May to November monthly anomalies averaged over the Gulf of St. Lawrence and over selected regions of the Gulf. The scorecards are colour-coded according to the monthly normalized anomalies based on the 1991–2020 climatologies for each month, but the numbers are the monthly average temperatures in °C. The 1991–2020 mean and standard deviation are indicated for each month on the right side of the table. The May to November average is also included. Data for 1981 are not shown as they begin only in September.

Fig. 24. AVHRR SST May to November monthly anomalies averaged over other selected regions of the Gulf. The scorecards are colour-coded according to the monthly normalized anomalies based on the 1991–2020 climatologies for each month, but the numbers are the monthly average temperatures in °C. The 1991–2020 mean and standard deviation are indicated for each month on the right side of the table. The May to November average is also included. Data for 1981 are not shown as they begin only in September.
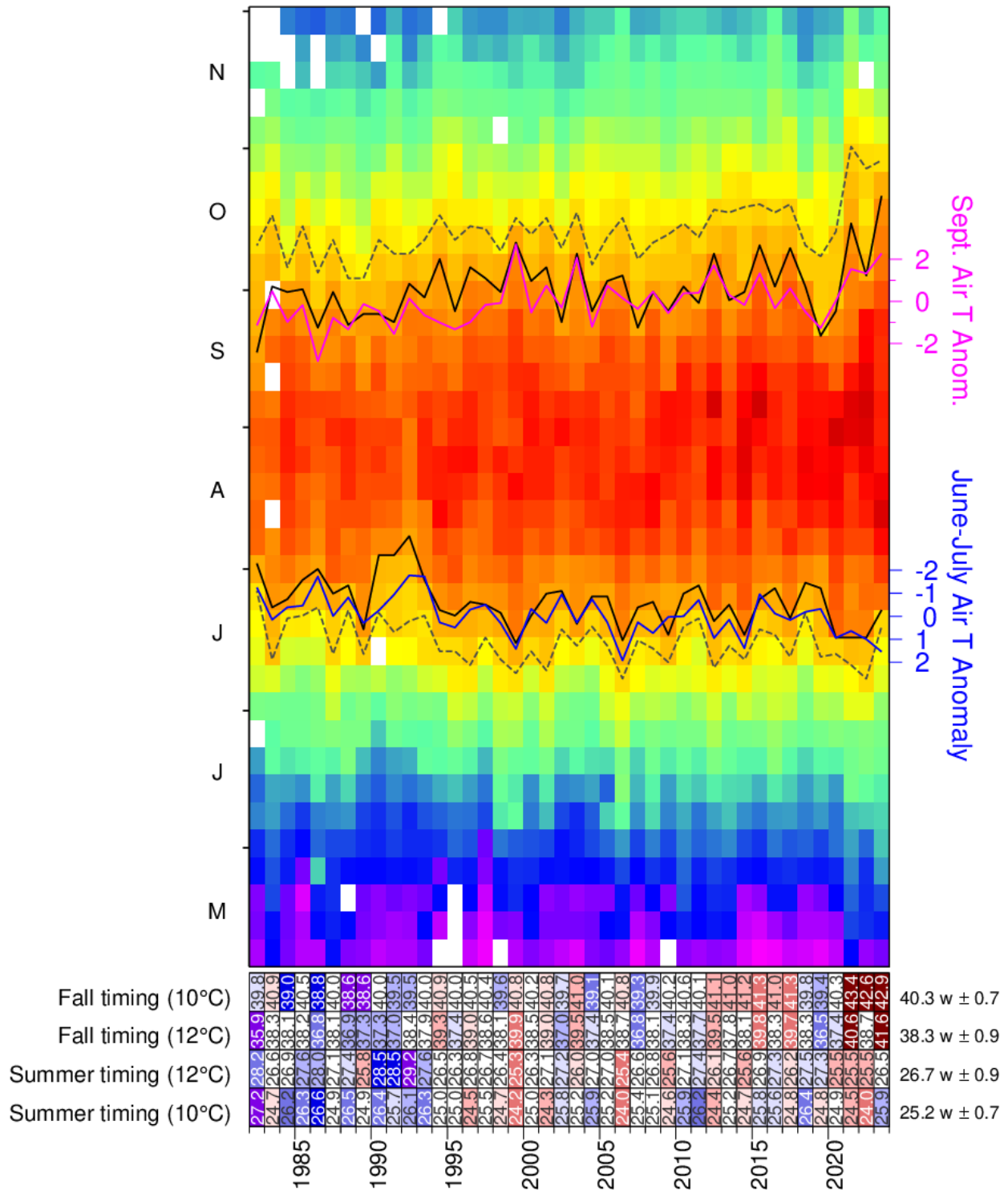
Fig. 25. Weekly average SST (1982–2023) matrix for the Gulf of St. Lawrence. Black lines show the first and last occurrence of the 12 °C isotherm and proxies based on June-July (blue line) and September (magenta) average air temperature anomalies are also shown (axes on right). Dashed gray lines show the first and last occurrence of the 10 °C isotherm. The scorecards are colour-coded according to the normalized anomalies based on the 1991–2020 time series, but the numbers are week numbers when the threshold was crossed. Updated from Galbraith and Larouche 2013.
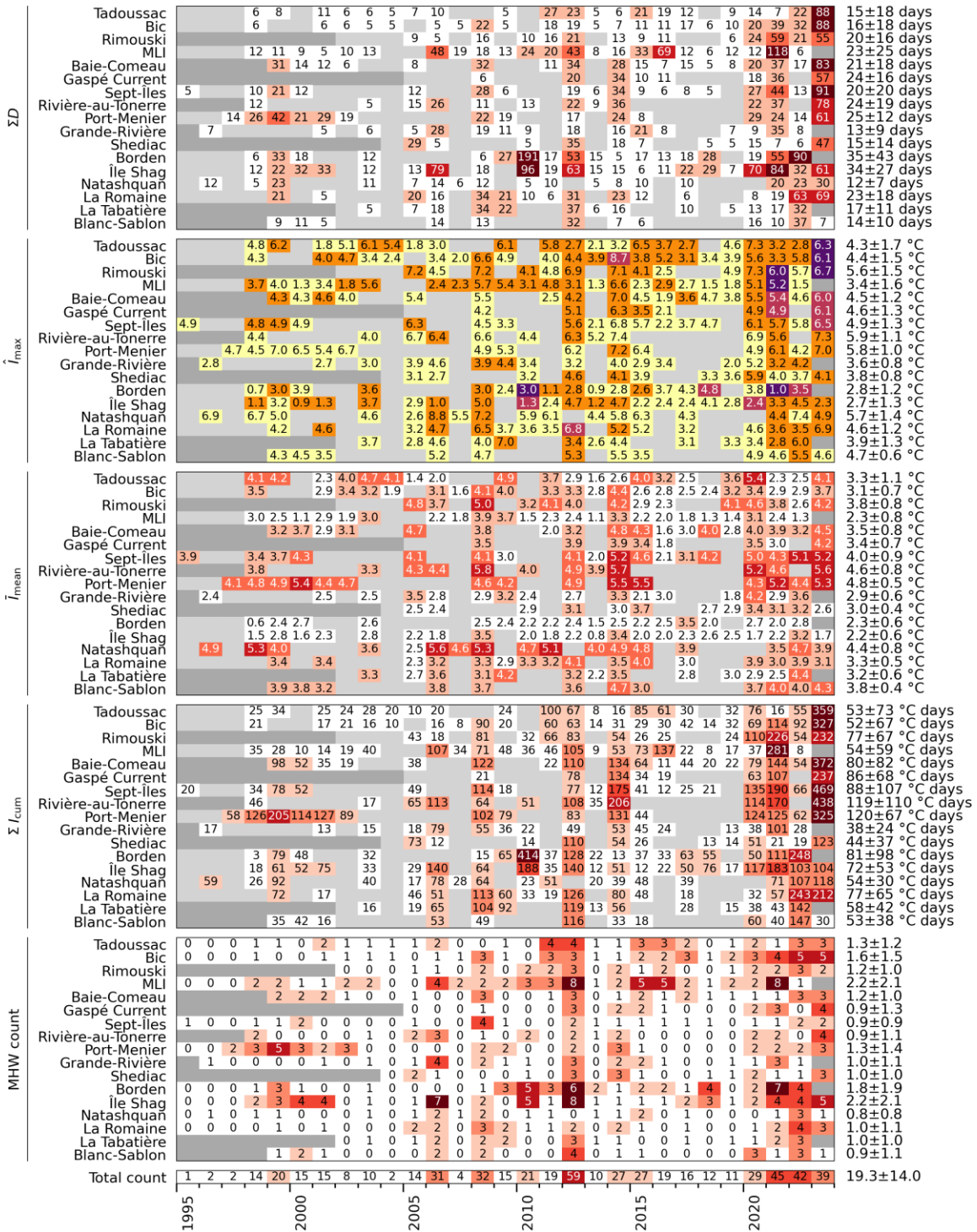
Fig. 26. Aggregated MHW metrics by station. From top to bottom are shown ΣD, Î$_{max}$, Ī$_{mean}$, ΣI$_{cum}$, and the number of MHW events. Boxes are colour-coded according to their values. To emphasize larger events, values up to the approximate mean of each panel (ΣD: 20 days, Ī$_{mean}$: 3 °C, ΣI$_{cum}$: 50 °C days, count: 2, total count: 20) are coloured white and shades of red darken with increasing values by approximately one standard deviation for each shade (ΣD: 20 days, Ī$_{mean}$: 1 °C, ΣI$_{cum}$: 50 °C days, count: 1, total count: 10). The Î$_{max}$ panel displays the metric's value and is colour-coded to the corresponding MHW category: yellow (moderate), orange (strong), burgundy (severe) or purple (extreme). The mean and standard deviation are shown to the right for each station. All results are based on daily thermograph network data.
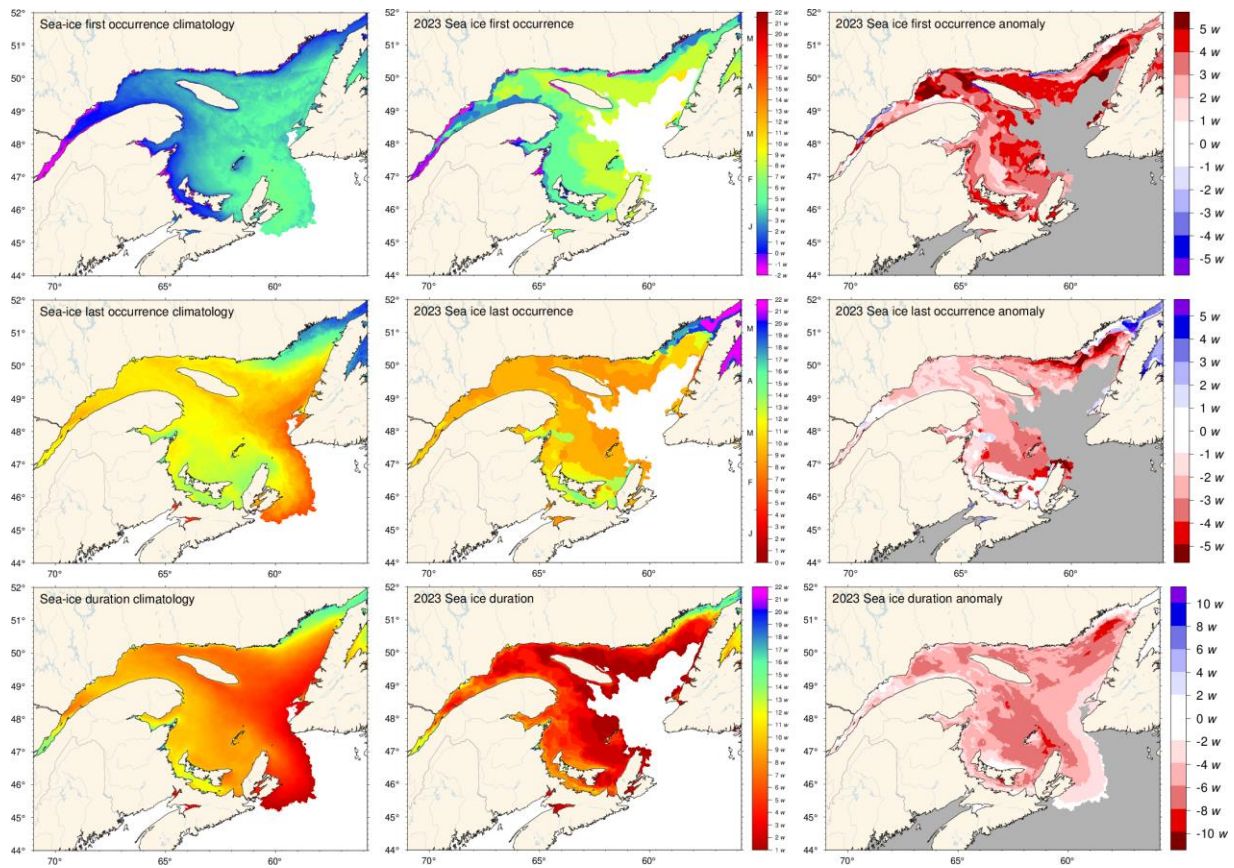
Fig. 27. First and last occurrence of ice and ice season duration based on weekly data. The 1991–2020 climatologies are shown (left) as well as the 2023 values (middle) and anomalies (right). First and last occurrence is defined here as the first and last weekly chart in which any amount of ice is recorded for each pixel and are illustrated as day-of-year. Ice duration sums the number of weeks with ice cover for each pixel. Climatologies are shown for pixels that had at least 15 years out of the 30 with occurrence of sea-ice, and therefore also show the area with 50% likelihood of having some sea-ice at any time during any given year.

50

Fig. 28. First and last day of ice occurrence, ice duration and maximum seasonal ice volume by region. The time when ice was first and last seen in days from the beginning of each year is indicated for each region, and the colour code expresses the anomaly based on the 1991–2020 climatology, with blue (cold) representing earlier first occurrence and later last occurrence. Negative numbers are in the previous year. The threshold to determine dates of first and last occurrence is 5% of the largest ice volume ever recorded in the region. Numbers in the table are the actual day of the year or volume, but the colour coding is according to normalized anomalies based on the climatology of each region. Duration is the number of days that the threshold was exceeded. All results based on weekly data.

51
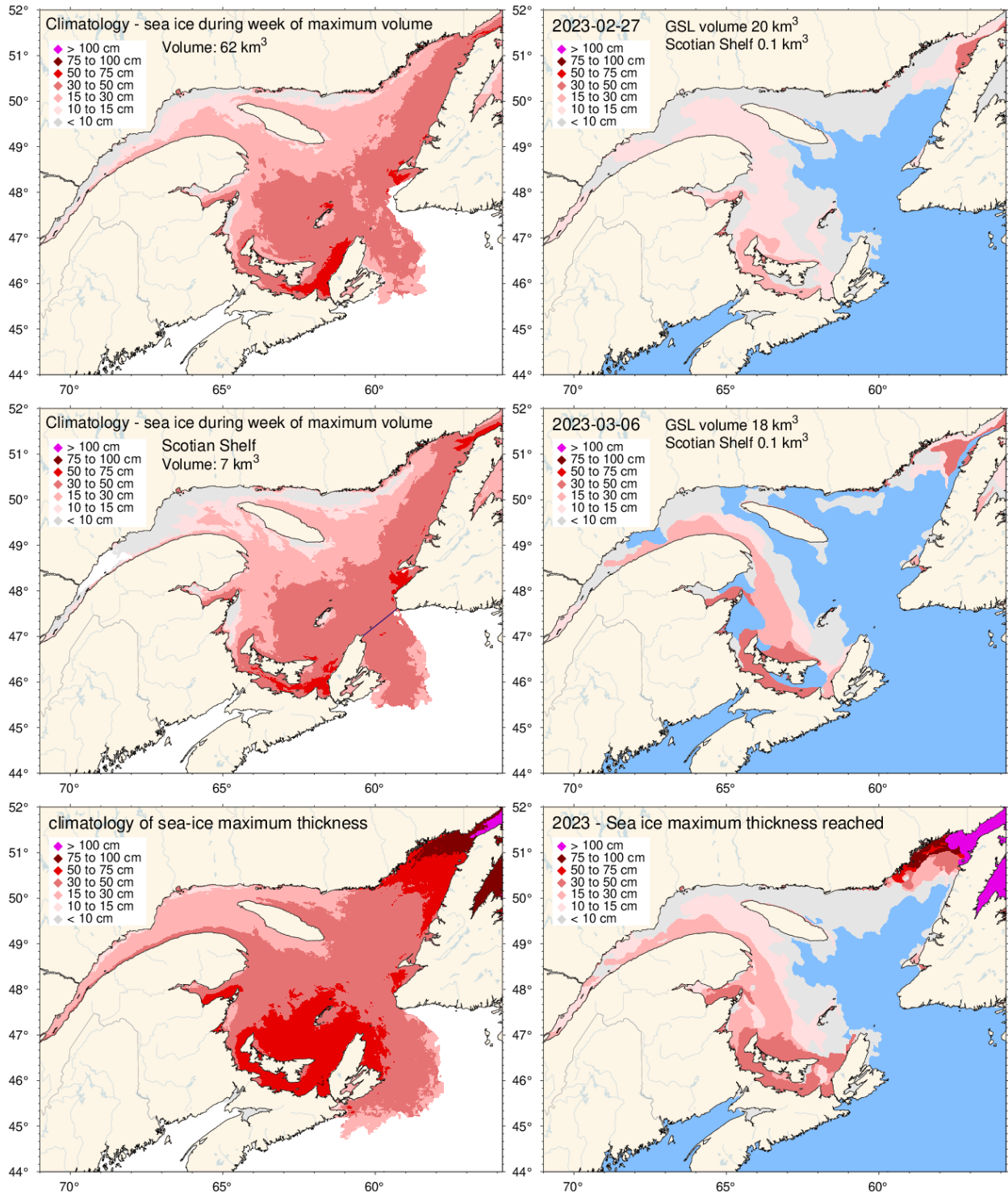
Fig. 29. Ice thickness maps for 2023 for the week of the year with the maximum volume including the portion covering the Scotian Shelf (upper right panel), with the maximum volume on the Scotian Shelf (middle right panel) and similarly for the 1991–2020 climatology of the weekly maximum (upper and middle left panels). Note that these maps reflect the ice thickness distribution on that week, and not the maximum observed at any given location during the year. That information is shown by the lower panels, showing the 1991–2020 climatology and 2023 distribution of the thickest ice recorded during the season at any location.
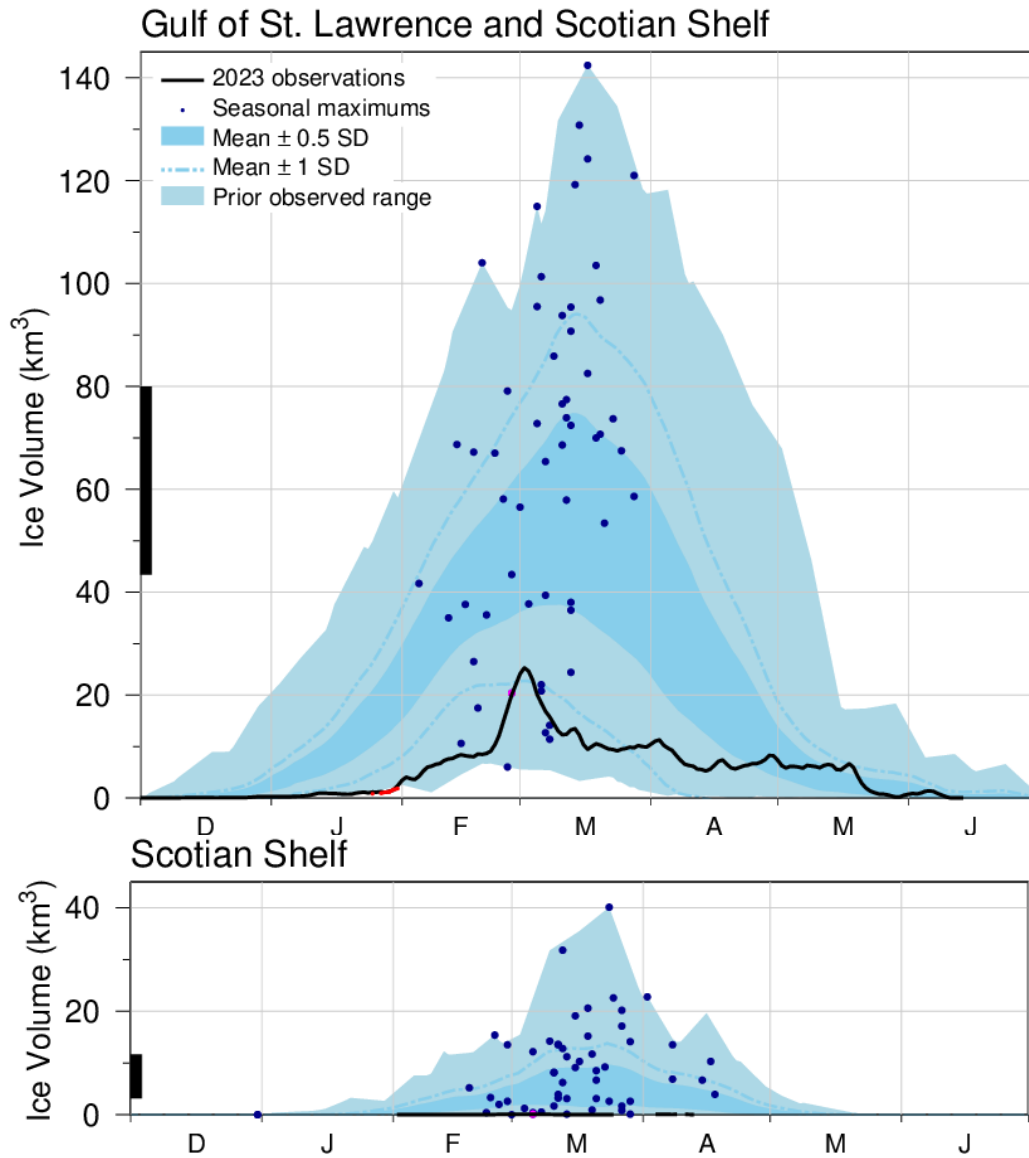
Fig. 30. Time series of the 2022–2023 daily mean ice volume for the Gulf of St. Lawrence and Scotian Shelf (top panel, black line) and for the Scotian Shelf (bottom panel, black line). Historical daily lows are shown in red. Also shown are the 1991–2020 climatological mean volume plus and minus 0.5 and 1 SD (dark blue area and dashed line), the minimum and maximum span of 1969–2022 observations (light blue) and the date and volumes of 1969–2022 seasonal weekly maxima (blue dots; 2023 weekly chart maximum shown in magenta). The black thick lines on the left indicates the mean volume plus and minus 0.5 SD of the annual maximum ice volume, which is higher than the peak of the mean daily ice volume distribution.
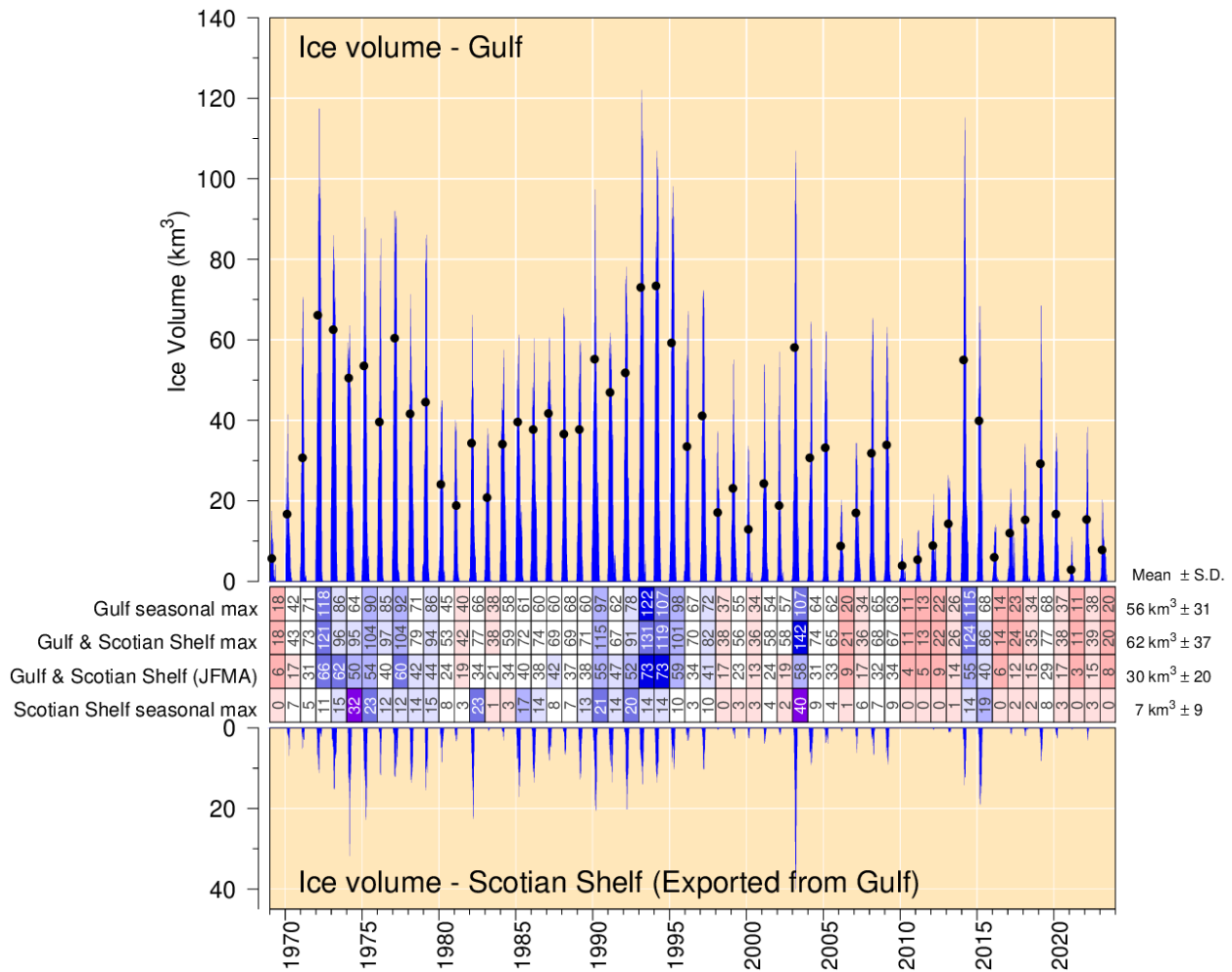
Fig. 31. Estimated weekly maximum ice volume in the Gulf of St. Lawrence (upper panel) and on the Scotian Shelf seaward of Cabot Strait defined by its narrowest crossing (lower panel). Dots show January-April averages of combined Gulf and Scotian Shelf volumes. Scorecards show Gulf seasonal maximums, combined Gulf and Shelf seasonal maximums, combined Gulf and Shelf January to April average, and Shelf-only annual maximum volumes, all from weekly ice data. The mean and standard deviation are indicated on the right side using the 1991–2020 climatology. The colour-coding are according to normalized anomalies based on the 1991–2020 climatologies, but the numbers are volumes in km^3.

54
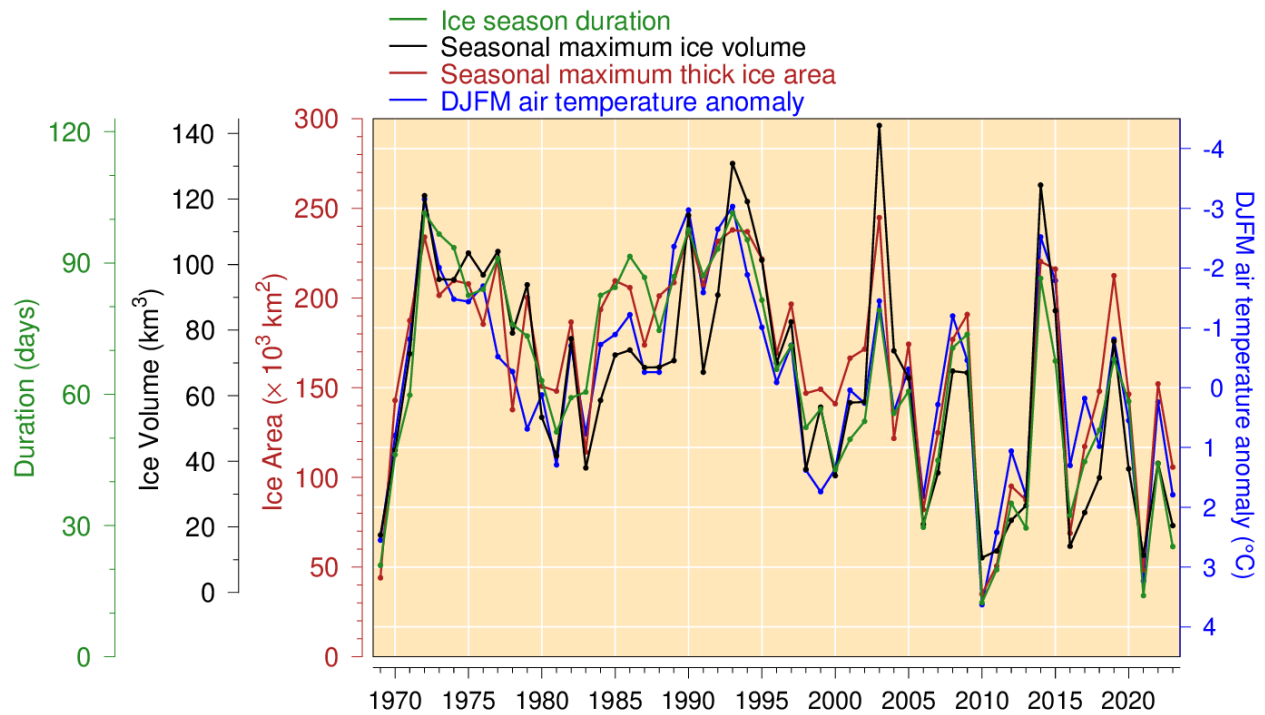
Fig. 32. Seasonal maximum ice volume and area including the portion on the Scotian Shelf (excluding ice less than 15 cm thick), ice season duration and December-to-March (DJFM) air temperature anomaly (Figure adapted from Hammill and Galbraith 2012, but here not excluding small floes and adding February and March data to the air temperature anomalies). All sea-ice products are based on weekly data. Mean duration obtained as spatial average of Fig. 27, excluding the Scotian Shelf, with zeros counted if no ice is present but the climatology has some. Linear relations indicate losses of 18 km³, 31 000 km² and 14 days of sea-ice season for each 1 °C increase in winter air temperature (R² of 0.75, 0.81 and 0.83 respectively).
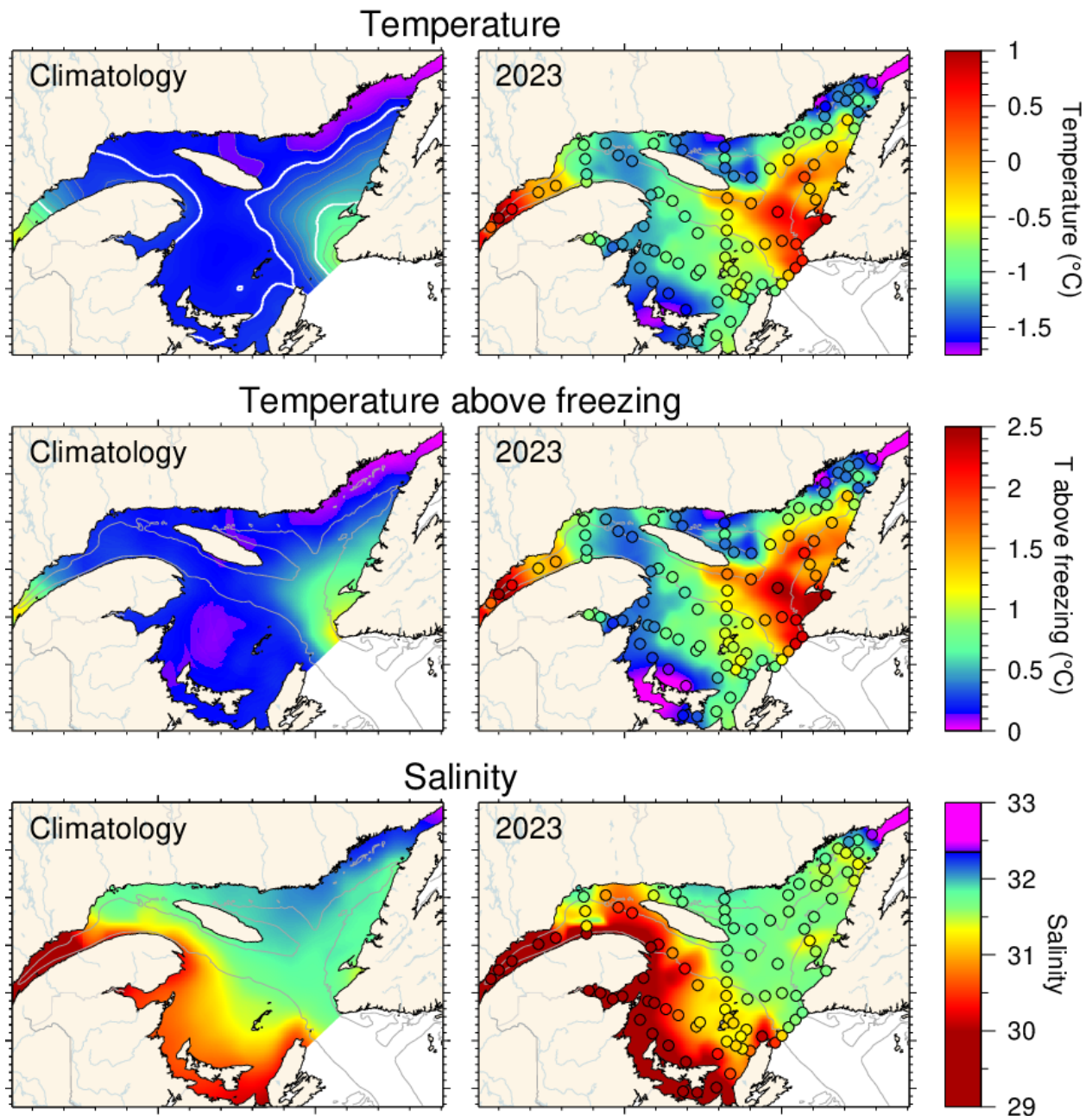
Fig. 33. Winter surface layer characteristics from the March 2023 survey compared with climatological means: surface water temperature (upper panel), temperature difference between surface water temperature and the freezing point (middle panel), and salinity (lower panel). Symbols are coloured according to the value observed at the station, using the same colour palette as the interpolated image. A good match is seen between the interpolation and the station observations where the station colours blend into the background. Black symbols indicate missing or bad data. The climatologies are based on 1996–2020 for salinity but exclude 2010 as an outlier for temperature and temperature above freezing. Near-freezing waters with salinity > 32.35 (indicated by the black line in the salinity colour palette) are considered to be too saline to have been formed from waters originating within the Gulf and are presumed to have been advected as an intrusion from the Labrador Shelf through the Strait of Belle Isle.
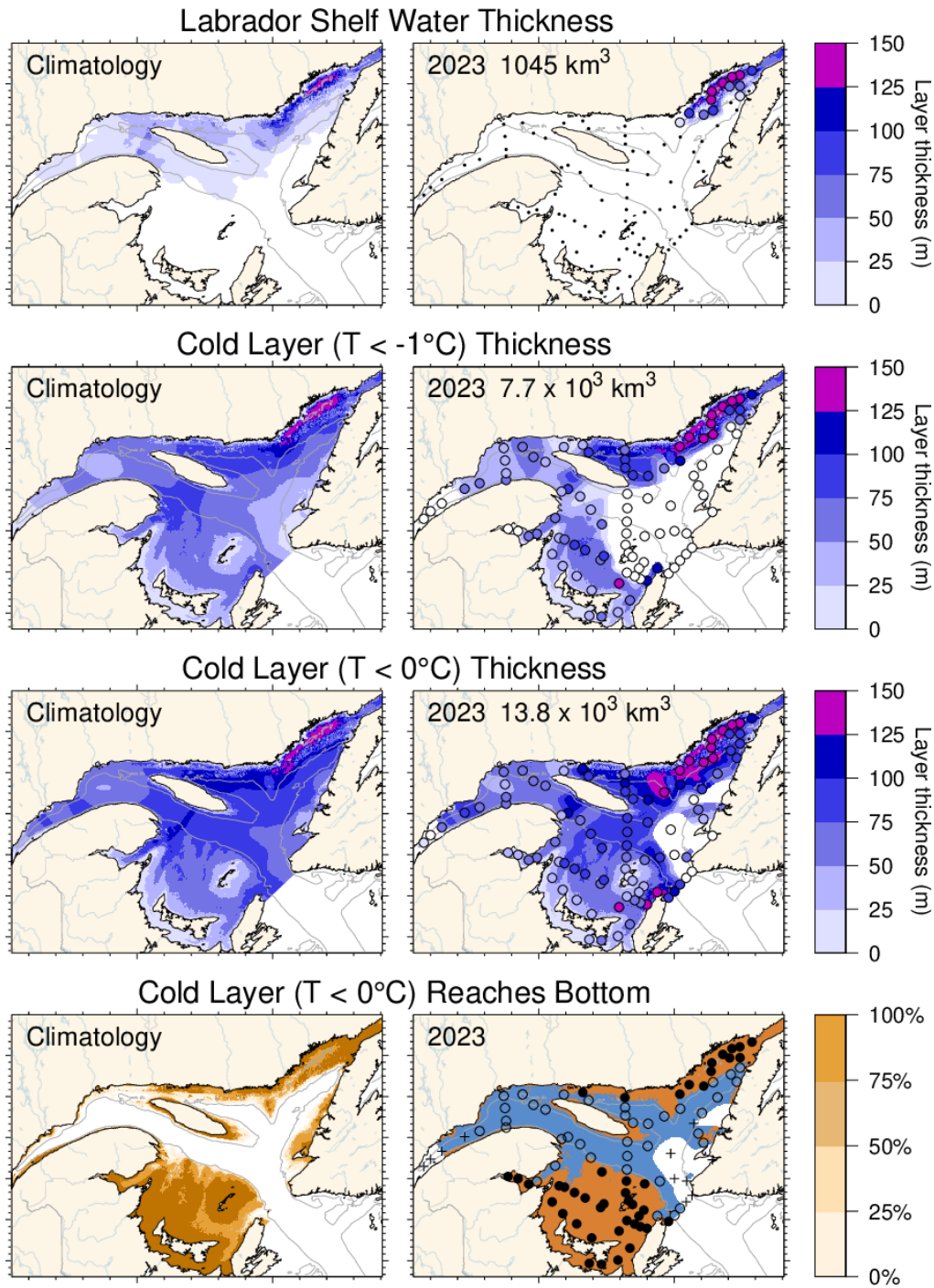
Fig. 34. Winter surface layer characteristics from the March 2023 survey compared with climatological means: estimates of the thickness of the Labrador Shelf water intrusion (upper panels), cold layer (T < -1 °C, T < 0 °C) thickness (middle panels), and maps indicating where the cold layer (T < 0 °C) reaches the bottom (in brown; lower panels). Station symbols are coloured according to the observed values as in Fig. 33. For the lower panels, the stations where the cold layer reached the bottom are indicated with filled circles while open circles represent stations where the layer did not reach the bottom. Crosses indicate no water present colder than the threshold of 0 °C. Integrated volumes are indicated for the first six panels (including an approximation for the Estuary but excluding the Strait of Belle Isle). The climatologies are based on 1997–2020 for the Labrador Shelf water intrusion, 1996–2020 for the cold layer (T < 0 °C) but excludes 2010 for T < -1 °C. The climatology of the cold layer reaching the bottom is expressed in classes of percentages.

57
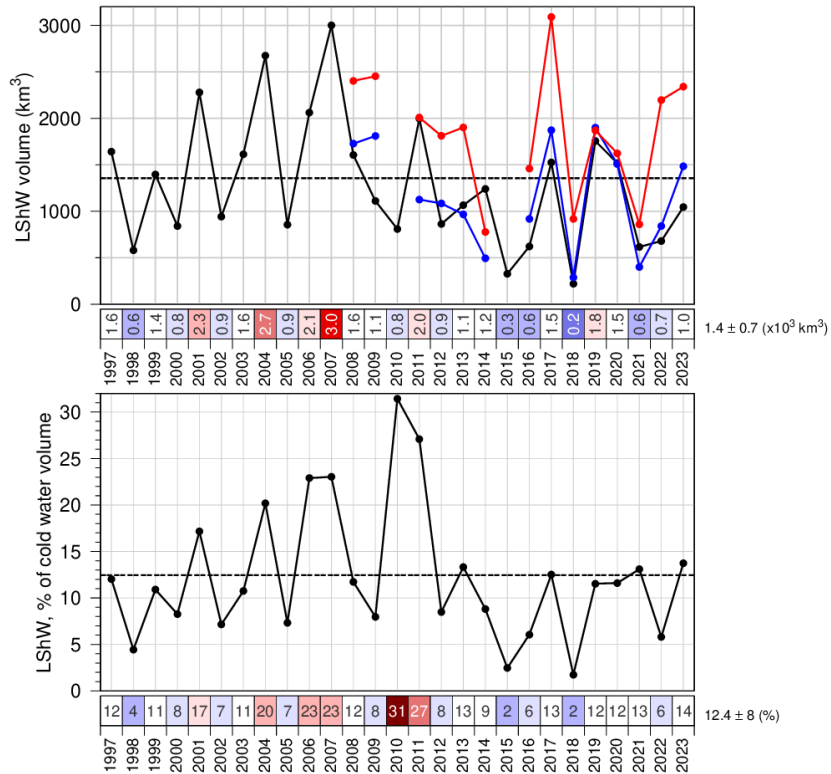
Fig. 35. Estimated volume of cold and saline Labrador Shelf water that flowed into the Gulf over the winter through the Strait of Belle Isle. The bottom panel shows the volume as a percentage of total cold-water volume (< -1ºC) of the entire Gulf. The numbers in the boxes are actual values colour-coded according to their 1997–2020 climatology anomaly. Coverage of Mecatina Trough was insufficient in 1996 to provide an estimated volume. The top panel also includes the volume integrated from estimated transport in the Strait of Belle Isle up to March 15th (blue) and up the end of the inflow in late spring (red), an update to Shaw & Galbraith 2023.
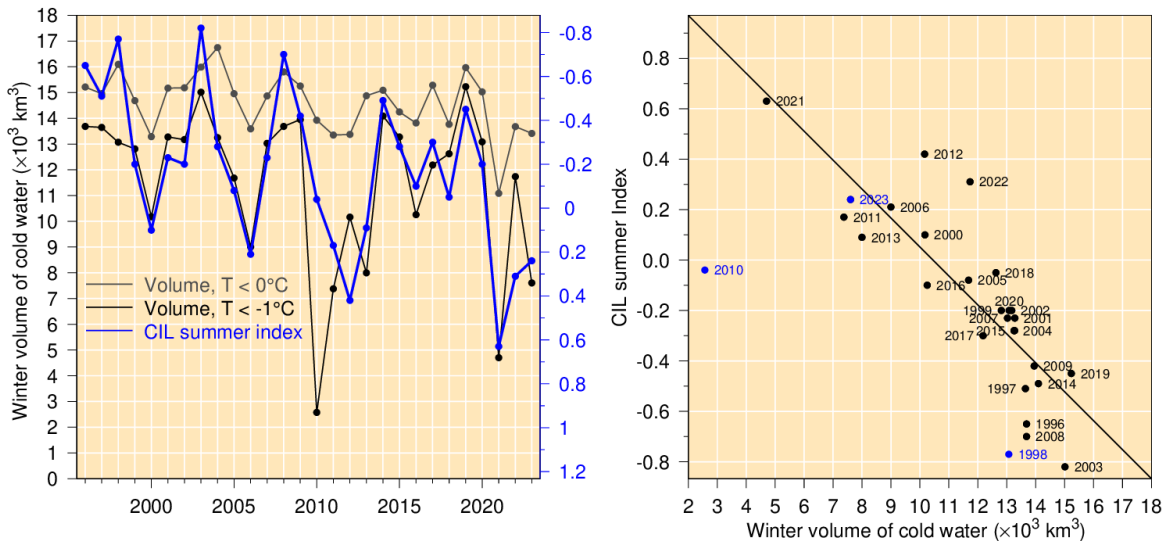
Fig. 36. Left panel: winter surface cold (T < -1 °C and T < 0 °C) layer volume (excluding the Estuary and the Strait of Belle Isle) time series (black and grey lines) and summer CIL index (blue line). Right panel: Relation between summer CIL index and winter cold-water volume with T < -1 °C (regression for 1996–2023 data pairs, excluding 1998 [see Galbraith 2006] and the 2010 mild winter). Note that the CIL scale in the left panel is reversed.
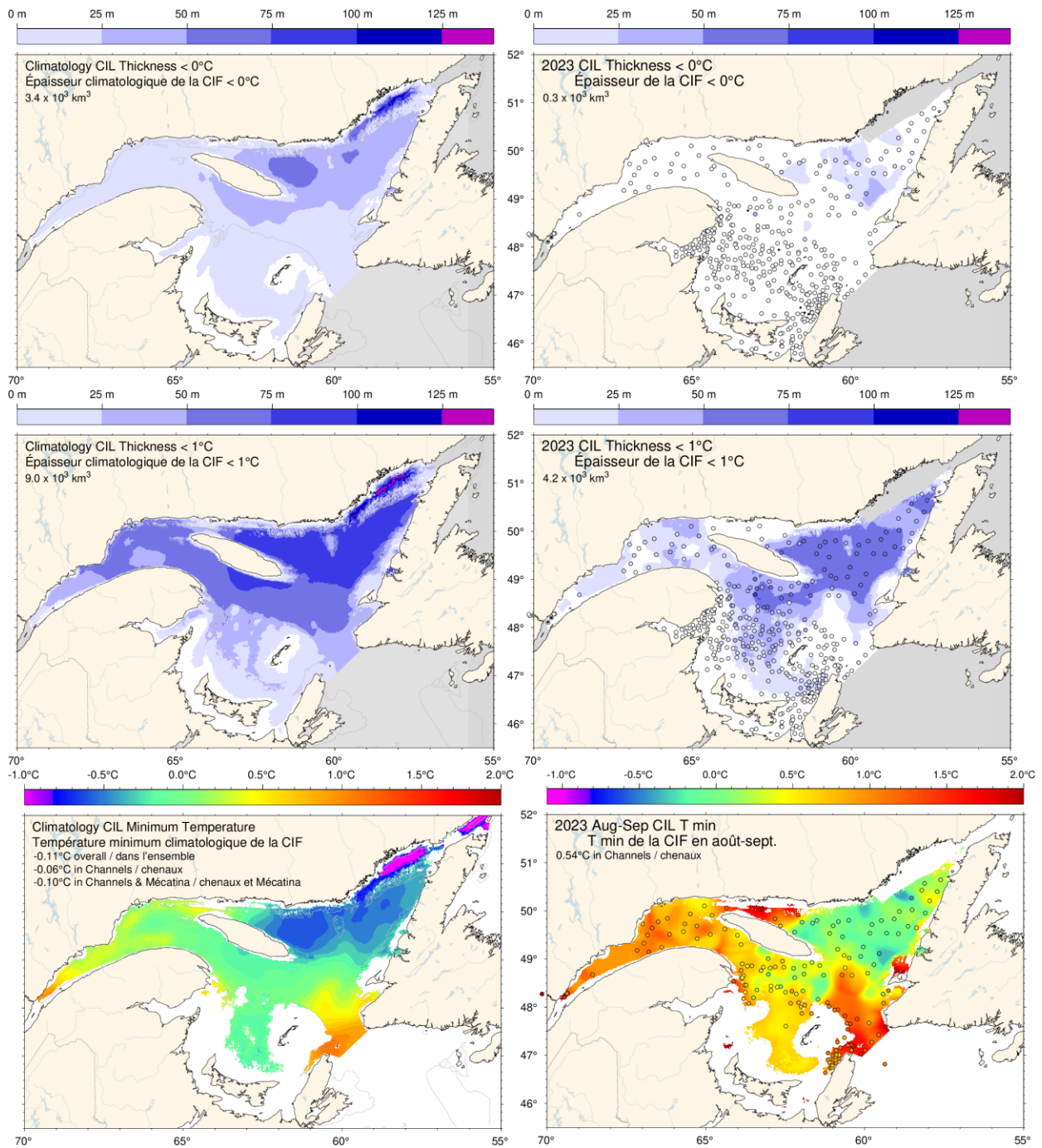
Fig. 37. Cold intermediate layer thickness (T < 0ºC, top panels; T < 1ºC, middle panels) and minimum temperature (bottom panels) in August and September 2023 (right) and 1991–2020 climatology (left). Station symbols are colour-coded according to their CIL thickness and minimum temperature. Integrated CIL volumes are indicated in the four top panels and area-averaged temperatures are indicated in the bottom two panels.

Fig. 38. CIL volume (top panel) delimited by 0ºC (in blue) and 1ºC (in red), and minimum temperature index (bottom panel) in the Gulf of St. Lawrence. The volumes are integrals of each of the annual interpolated thickness grids such as those shown in the top panels of Fig. 37 excluding Mécatina Trough and the Strait of Belle Isle. Rectangles on the right side show 1991–2020 mean ± 0.5 SD. In the lower panel, the black line is the updated Gilbert and Pettigrew (1997) index interpolated to 15 July (with dashed lines showing mean ± 0.5 SD) and the green line is the spatial average of each of the annual interpolated grids such as those shown in the two bottom panels of Fig. 37, excluding Mécatina Trough, the Strait of Belle Isle and the Magdalen Shallows. The numbers in the boxes are normalized anomalies relative to 1991–2020 climatologies.

60

Fig. 39. Volume of the CIL colder than 0 ºC (blue) and colder than 1ºC (red) in August and September (data mostly in September on Magdalen Shallows and August elsewhere). The volume of the CIL colder than 1 ºC in November for available years since 2006 is also shown for the St. Lawrence Estuary (black dashed line). Red and blue dashed lines are 1991–2020 averages and rectangles on the right side show the 1991–2020 mean ± 0.5 SD.
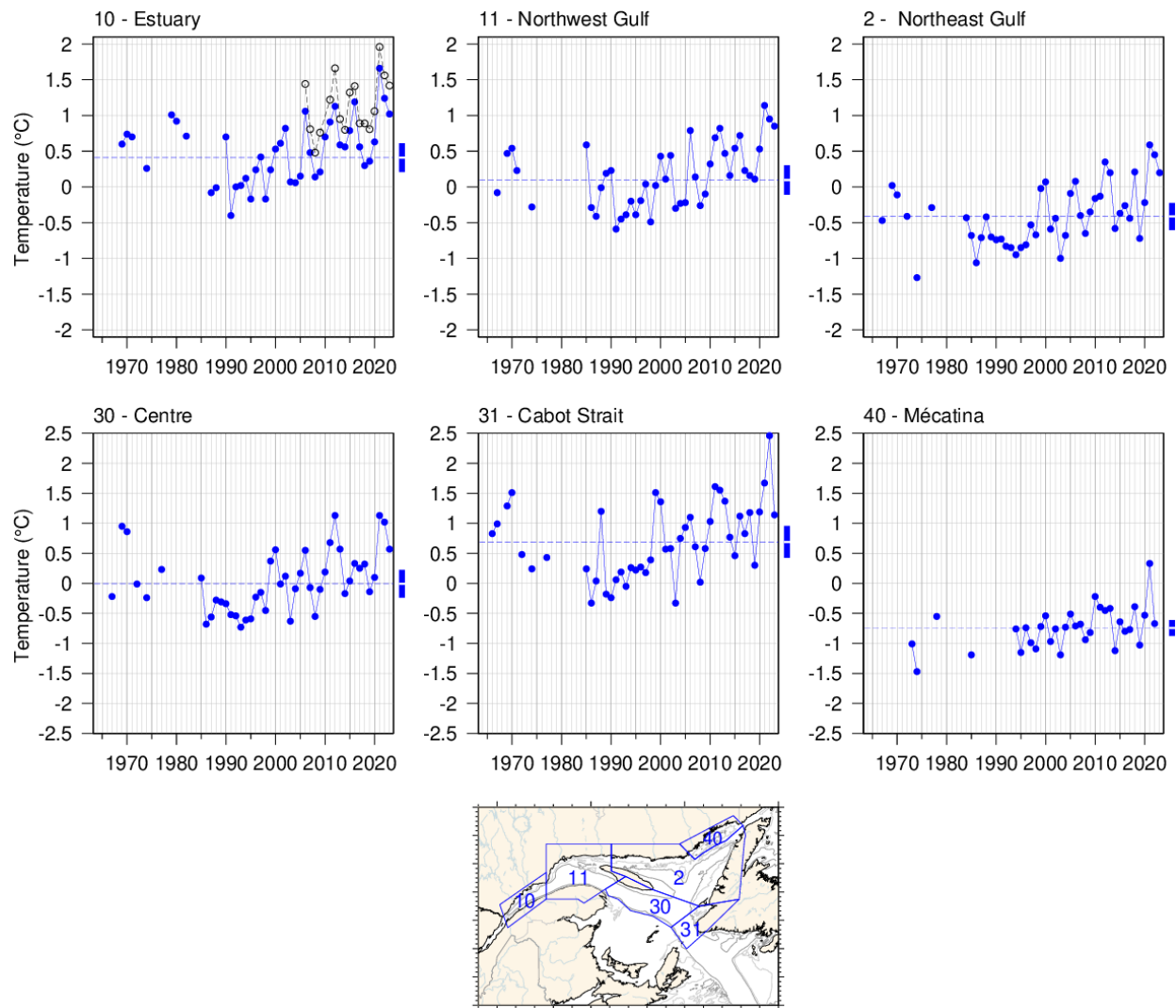
Fig. 40. Temperature minimum of the August and September CIL spatially averaged for selected areas where the CIL minimum temperature can be clearly identified. The spatial average of the November CIL temperature minimum for available years since 2006 is also shown for the St. Lawrence Estuary (black dashed line). Blue dashed lines are 1991–2020 averages and rectangles on the right side of panels show the 1991–2020 mean ± 0.5 SD.
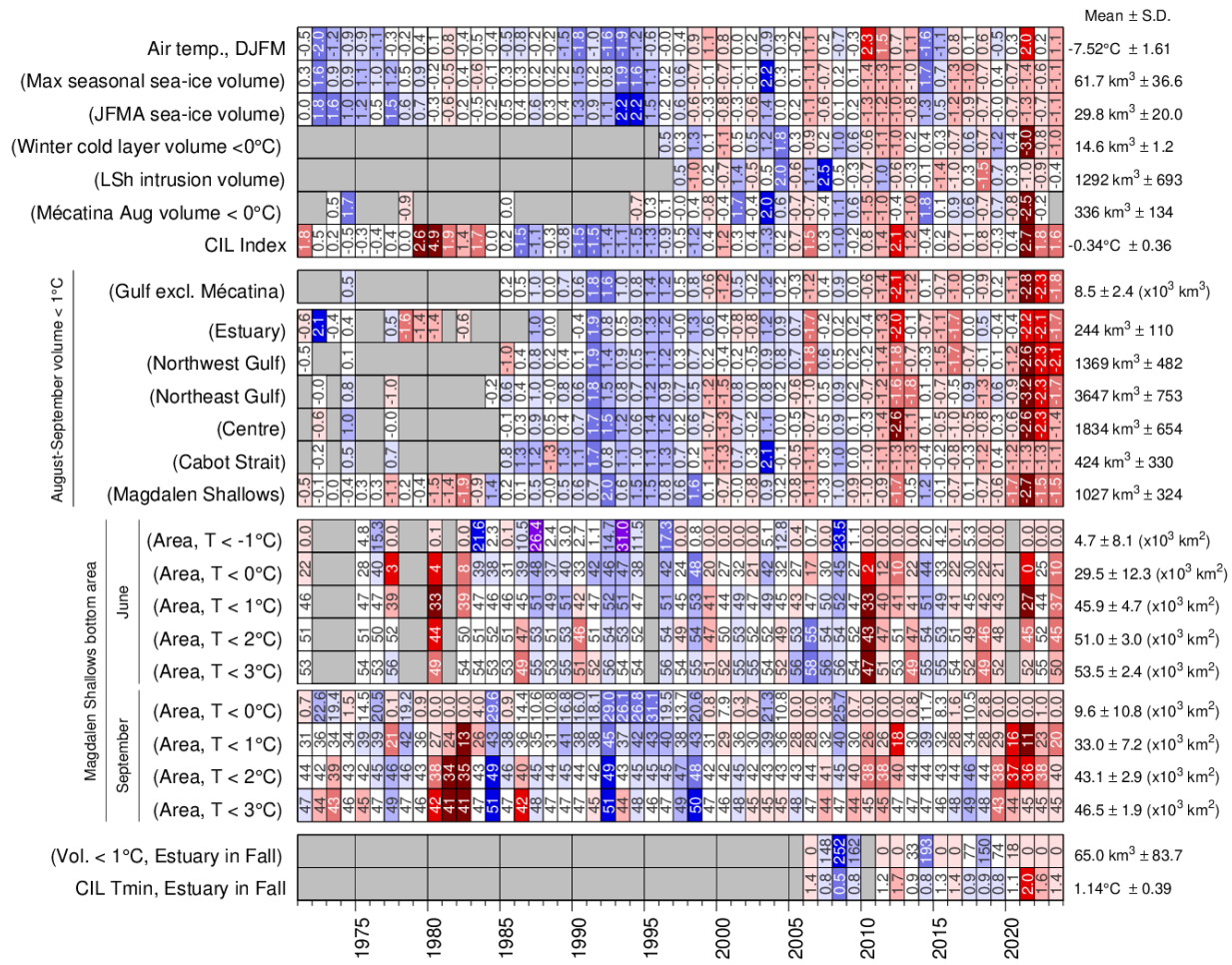
Fig. 41. Winter and summertime CIL related properties. The top block shows the scorecard time series for Dec-Jan-Feb-March air temperature (Fig. 5), yearly maximum sea-ice volume (Gulf + Scotian Shelf), January-April average sea-ice volume, winter (March) cold-layer (< 0 °C) volume, volume of Labrador Shelf Water intrusion into the Gulf observed in March, the August volume of cold water (< 0 °C) observed in the Mécatina Trough and the Gilbert and Pettigrew (1997) CIL index. Labels in parentheses have their colour coding reversed (blue for high values). The second block shows scorecard time series for August–September CIL volumes (< 1 °C) for regions of the Gulf. The third block shows the scorecard time series for the bottom areas of the Magdalen Shallows covered by waters colder than 0, 1, 2, and 3 °C during the June and September survey. The last block shows the November survey CIL volume (< 1 °C) and average CIL minimum temperature in the Estuary. Numbers in cells express anomalies in units of standard deviation, except for bottom areas and Estuary metrics which are expressed in physical units (because of the occurrence of zeros in areas and volumes).
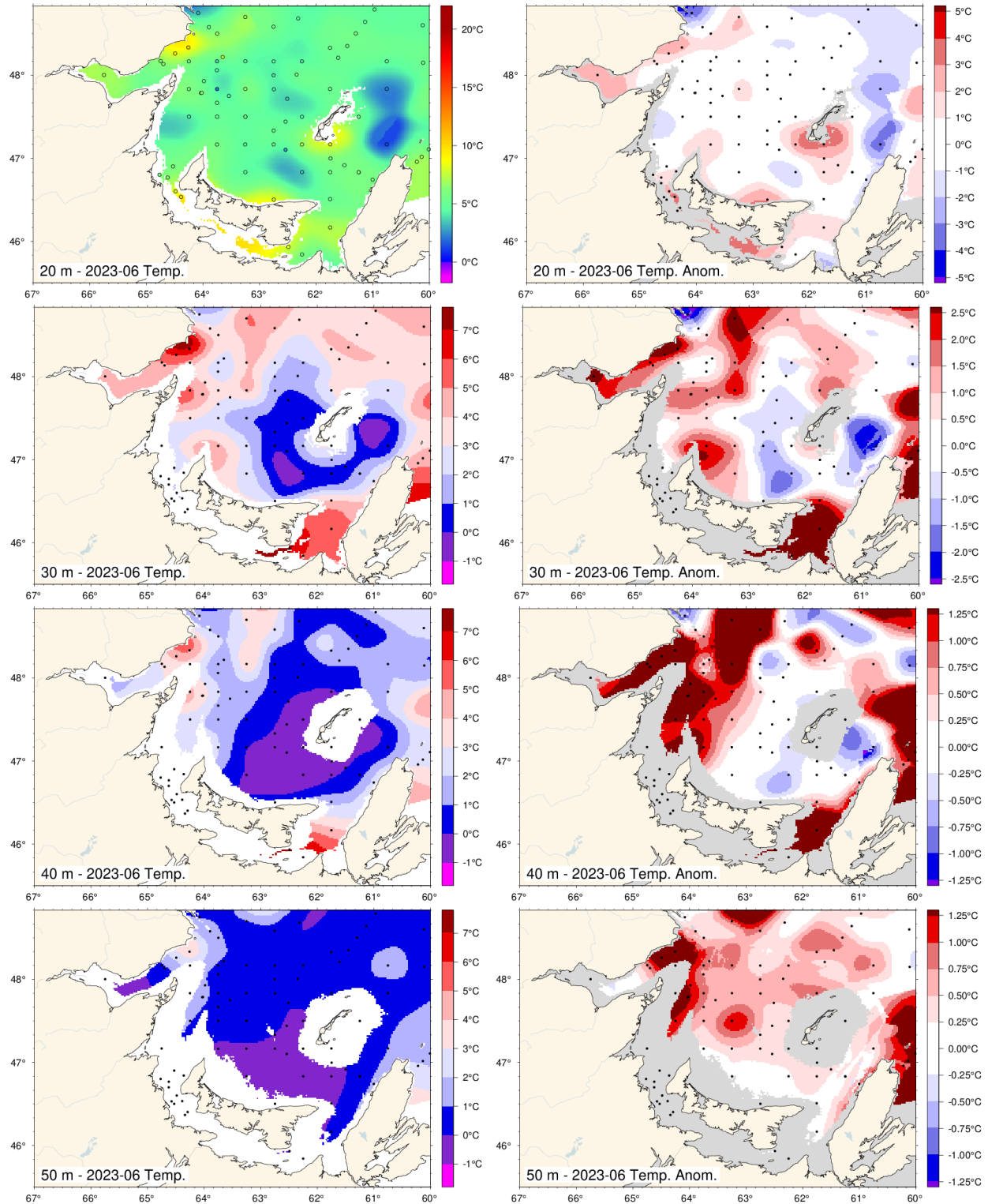
Fig. 42. June depth-layer temperature and anomaly fields on the Magdalen Shallows at 20 m, 30 m, 40 m and 50 m. Anomalies are based on 1991–2020 climatologies for all available years (appearing on Fig. 43). Dots are station occupations.

Fig. 43. Depth-layer average temperature anomalies for western and eastern Magdalen Shallows for the June mackerel survey. The SST data are June averages from AVHRR remote sensing. The colour-coding are according to normalized anomalies based on the 1991–2020 climatologies, but the numbers are mean temperatures in ºC.
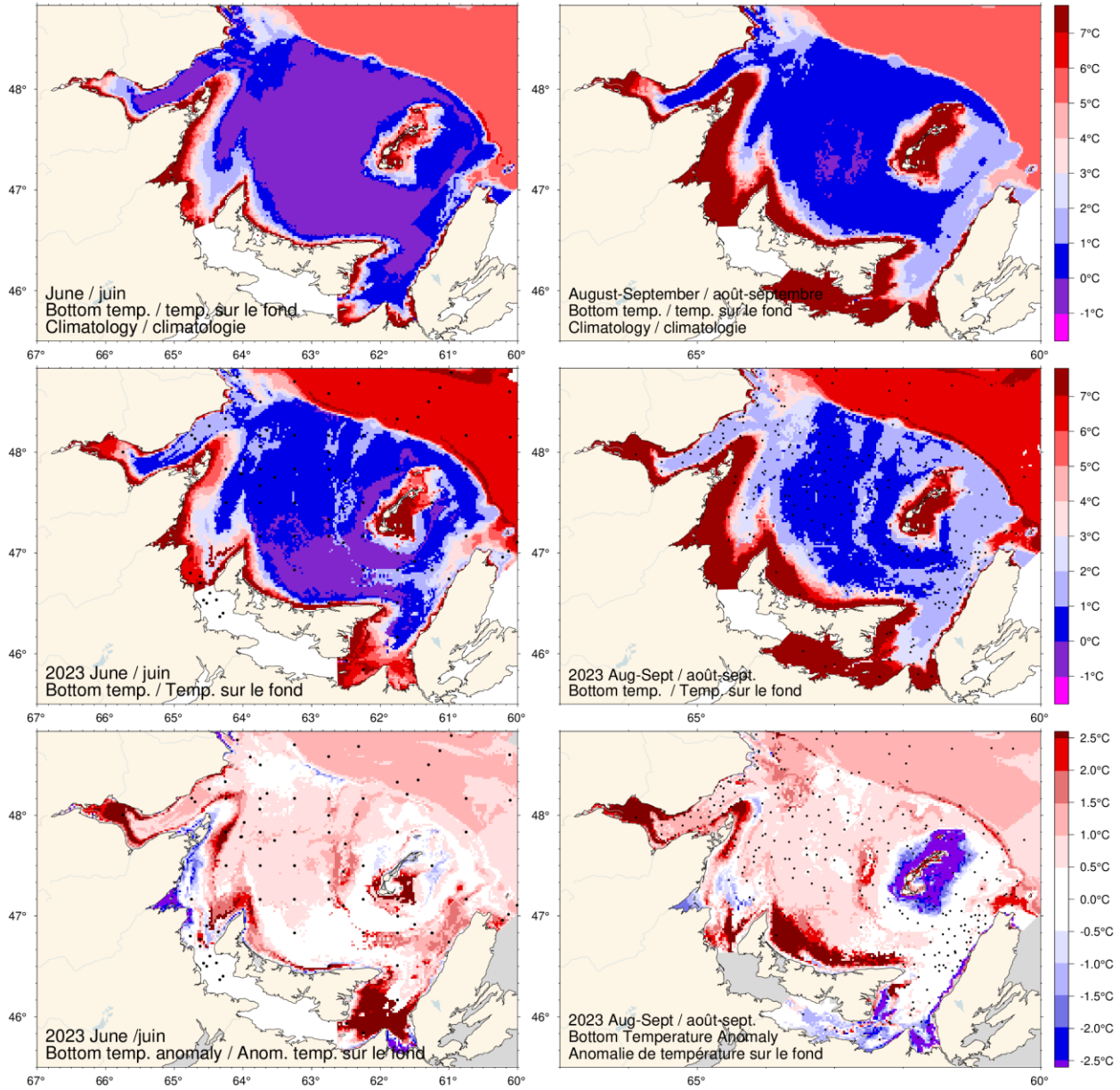
Fig. 44. June (left) and August-September (right) bottom temperature 1991–2020 climatology (top), 2023 observations (middle) and anomaly (bottom) for the Magdalen Shallows.
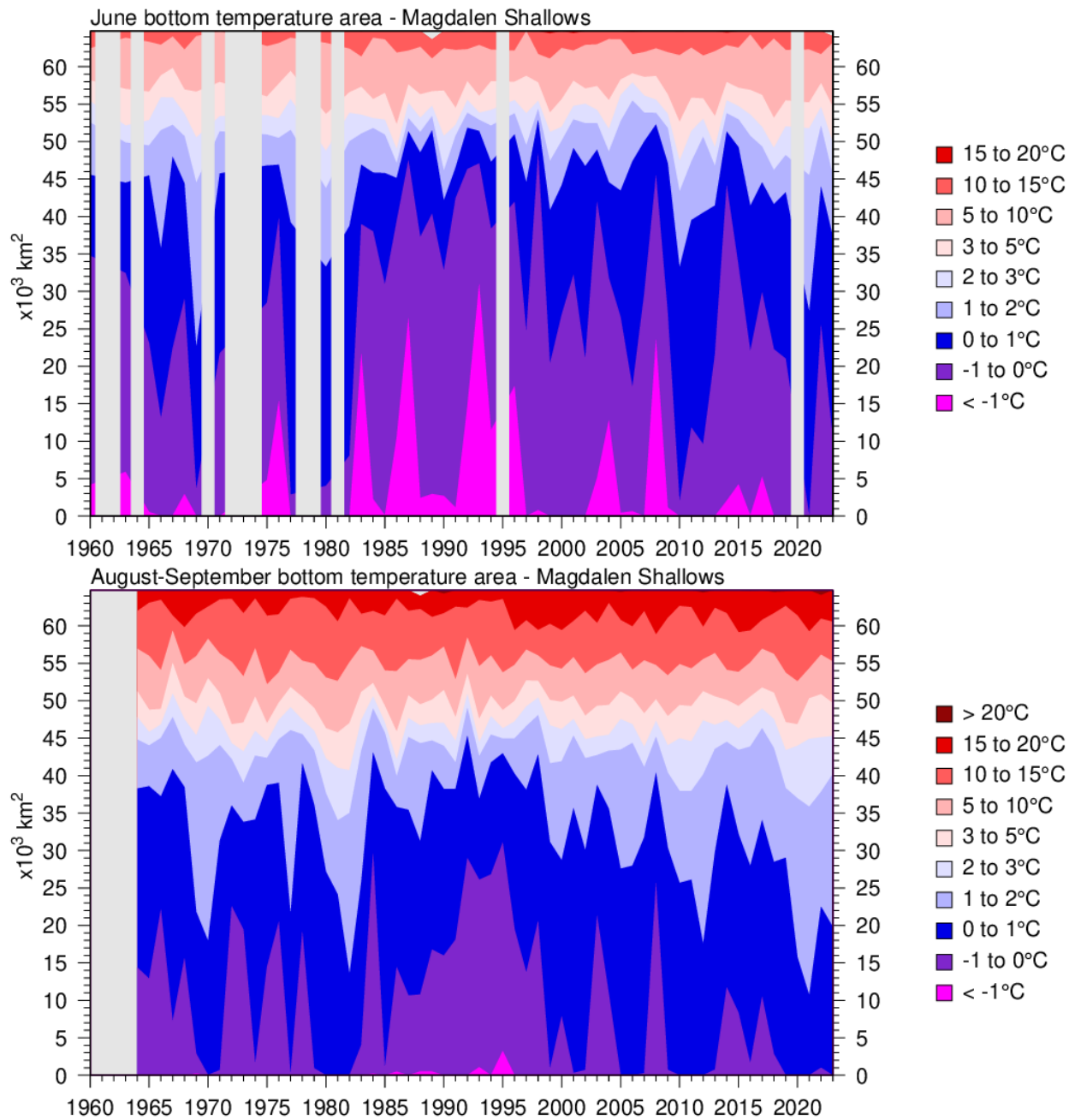
Fig. 45. Time series of the bottom areas covered by different temperature bins in June (top) and August-September (bottom) for the Magdalen Shallows (including Baie des Chaleurs).
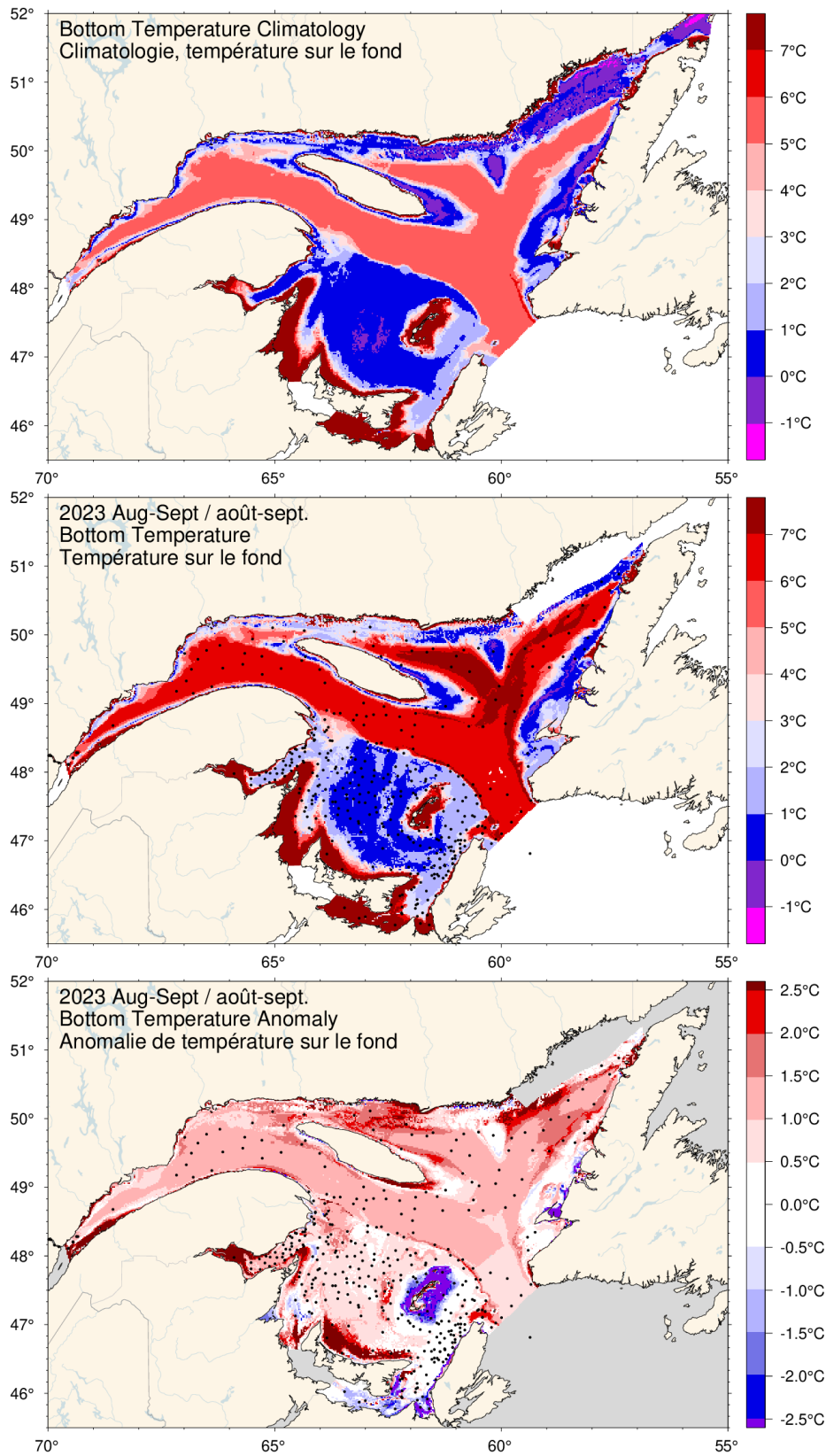
Fig. 46. August-September bottom temperature climatology (top), 2023 observations (middle) and anomaly (bottom).
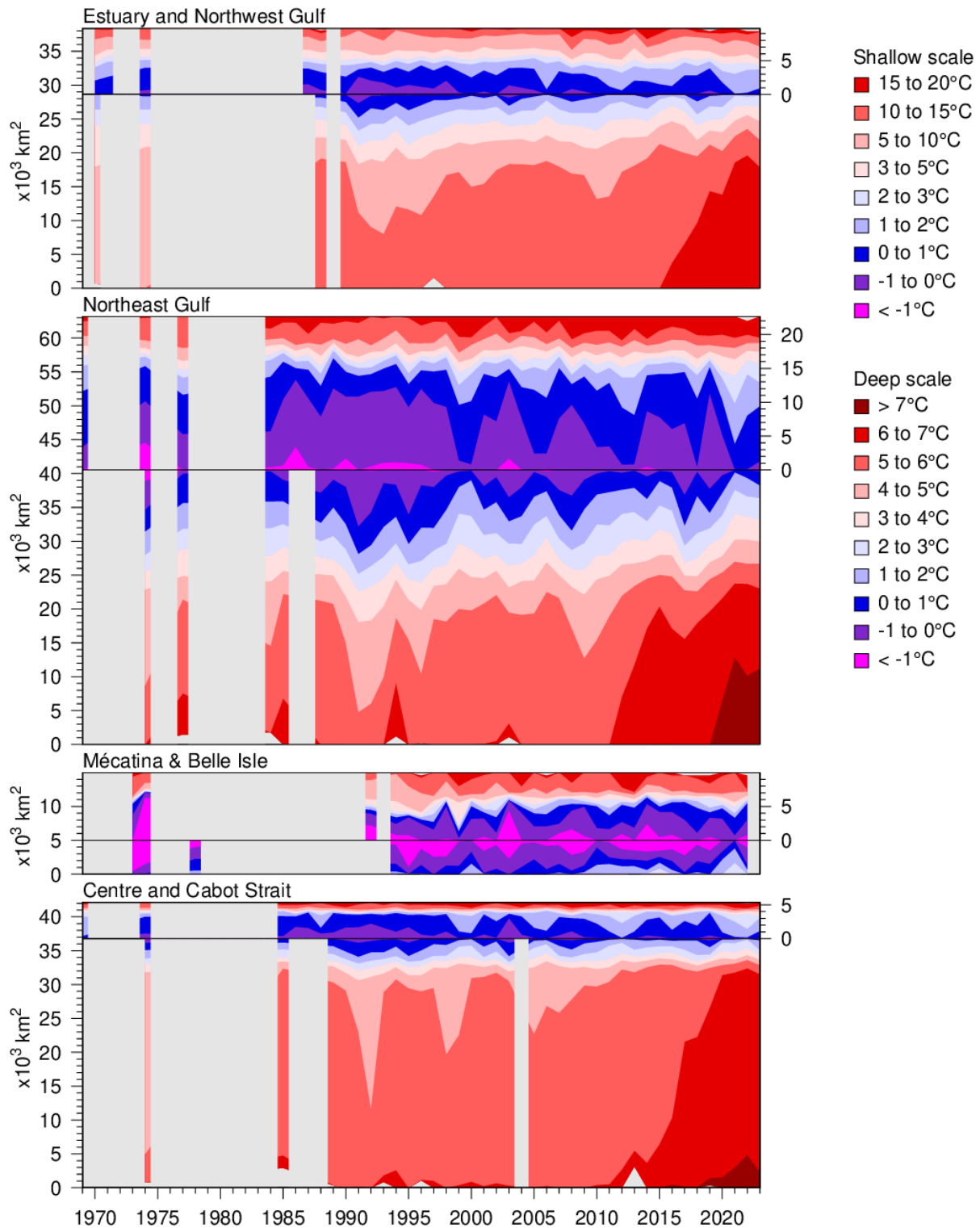
Fig. 47. Time series of the bottom areas covered by different temperature bins in August and September for regions of the northern Gulf. The panels are separated by a black horizontal line into shallow (< 100 m) and deep (> 100 m) areas to distinguish between warmer waters above and below the CIL. The shallow areas are shown on top using the area scale on the right-hand side and have warmer waters shown starting from the top end. The deep areas are shown below the horizontal line and have warmer waters starting at the bottom end. The CIL areas above and below 100 m meet near the horizontal line.
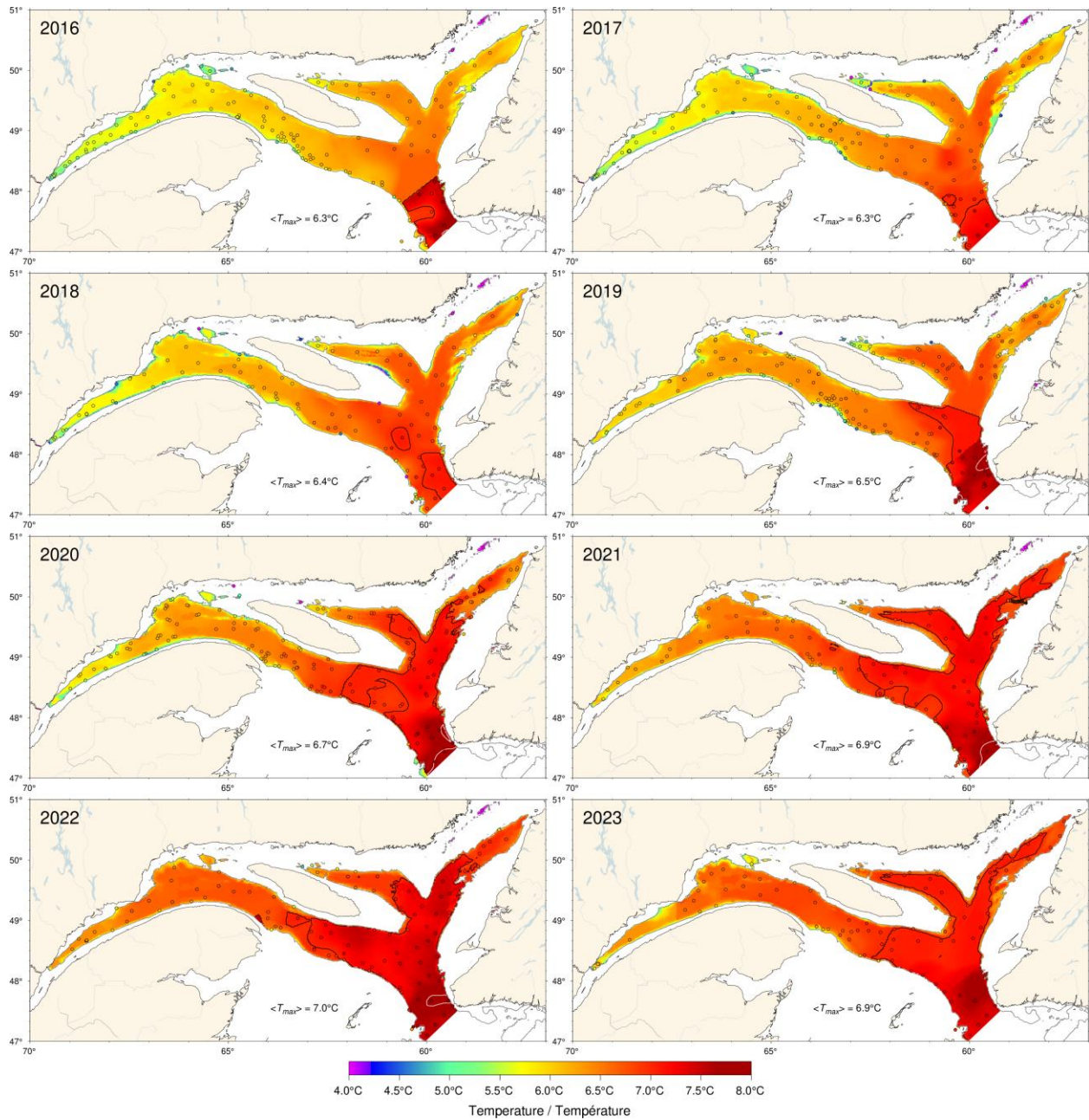
Fig. 48. Map of the deep temperature maximum found typically between 200 m and 300 m, 2015–2022. Maps are interpolated from August-September data available for each year. For 2017, 2020, 2021 and 2022, casts made in Cabot Strait during the fall survey were used to fill August sampling gaps (from the earlier BIO survey in October for 2022). The black and white contours are for 7 and 8 °C, respectively.

70
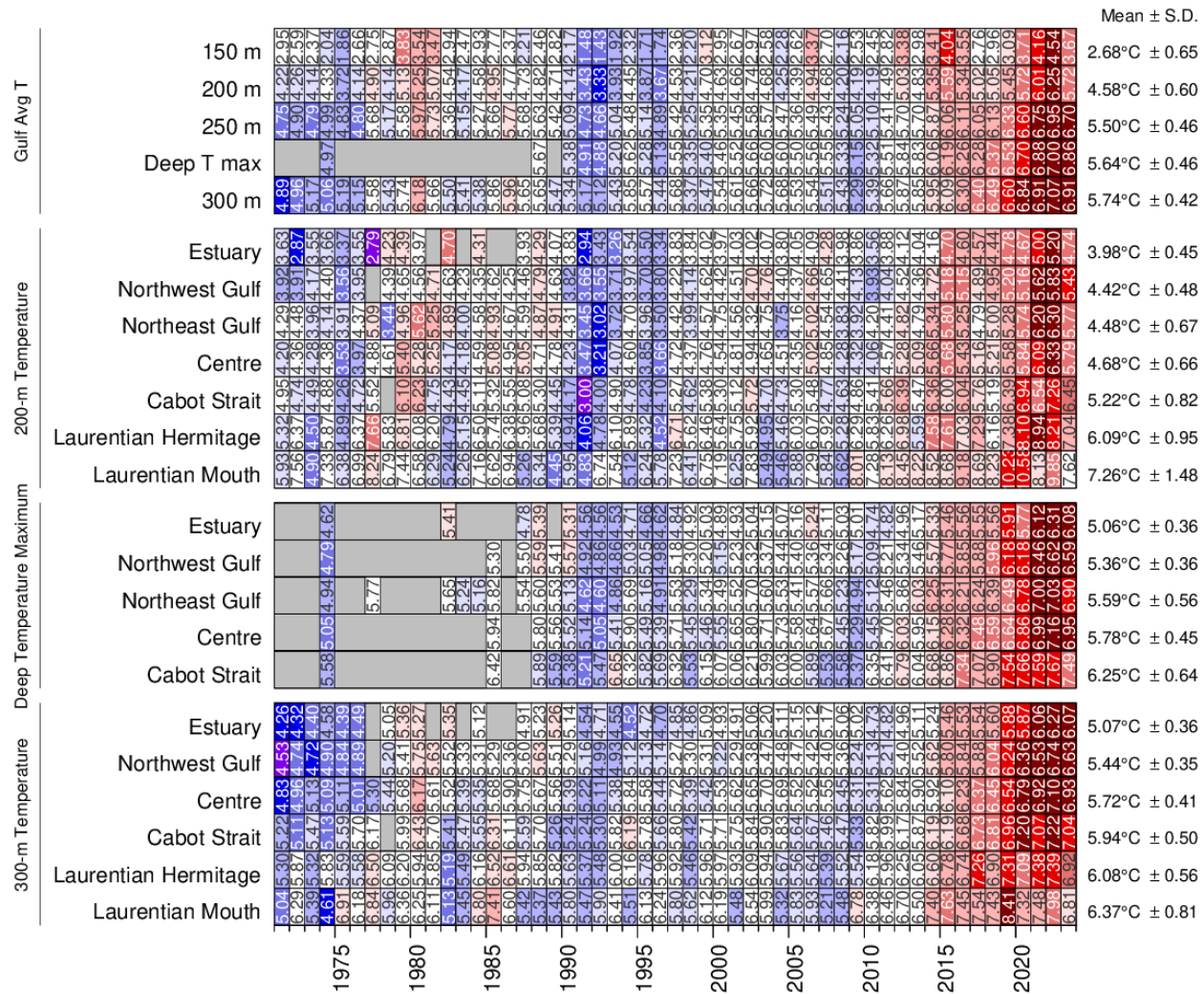
Fig. 49. Deep layer temperature. Gulf averages for temperature are shown for 150, 200, 250, 300 m, as well as for the deep temperature maximum usually found between 200 m and 300 m. Regional averages are shown for 200 m and 300 m, and deep temperature maximum. The numbers on the right are the 1991–2020 climatological means and standard deviations. The numbers in the boxes are average temperatures. The colour-coding is according to the temperature anomaly relative to the 1991–2020 climatology of each region and depth.
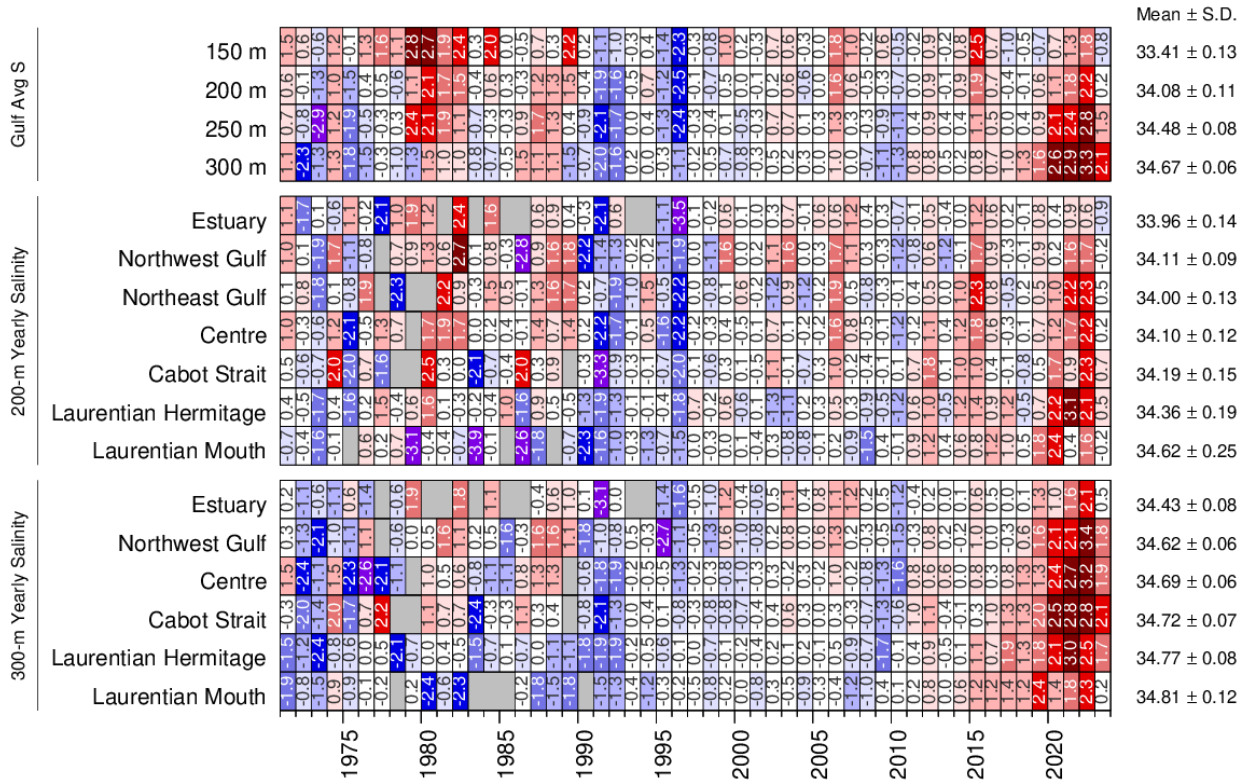
Fig. 50. Deep layer salinity. Gulf averages for salinity are shown for 150, 200, 250, and 300 m. Regional averages are shown for 200 m and 300 m. The numbers on the right are the 1991–2020 climatological means and standard deviations. The numbers in the boxes are normalized anomalies.

72
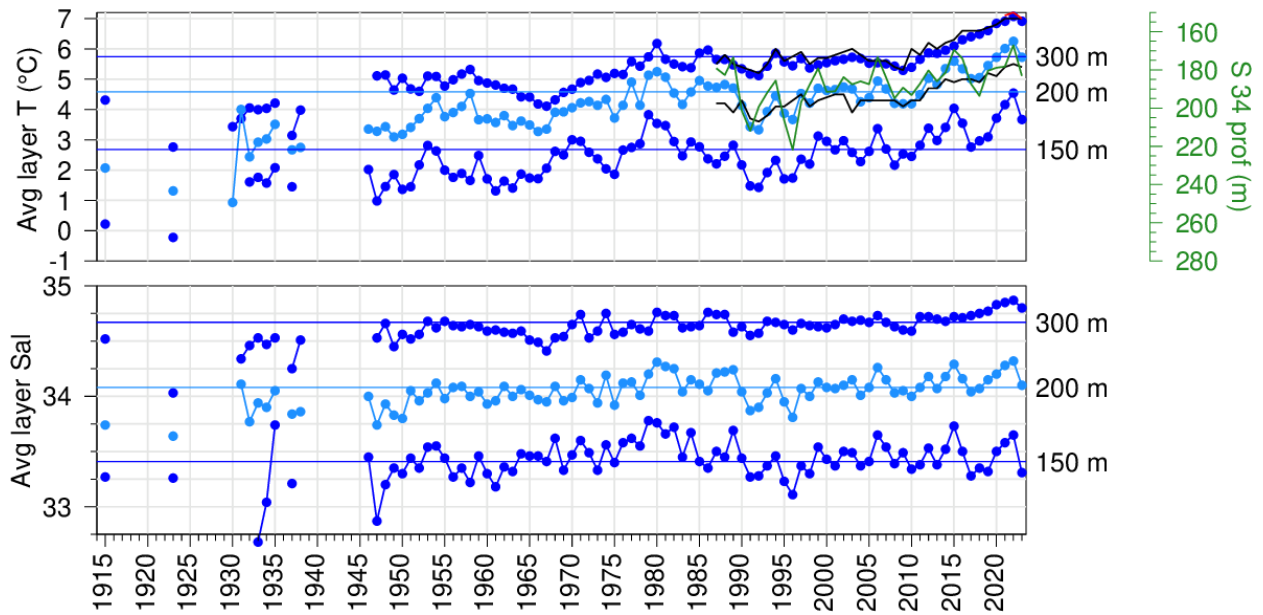
Fig. 51. Layer-averaged temperature and salinity time series for the Gulf of St. Lawrence. The temperature and salinity panels show the 150 m, 200 m, and 300 m annual averages and the horizontal lines are 1991–2020 means. The black line overlying temperature at 300 m is the average temperature of waters of salinity 34.7 in August (1987-2023) while the red line is for salinity 34.8 (2021-2023) more typical of the salinity found at 300 m in recent years. The black line overlying temperature at 200 m is the average temperature of waters of salinity 34 in August, while the green line is its averaged depth (scale shown on right).
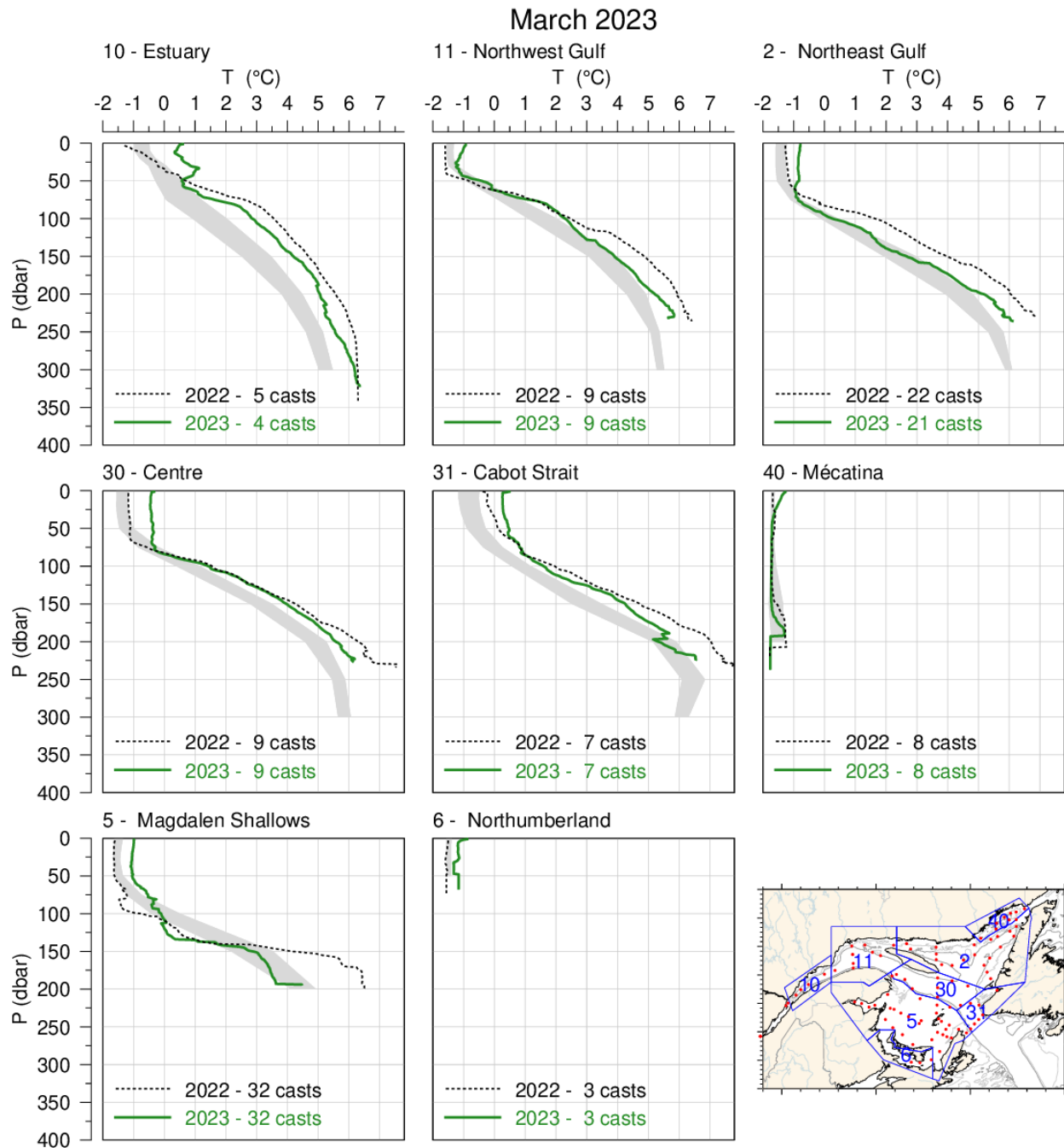
Fig. 52. Mean temperature profiles observed in each region of the Gulf during the March 2023 survey. The shaded area represents the 1991–2020 (but mostly 1996–2020) climatological monthly mean ± 0.5 SD. Mean profiles for 2022 are also shown for comparison.
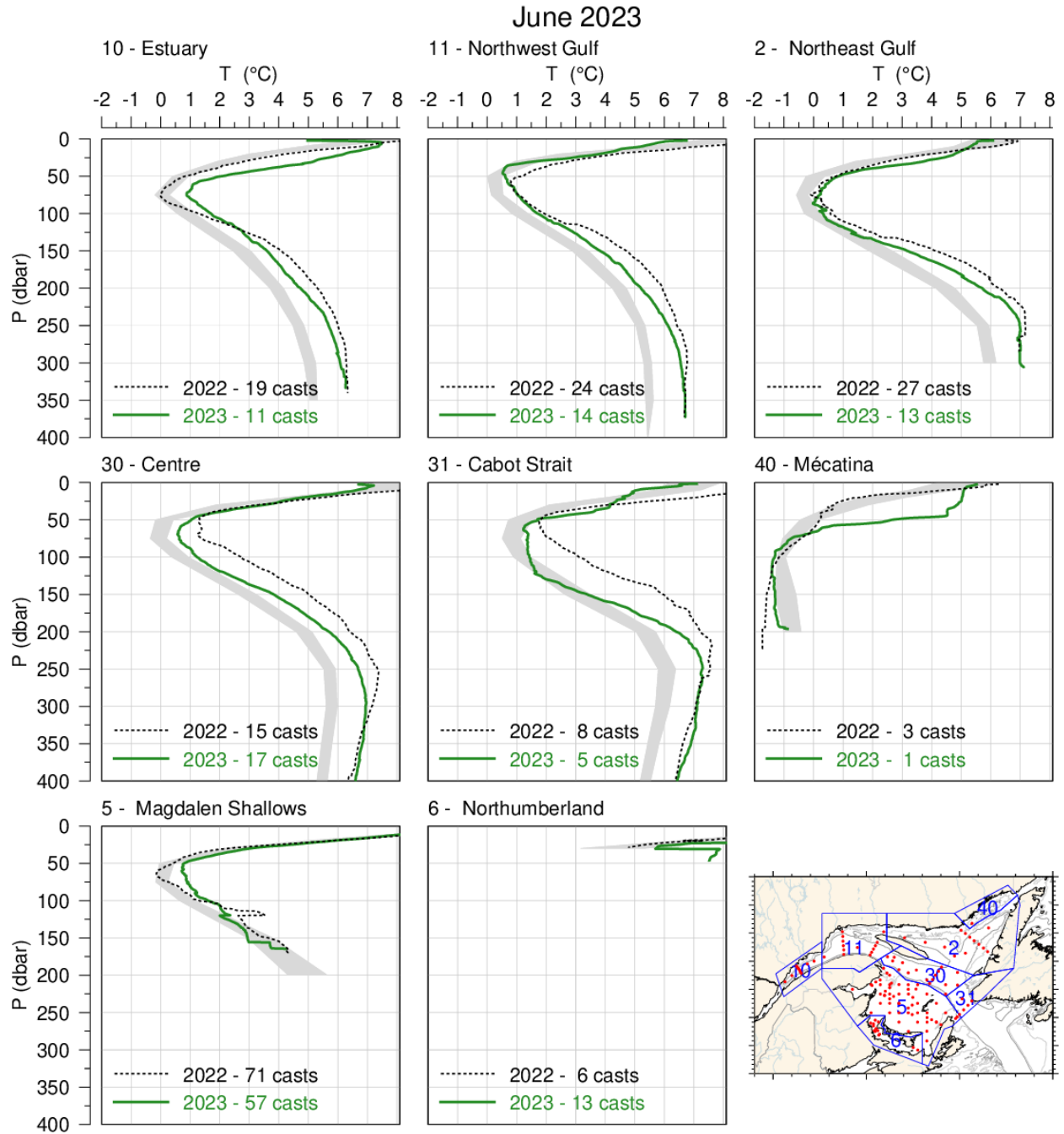
June 2023

Fig. 53. Mean temperature profiles observed in each region of the Gulf during June 2023. The shaded area represents the 1991–2020 climatological monthly mean ± 0.5 SD. Mean profiles for 2022 are also shown for comparison.
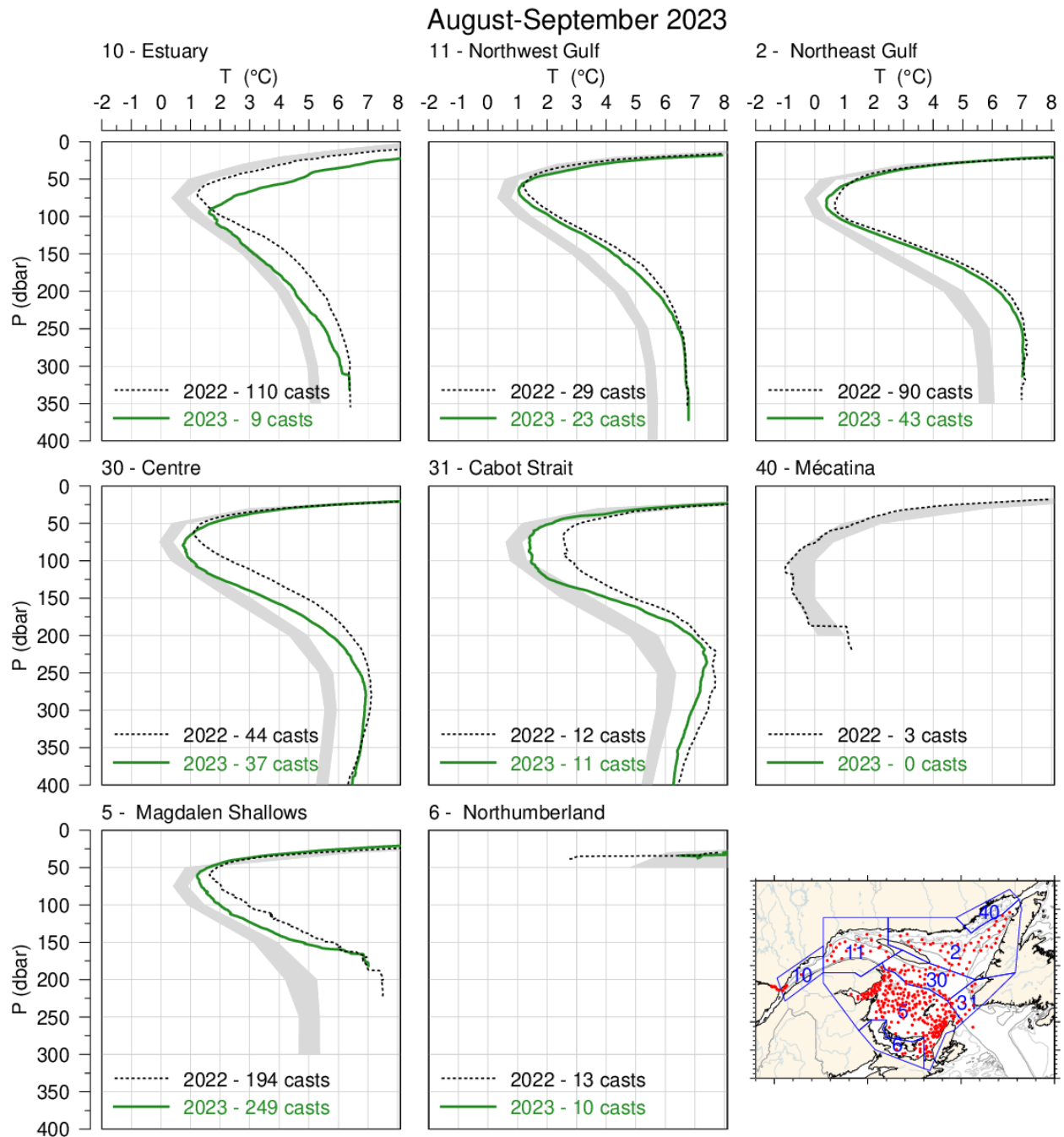
Fig. 54. Mean temperature profiles observed in each region of the Gulf during August and September 2023. The shaded area represents the 1991–2020 climatological monthly mean ± 0.5 SD for August for all regions except the Magdalen Shallows for which September is shown. Mean profiles for 2022 are also shown for comparison.

October 2023

Fig. 55. Mean temperature profiles observed in each region of the Gulf during the October 2023 AZMP survey. The shaded area represents the 1991–2020 climatological monthly mean ± 0.5 SD. Mean profiles for 2022 are also shown for comparison.

Estuary

	2022				2023			
	Mar	June	Aug	Oct	Mar	June	Aug	Oct
0 m	-1.29	8.6	12.4	5.9	0.5	7.7	10.5	9.5
10 m	-0.91	6.7	7.9	5.4	0.4	7.5	9.2	9.5
20 m	-0.49	4.3	5.7	5.2	0.6	6.5	8.2	8.6
30 m	-0.20	2.8	4.0	4.7	0.9	5.4	6.1	7.7
50 m	0.7	0.9	2.2	3.3	0.6	2.3	4.3	5.8
75 m	2.6	-0.0	1.4	1.8	1.6	1.1	2.2	3.2
100 m	3.6	1.3	2.1	2.0	2.9	1.6	1.7	2.0
150 m	4.7	4.1	4.4	3.8	4.2	3.5	2.7	3.2
200 m	5.56	5.31	5.39	4.99	5.05	4.73	4.25	5.05
250 m	6.13	6.00	6.02	5.77	5.55	5.68	5.25	5.89
300 m	6.25	6.30	6.34	6.21	6.18	6.10	5.98	6.27
350 m	6.29	6.33	6.40	6.35		6.26		6.43

Northwest Gulf

	2022				2023			
	Mar	June	Aug	Oct	Mar	June	Aug	Oct
0 m	-1.60	9.2	15.0	6.4	-0.93	6.0	13.3	10.7
10 m	-1.60	7.2	12.2	6.3	-1.02	5.2	12.9	10.7
20 m	-1.59	4.4	5.0	5.8	-1.14	3.8	8.7	9.0
30 m	-1.58	2.9	2.7	4.6	-1.20	1.6	5.0	6.2
50 m	-0.84	1.3	1.3	2.8	-0.44	0.6	1.4	3.7
75 m	1.2	1.1	1.5	2.2	1.1	1.0	1.1	1.9
100 m	2.5	1.9	2.5	2.5	2.3	1.7	2.0	1.8
150 m	4.9	4.7	4.7	4.6	3.9	3.8	3.6	3.7
200 m	5.95	5.89	5.95	5.89	5.21	5.21		5.43
250 m		6.43	6.46	6.51		6.12		6.43
300 m		6.76	6.69	6.68		6.54		6.67
350 m		6.69	6.76	6.73		6.67		6.70
400 m		6.75						

Northeast Gulf

	2022				2023			
	Mar	June	Aug	Nov	Mar	June	Aug	Oct
0 m	-1.27	6.9	18.7	9.0	-0.74	5.5	16.4	8.4
10 m	-1.27	6.1	18.2	9.0	-0.76	5.3	15.2	8.3
20 m	-1.24	4.0	11.2	8.8	-0.81	4.8	8.0	7.8
30 m	-1.22	2.5	5.4	8.4	-0.81	3.7	4.1	5.5
50 m	-1.11	0.8	1.6	3.7	-0.78	0.8	1.5	1.6
75 m	-0.37	-0.0	0.9	1.7	-0.80	0.2	0.5	0.9
100 m	1.5	0.6	1.1	1.9	0.1	0.5	1.0	1.2
150 m	3.9	4.1	4.3	4.6	2.5	3.2	4.0	3.9
200 m	6.09	6.28	6.47	6.51	4.96	5.71	6.28	6.11
250 m		7.17	7.00	6.89		6.98	7.00	7.00

Mécatina

	2022				2023			
	Mar	June	Aug	Nov	Mar	June	Aug	Oct
0 m	-1.69	5.9	16.9	8.6	-1.25	5.5		6.0
10 m	-1.69	4.5	13.8	8.7	-1.41	5.1		5.9
20 m	-1.69	1.5	6.8	8.7	-1.53	5.0		5.2
30 m	-1.60	0.7	3.4	8.7	-1.62	4.8		4.8
50 m	-1.62	0.2	1.3	3.5	-1.71	2.7		3.7
75 m	-1.71	-0.4	0.0	1.1	-1.72	-0.8		2.4
100 m	-1.73	-1.2	0.4		-1.72	-1.3		1.4
150 m	-1.59	-1.6	-0.6	-0.3	-1.72	-1.3		0.7
200 m	-1.25	-1.64	1.13	0.20	-1.29	-0.91		1.85

Centre

	2022				2023			
	Mar	June	Sep	Oct	Mar	June	Sep	Oct
0 m	-1.16	9.4	13.9	9.6	-0.39	7.2	15.4	10.5
10 m	-1.17	8.3	13.6	9.5	-0.42	6.7	14.4	10.5
20 m	-1.16	5.5	8.3	9.6	-0.43	4.8	6.1	10.4
30 m	-1.15	3.3	4.1	8.0	-0.40	3.5	3.1	5.7
50 m	-1.11	1.3	1.4	2.8	-0.37	1.0	1.1	1.5
75 m	-0.58	1.4	1.3	1.8	-0.29	0.6	0.9	1.0
100 m	1.5	2.7	2.2	2.6	1.3	1.2	1.5	1.3
150 m	4.2	5.0	4.8	3.8	3.8	3.8	4.0	3.6
200 m	6.30	6.41	6.23	6.39	5.51	5.70	6.03	5.79
250 m		7.28	6.92	7.15		6.69	6.59	6.84
300 m		7.15	6.95	7.21		6.93	6.88	6.95
350 m		6.72	6.74	6.80		6.81	6.75	6.67
400 m		6.50	6.52	6.39		6.64		6.49
450 m		6.16		6.17		6.45		6.20

Cabot Strait

	2022				2023			
	Mar	June	Sep	Nov	Mar	June	Sep	Oct
0 m	-0.23	9.2	10.2	9.4	0.2	6.6	17.7	11.7
10 m	-0.23	9.1	10.2	8.9	0.2	5.1	16.3	11.4
20 m	-0.21	7.1	8.7	8.8	0.2	4.6	8.5	8.2
30 m	-0.09	4.4	8.0	8.7	0.3	4.2	3.8	4.5
50 m	0.1	1.8	2.5	5.3	0.4	1.7	1.6	2.2
75 m	0.8	2.1	3.4	2.7	0.8	1.4	1.3	2.0
100 m	1.9	3.0	4.1	2.8	1.6	1.4	1.4	1.8
150 m	4.7	6.0		5.5	4.3	3.4	4.2	4.3
200 m	7.02	7.23		7.41	5.82	6.41	6.76	6.38
250 m		7.52		7.54		7.28	7.13	7.16
300 m		7.05		7.19		7.11	6.91	7.06
350 m		6.63		6.77		6.90		6.52
400 m		6.37		6.31		6.43		6.18
450 m		6.11		6.14		6.30		6.04

Magdalen Shallows

	2022				2023			
	Mar	June	Sep	Nov	Mar	June	Sep	Oct
0 m	-1.59	10.3	16.3	8.7	-0.98	9.6	16.5	13.6
10 m	-1.63	9.1	16.0	8.7	-0.99	8.7	15.5	13.0
20 m	-1.64	5.7	12.0	8.3	-1.02	5.8	9.7	11.4
30 m	-1.63	2.4	6.7	7.7	-1.04	3.3	5.6	9.2
50 m	-1.62	0.4	2.8	4.7	-1.04	0.8	1.8	4.6
75 m	-1.23	0.1	2.5	2.4	-0.60	0.9	1.5	2.4
100 m	-0.90	1.1	3.0	2.5	-0.44	1.4	1.9	1.9
150 m	4.1	3.6	5.8	3.9	2.7	2.9	5.1	3.8

Fig. 56. Depth-layer monthly average temperature summary for months during which the Gulf-wide oceanographic surveys took place in 2022 and 2023. The colour-coding is according to the temperature anomaly relative to the monthly 1991–2020 climatology of each region.

Estuary

	2022				2023			
	Mar	June	Aug	Oct	Mar	June	Aug	Oct
Strat.	2.71	7.0	6.6	3.8	3.25	4.1	4.5	3.9
0 m	28.5	23.4	24.6	26.9	27.2	25.5	24.8	25.5
10 m	28.9	24.8	28.6	28.2	28.0	25.9	25.7	26.3
20 m	29.5	27.9	29.5	29.5	29.3	27.0	26.5	27.5
30 m	30.2	29.8	30.3	30.4	29.9	27.7	28.0	28.5
50 m	31.9	31.3	31.4	31.4	31.3	30.1	29.5	29.8
75 m	32.9	32.0	32.2	32.1	32.2	31.7	31.3	31.2
100 m	33.3	32.6	32.7	32.6	32.9	32.4	32.1	31.8
150 m	33.9	33.6	33.7	33.5	33.6	33.3	32.9	33.1
200 m	34.29	34.17	34.20	34.01	34.00	33.84	33.60	33.97
250 m	34.56	34.49	34.49	34.37	34.24	34.29	34.09	34.37
300 m	34.62	34.63	34.64	34.57	34.53	34.48	34.43	34.55
350 m	34.63	34.64	34.66	34.64		34.56		34.62

Northwest Gulf

	2022				2023			
	Mar	June	Aug	Oct	Mar	June	Aug	Oct
Strat.	0.56	4.0	4.6	2.0	0.92	2.4	3.4	2.7
0 m	31.2	27.8	28.5	29.8	30.5	29.1	29.4	29.2
10 m	31.2	29.0	29.0	30.4	30.6	29.7	29.4	29.3
20 m	31.3	30.4	30.5	30.7	31.1	30.5	30.5	30.2
30 m	31.4	30.9	31.4	31.2	31.3	31.1	31.1	30.9
50 m	31.9	31.7	32.0	31.9	31.7	31.6	31.8	31.5
75 m	32.5	32.3	32.5	32.4	32.2	32.1	32.1	32.0
100 m	32.9	32.8	33.0	32.9	32.7	32.5	32.6	32.4
150 m	33.9	33.8	33.8	33.7	33.4	33.4	33.3	33.3
200 m	34.36	34.29	34.33	34.29	33.99	33.99		34.09
250 m		34.64	34.61	34.62		34.42		34.57
300 m		34.83	34.82	34.80		34.66		34.74
350 m		34.90	34.88	34.87		34.76		34.82
400 m		34.89						

Northeast Gulf

	2022				2023			
	Mar	June	Aug	Nov	Mar	June	Aug	Oct
Strat.	0.07	2.2	4.0	1.3	0.10	0.8	3.5	1.6
0 m	31.7	29.7	30.2	30.8	31.6	31.2	30.0	30.6
10 m	31.7	30.3	30.3	30.8	31.6	31.2	30.2	30.6
20 m	31.7	31.1	30.8	30.9	31.7	31.3	30.9	30.7
30 m	31.8	31.4	31.3	31.0	31.7	31.4	31.3	31.1
50 m	31.8	31.8	31.8	31.7	31.8	31.7	31.7	31.8
75 m	32.0	32.1	32.1	32.2	31.9	32.0	32.0	32.1
100 m	32.5	32.6	32.5	32.7	32.1	32.3	32.5	32.5
150 m	33.5	33.5	33.6	33.6	32.9	33.1	33.4	33.4
200 m	34.27	34.28	34.34	34.37	33.74	34.04	34.26	34.20
250 m		34.77	34.65	34.60		34.63	34.65	34.69

Mécatina

	2022				2023			
	Mar	June	Aug	Nov	Mar	June	Aug	Oct
Strat.	0.13	1.4	3.7	1.2	0.48	0.5		0.7
0 m	31.9	30.7	30.1	30.9	31.7	31.3		31.1
10 m	31.9	30.8	30.4	30.9	31.8	31.3		31.1
20 m	32.0	31.2	31.1	30.9	31.9	31.3		31.2
30 m	32.0	31.4	31.5	30.9	32.1	31.3		31.4
50 m	32.1	31.8	31.9	31.7	32.3	31.5		31.6
75 m	32.1	32.1	32.1	32.1	32.4	32.0		31.8
100 m	32.3	32.4	32.5	32.2	32.4	32.2		31.9
150 m	32.4	32.5	32.5	32.4	32.4	32.3		32.3
200 m	32.52	32.55	32.81	32.60	32.47	32.36		32.72

Centre

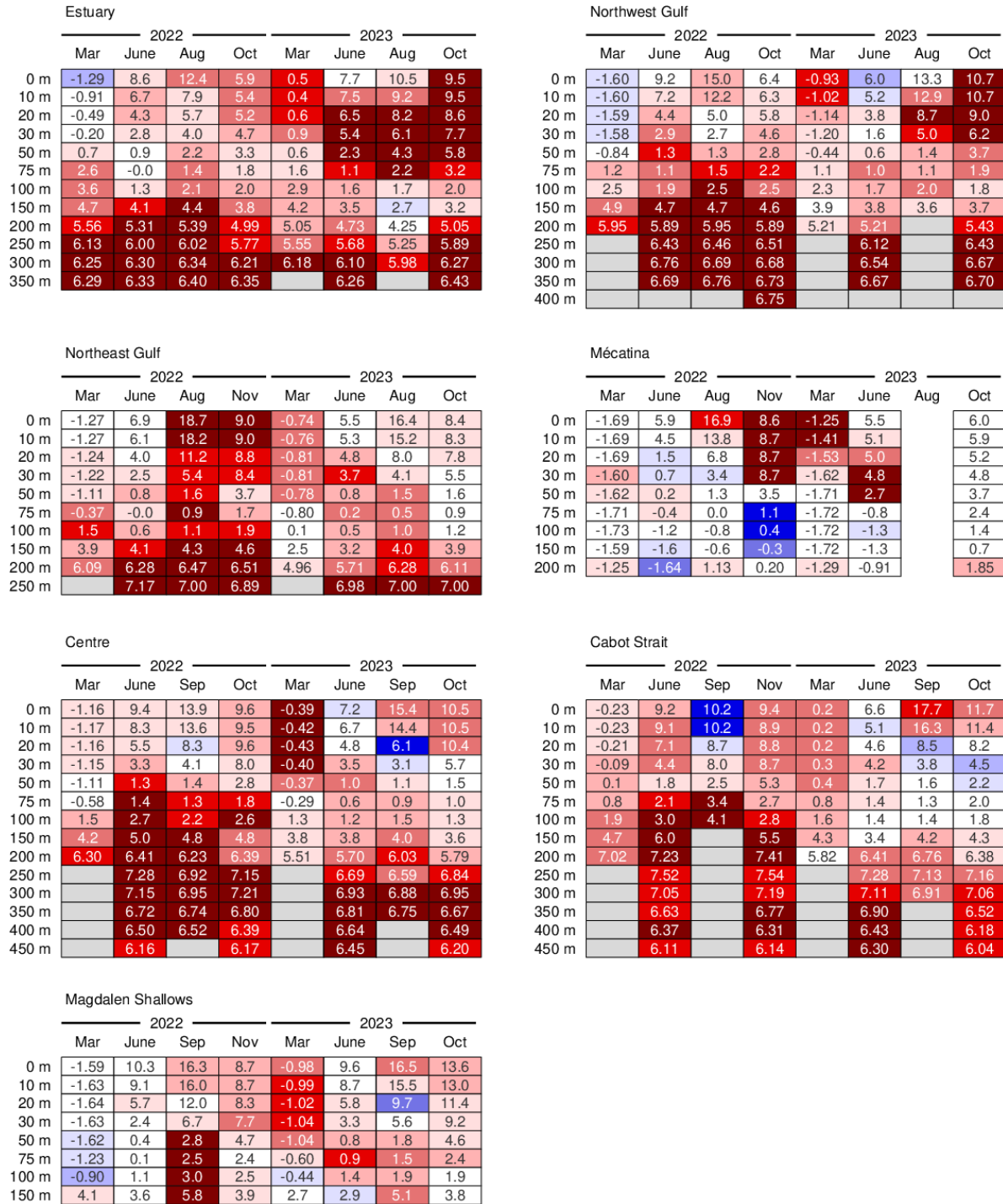|	2022				2023			
	Mar	June	Sep	Oct	Mar	June	Sep	Oct
Strat.	0.17	2.2	3.6	2.0	0.22	1.4	4.0	2.3
0 m	31.5	30.3	29.4	30.3	31.3	30.7	29.4	30.2
10 m	31.6	30.6	29.6	30.3	31.3	30.9	29.7	30.2
20 m	31.7	31.1	30.6	30.4	31.4	31.2	30.9	30.8
30 m	31.7	31.5	31.2	30.8	31.4	31.4	31.5	31.1
50 m	31.7	31.9	31.9	31.9	31.5	31.7	31.9	31.8
75 m	31.9	32.3	32.4	32.4	31.7	32.0	32.2	32.1
100 m	32.6	32.9	32.8	32.8	32.3	32.4	32.6	32.4
150 m	33.6	33.8	33.8	33.7	33.3	33.3	33.3	33.3
200 m	34.39	34.39	34.34	34.35	34.00	34.07	34.25	34.12
250 m		34.77	34.70	34.71		34.53	34.60	34.60
300 m		34.92	34.86	34.88		34.78	34.80	34.81
350 m		34.97	34.95	34.96		34.91	34.84	34.94
400 m		34.98	34.98	34.99		34.94		34.95
450 m		35.00		34.99		34.98		34.95

Cabot Strait

	2022				2023			
	Mar	June	Sep	Nov	Mar	June	Sep	Oct
Strat.	0.31	1.5	2.7	1.9	0.08	1.2	5.0	3.0
0 m	31.3	31.1	29.6	29.9	31.6	30.8	28.6	29.7
10 m	31.5	31.1	29.7	30.1	31.6	30.9	29.0	29.8
20 m	31.5	31.2	30.6	30.4	31.6	31.2	30.2	30.8
30 m	31.6	31.4	30.8	30.7	31.6	31.5	31.3	31.6
50 m	31.7	31.9	31.9	31.6	31.7	31.7	31.9	32.0
75 m	31.9	32.4	32.7	32.4	31.9	32.1	32.2	32.4
100 m	32.6	32.8	33.2	32.8	32.3	32.3	32.4	32.6
150 m	33.6	34.0		33.8	33.5	33.2	33.5	33.5
200 m	34.42	34.57		34.53	34.08	34.26	34.45	34.29
250 m		34.82		34.78		34.73	34.77	34.71
300 m		34.92		34.89		34.84	34.90	34.87
350 m		34.97		34.97		34.94		34.93
400 m		34.99		34.99		34.98		34.96
450 m		35.00		34.99		34.99		34.96

Magdalen Shallows

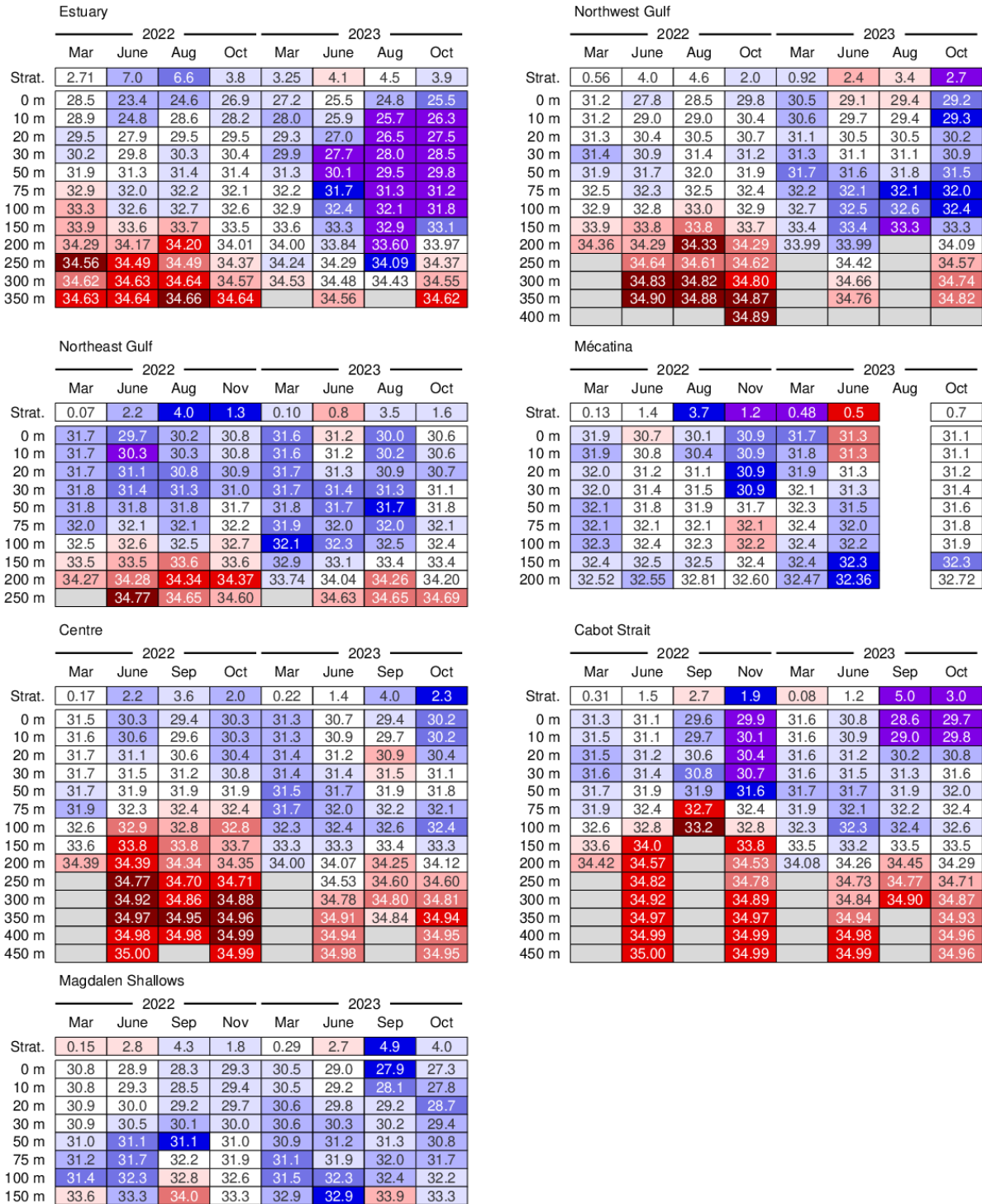|	2022				2023			
	Mar	June	Sep	Nov	Mar	June	Sep	Oct
Strat.	0.15	2.8	4.3	1.8	0.29	2.7	4.9	4.0
0 m	30.8	28.9	28.3	29.3	30.5	29.0	27.9	27.3
10 m	30.8	29.3	28.5	29.4	30.5	29.2	28.1	27.8
20 m	30.9	30.0	29.2	29.7	30.6	29.8	29.2	28.7
30 m	30.9	30.5	30.1	30.0	30.6	30.3	30.2	29.4
50 m	31.0	31.1	31.1	31.0	30.9	31.2	31.3	30.8
75 m	31.2	31.7	32.2	31.9	31.1	31.9	32.0	31.7
100 m	31.4	32.3	32.8	32.6	31.5	32.3	32.4	32.2
150 m	33.6	33.3	34.0	33.3	32.9	32.9	33.9	33.3

Fig. 57. Depth-layer monthly average stratification (strat.) and salinity summary for months of the Gulf-wide oceanographic surveys in 2022 and 2023. Stratification is defined as the density difference at 50 m and the surface and its colour-coding is reversed (blue for positive anomaly because usually associated with low surface salinity).
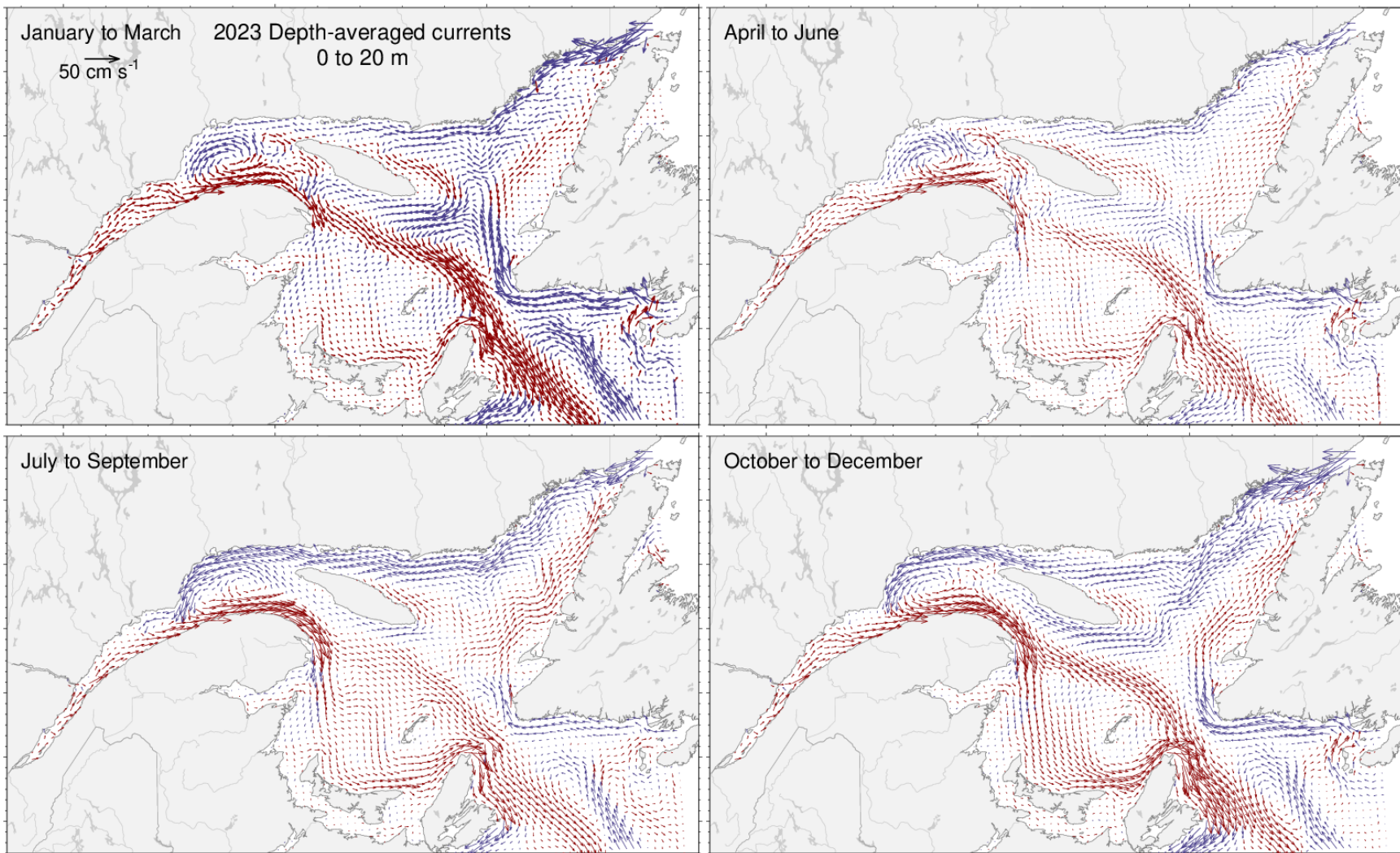
79

Fig. 58. Depth-averaged currents from 0 m to 20 m for each three-month period of 2023. Vectors drawn in blue are towards the west and those drawn in red are towards the east.
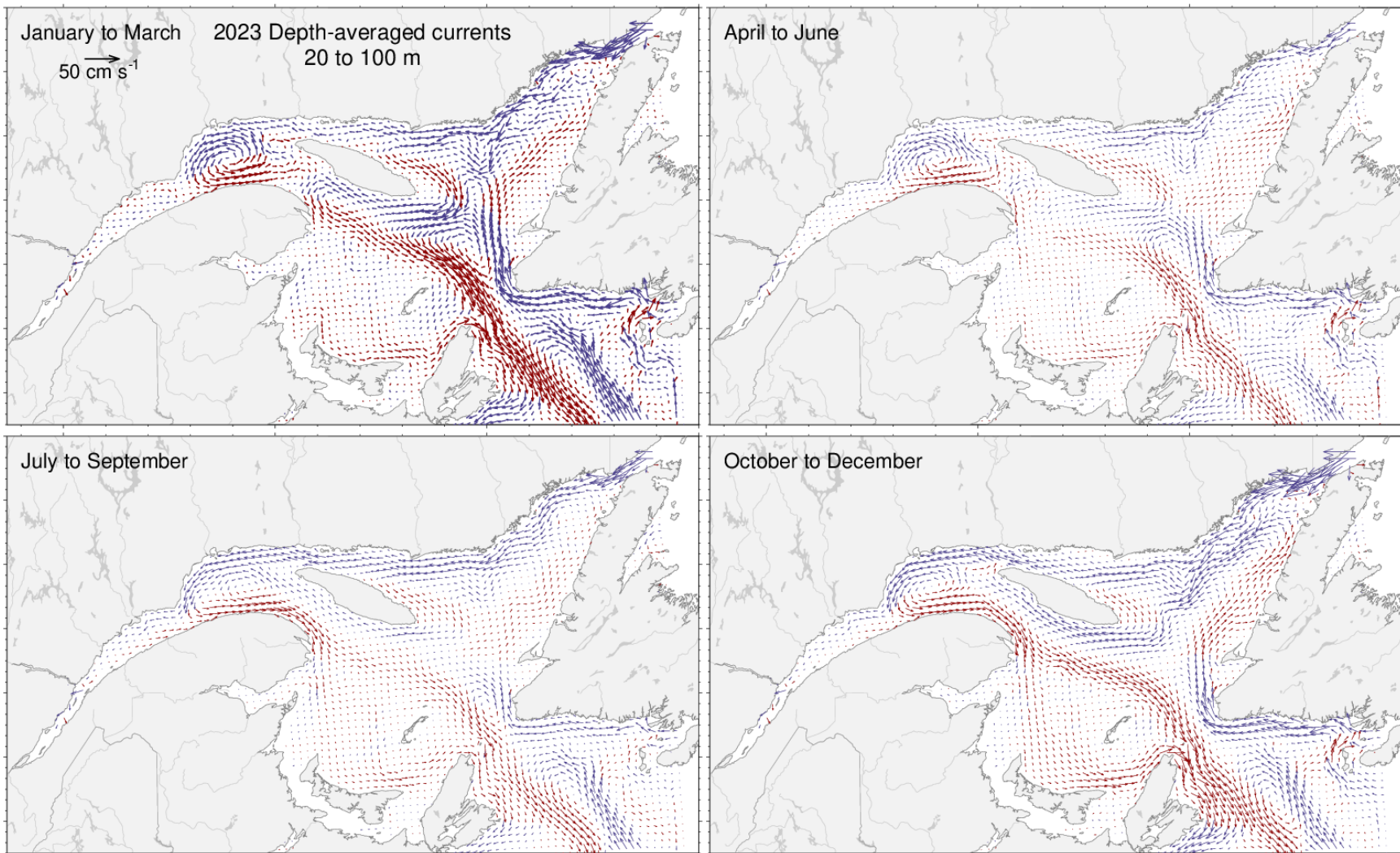
Fig. 59. Depth-averaged currents from 20 m to 100 m for each three-month period of 2023. Vectors drawn in blue are towards the west and those drawn in red are towards the east.
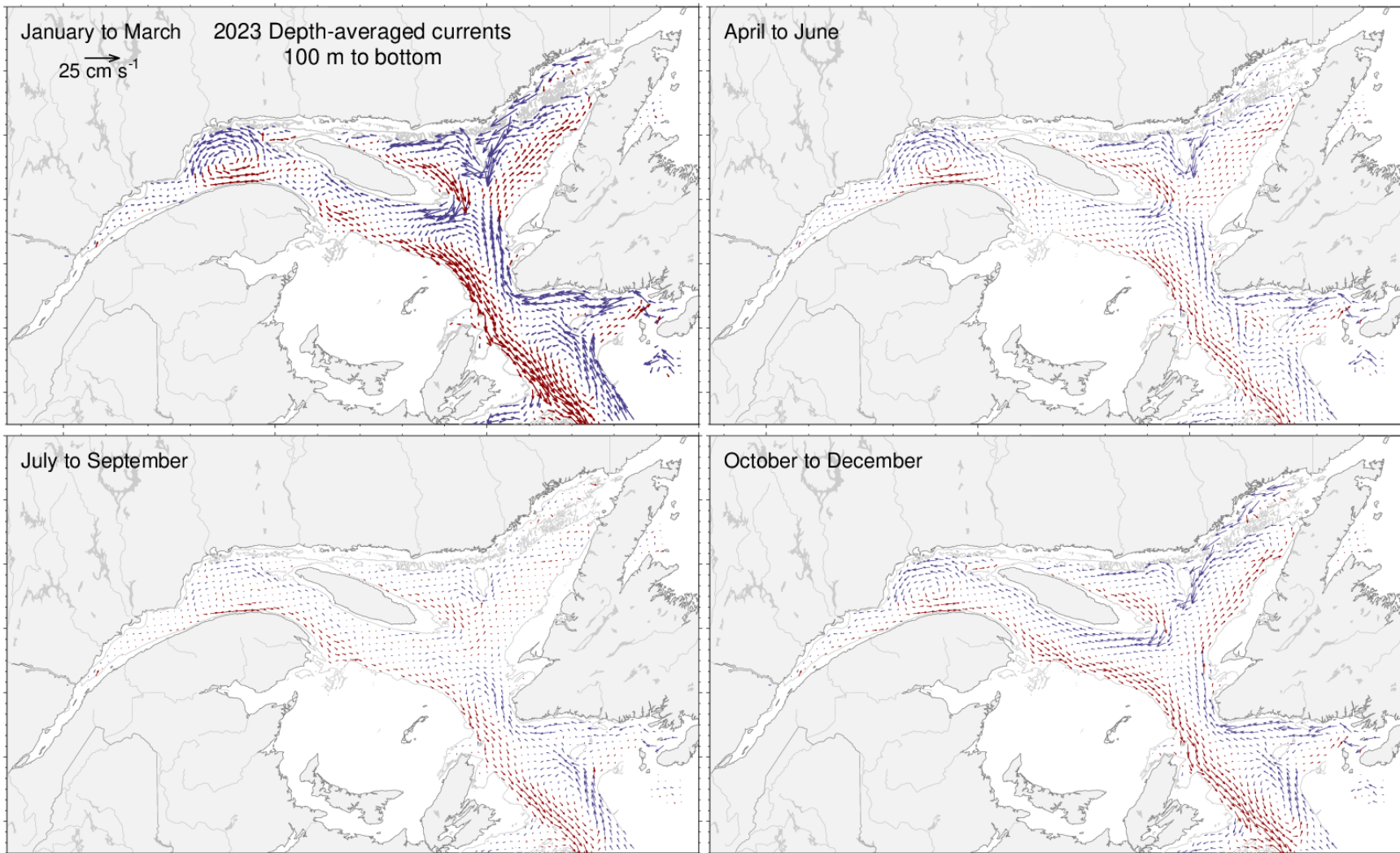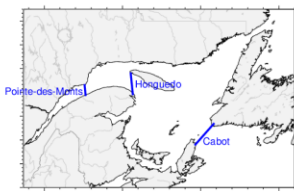
Fig. 60. Depth-averaged currents from 100 m to the bottom for each three-month period of 2023. Vectors drawn in blue are towards the west and those drawn in red are towards the east.
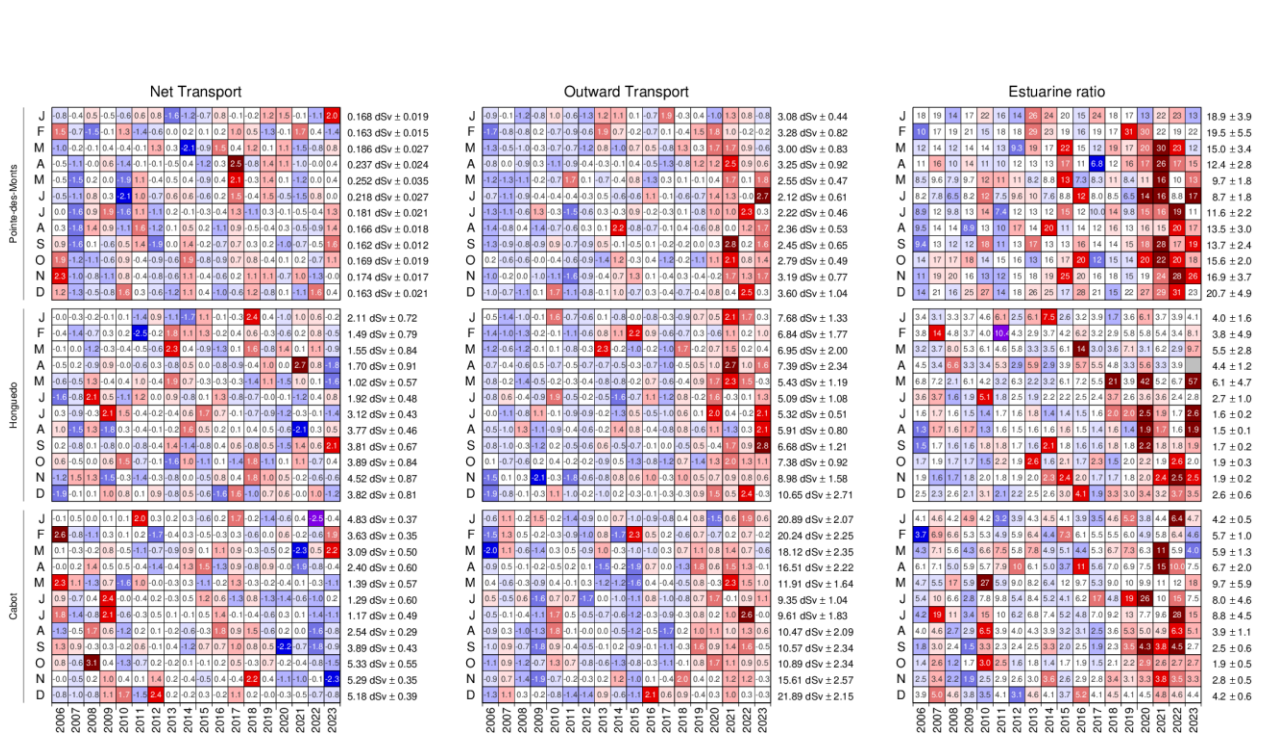
Fig. 61. Monthly averaged modelled transports (positive eastward) and estuarine ratio across sections of the Gulf of St. Lawrence since 2006. The numbers on the right are the 2006–2020 means and standard deviations. The numbers in the boxes are normalized anomalies for transport panels, but ratio values are indicated in the right panel. Colours indicate the magnitude of the anomaly. dSv (deci-Sverdrup) are units of transport equal to 10^5 m^{3}s^{-1}.
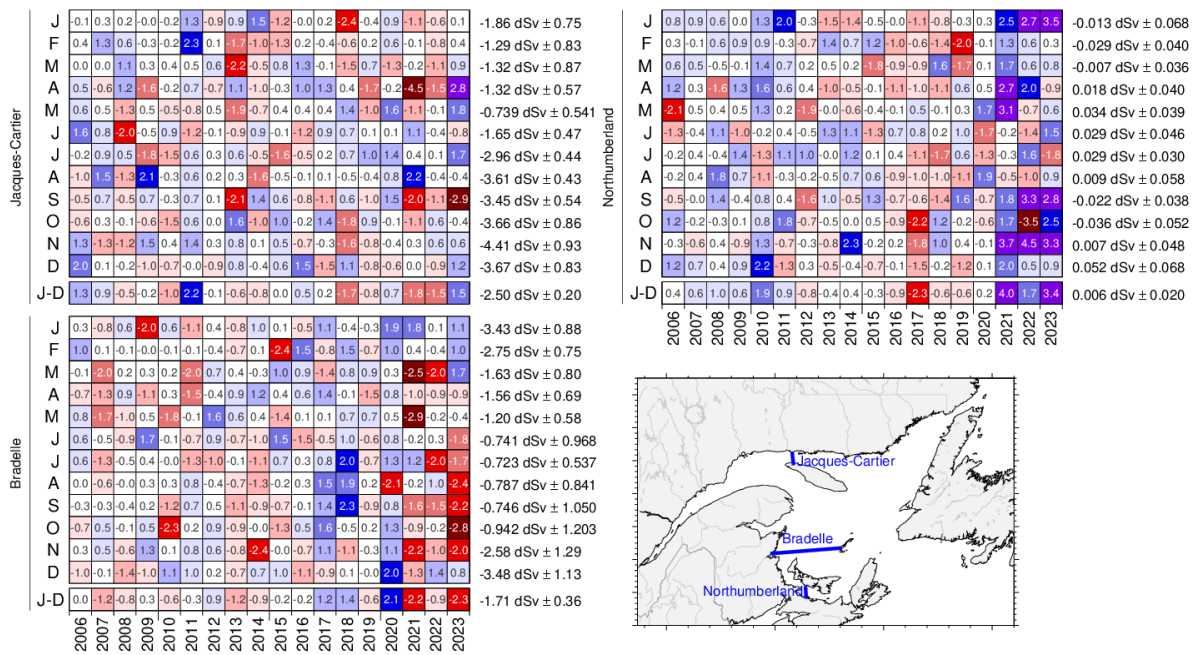
Fig. 62. Monthly and annual averaged modelled transports across sections of the Gulf of St. Lawrence since 2006. The numbers on the right are the 2006–2020 means and standard deviations, with positive values towards east and north. The numbers in the boxes are normalized anomalies. Since most mean transports are negative, negative anomalies are coded in red (e.g., negative anomalies are shown in red as stronger negative transport).
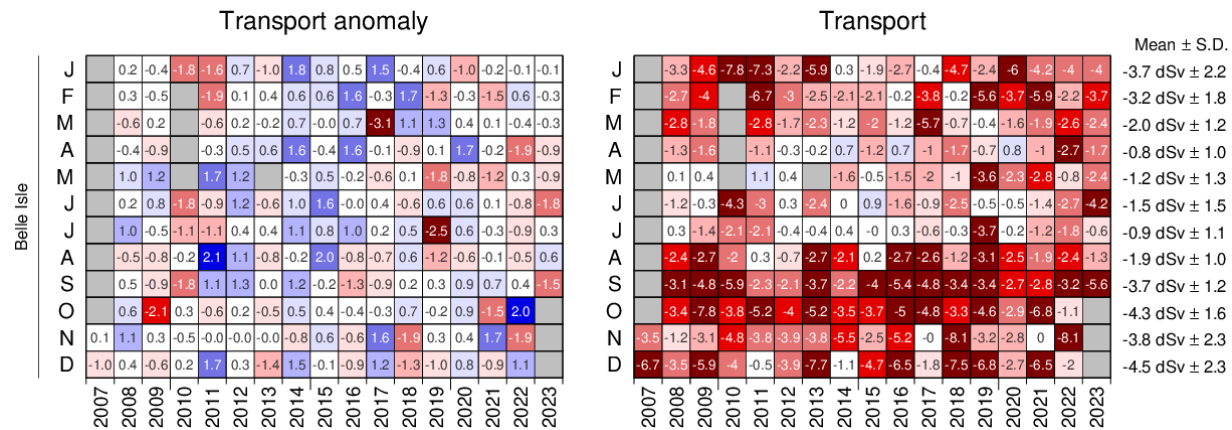

Fig. 63. Monthly-averaged transports estimates (right) and transport anomaly (left) across the Strait of Belle Isle section since 2007. The interannual means and standard deviations are shown to the right, with positive values towards the Labrador Shelf. The values are normalized anomalies in the left panel, and transport in units of deci-Sverdrups (10^5 m^3 s^{-1}) in the right panel. Colours indicate the magnitude of the anomaly or transport. Colours are reversed, red indicating a stronger (negative) transport towards the Gulf of St. Lawrence. See Fig. 13 for mooring location.
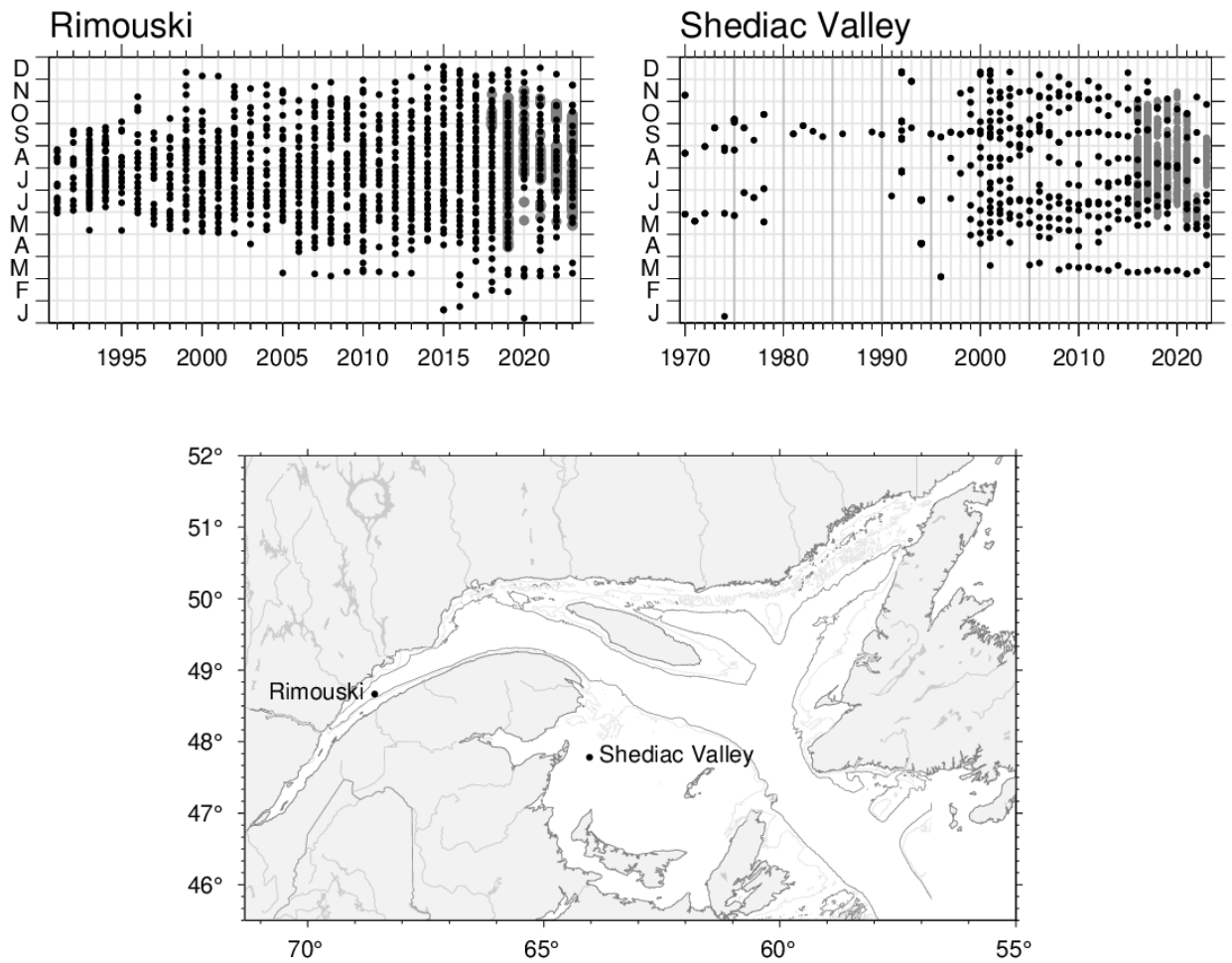
Fig. 64. Sampling frequency and positions of the AZMP stations Rimouski and Shediac Valley. Gray overlays show temperature and salinity casts made by oceanographic buoys. In 2023 at Shediac Valley, 138 temperature and salinity profiles were made by the PMZA-VAS automatic oceanographic buoy between 2023-05-19 and 2023-07-16. At Rimouski station, 333 full depth temperature and salinity profiles made by the PMZA-RIKI automatic oceanographic buoy between 2023-05-12 and 2023-10-12.
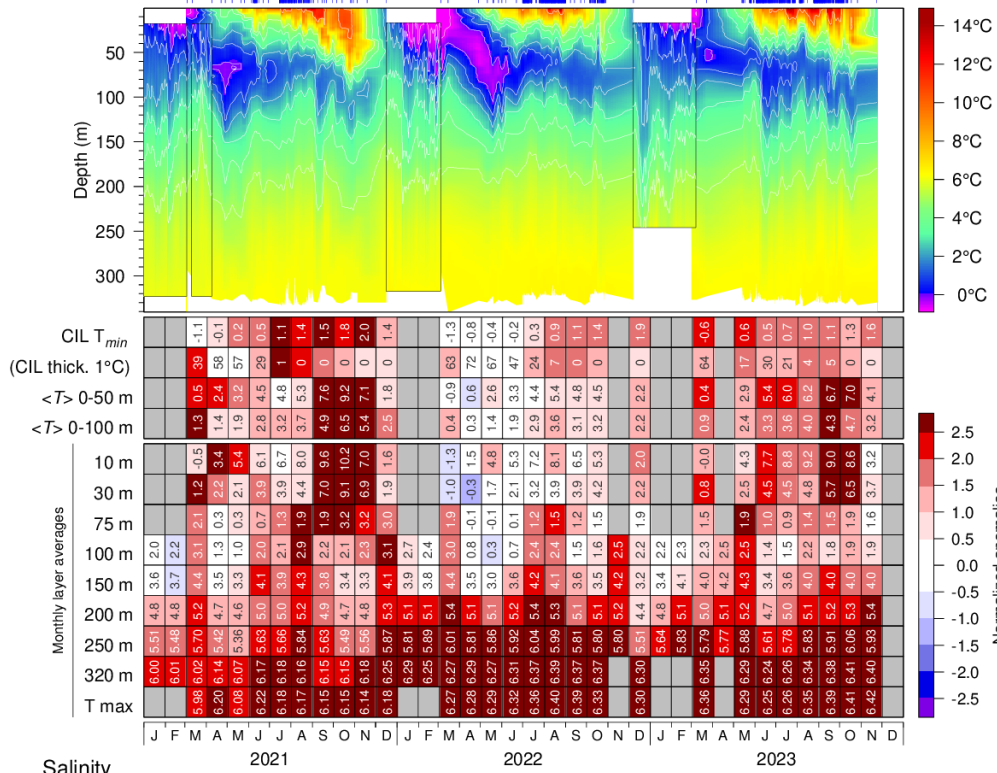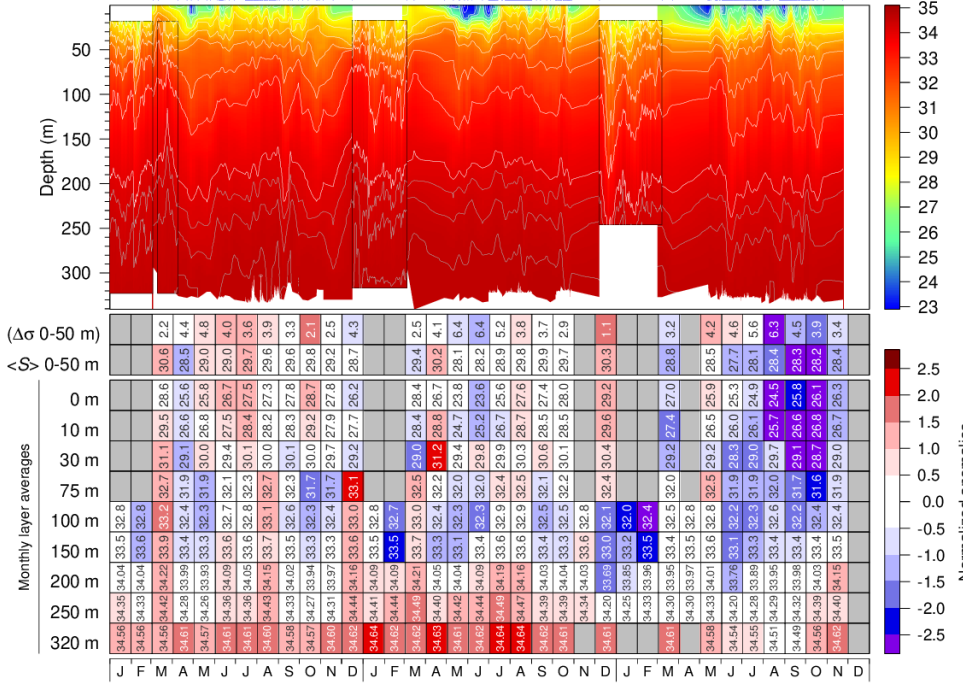
Fig. 65. Isotherm (top) and isohaline (bottom) time series at the Rimouski station; tick marks above indicate full-depth casts (mostly from a Viking buoy). The scorecard tables are monthly layer averages colour-coded according to the anomaly relative to the 1991–2020 monthly climatology for the station (yearly climatology for 200 m and deeper). Thickness of the CIL and stratification have reversed colour codes where blue indicates thicker CIL (associated with colder water) and more stratification (associated with low surface salinity). The box insets and some of the monthly averages are from mooring data.

Shediac Valley - Temperature

Depth (m)

Temperature scale: 18°C, 16°C, 14°C, 12°C, 10°C, 8°C, 6°C, 4°C, 2°C, 0°C

Normalized anomalies: 2.5, 2.0, 1.5, 1.0, 0.5, 0.0, -0.5, -1.0, -1.5, -2.0, -2.5

<T> 0-50 m
<T> 0m-bottom

Monthly layer averages: 0 m, 10 m, 20 m, 30 m, 50 m, 75 m

J F M A M J J A S O N D | J F M A M J J A S O N D | J F M A M J J A S O N D
2021 | 2022 | 2023

Salinity

Depth (m)

Salinity scale: 35, 34, 33, 32, 31, 30, 29, 28, 27, 26, 25, 24, 23

(Δσ 0-50 m)
<S> 0-50 m

Monthly layer averages: 0 m, 10 m, 20 m, 30 m, 50 m, 75 m

Normalized anomalies: 2.5, 2.0, 1.5, 1.0, 0.5, 0.0, -0.5, -1.0, -1.5, -2.0, -2.5

J F M A M J J A S O N D | J F M A M J J A S O N D | J F M A M J J A S O N D
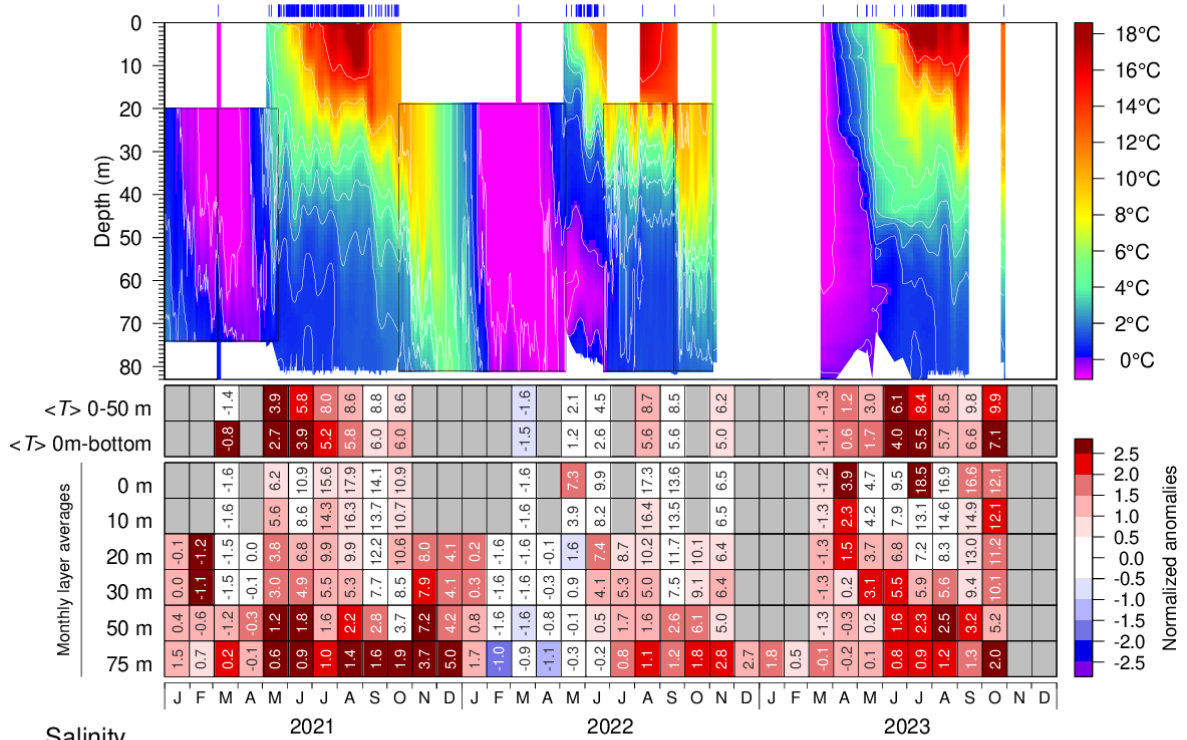2021 | 2022 | 2023

Fig. 66. Isotherm (top) and isohaline (bottom) time series at the Shediac Valley station; tick marks above indicate casts (mostly from automatic buoys). Scorecard tables are monthly layer averages colour-coded according to the anomaly relative to the 1991–2020 monthly climatology for the station (input to climatology is sparse prior to 1999). Higher than normal stratification is coded in blue (associated with low surface salinity). The box insets and 20 m, 30 m, 50 m and 75 m monthly layer averages are mostly from mooring data. Internal tide oscillations are smoothed out.
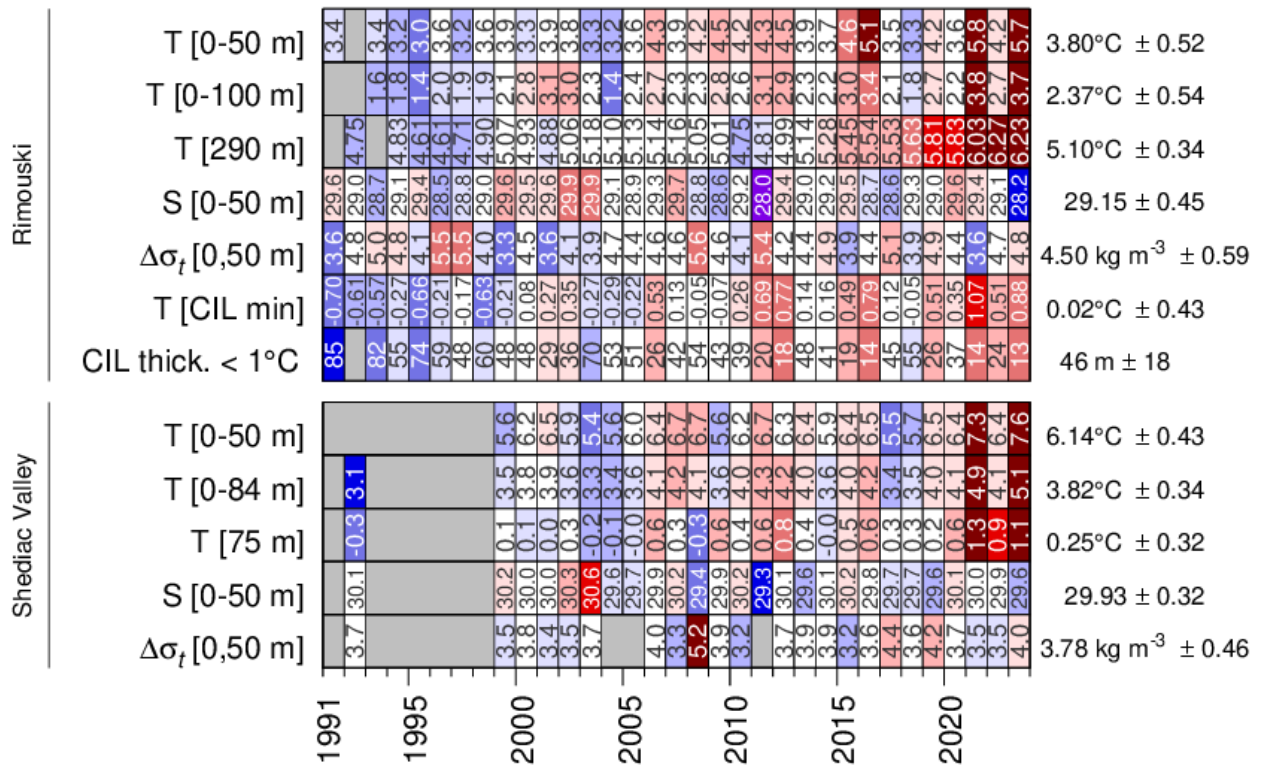
87

Rimouski

- T [0-50 m] — 3.80°C ± 0.52
- T [0-100 m] — 2.37°C ± 0.54
- T [290 m] — 5.10°C ± 0.34
- S [0-50 m] — 29.15 ± 0.45
- $\Delta\sigma_t$ [0,50 m] — 4.50 kg m^{-3} ± 0.59
- T [CIL min] — 0.02°C ± 0.43
- CIL thick. < 1°C — 46 m ± 18

Shediac Valley

- T [0-50 m] — 6.14°C ± 0.43
- T [0-84 m] — 3.82°C ± 0.34
- T [75 m] — 0.25°C ± 0.32
- S [0-50 m] — 29.93 ± 0.32
- $\Delta\sigma_t$ [0,50 m] — 3.78 kg m^{-3} ± 0.46

Years: 1991, 1995, 2000, 2005, 2010, 2015, 2020

Fig. 67. May to October temperature and salinity layer averages, stratification (expressed as the density difference between 0 m and 50 m), and CIL temperature minimum and thickness (T < 1 °C) for high frequency monitoring stations. Numbers in panels are monthly average values colour-coded according to the anomaly relative to the 1991–2020 climatology. Three months of anomaly data, between May and October, are required to show an average anomaly for any given year, except for deep water temperature at Rimouski station. Data in either July or August are also required for stratification at Shediac Valley. Temperatures at 290 m and 75 m at Rimouski station and Shediac Valley station are considered to represent near-bottom temperatures.
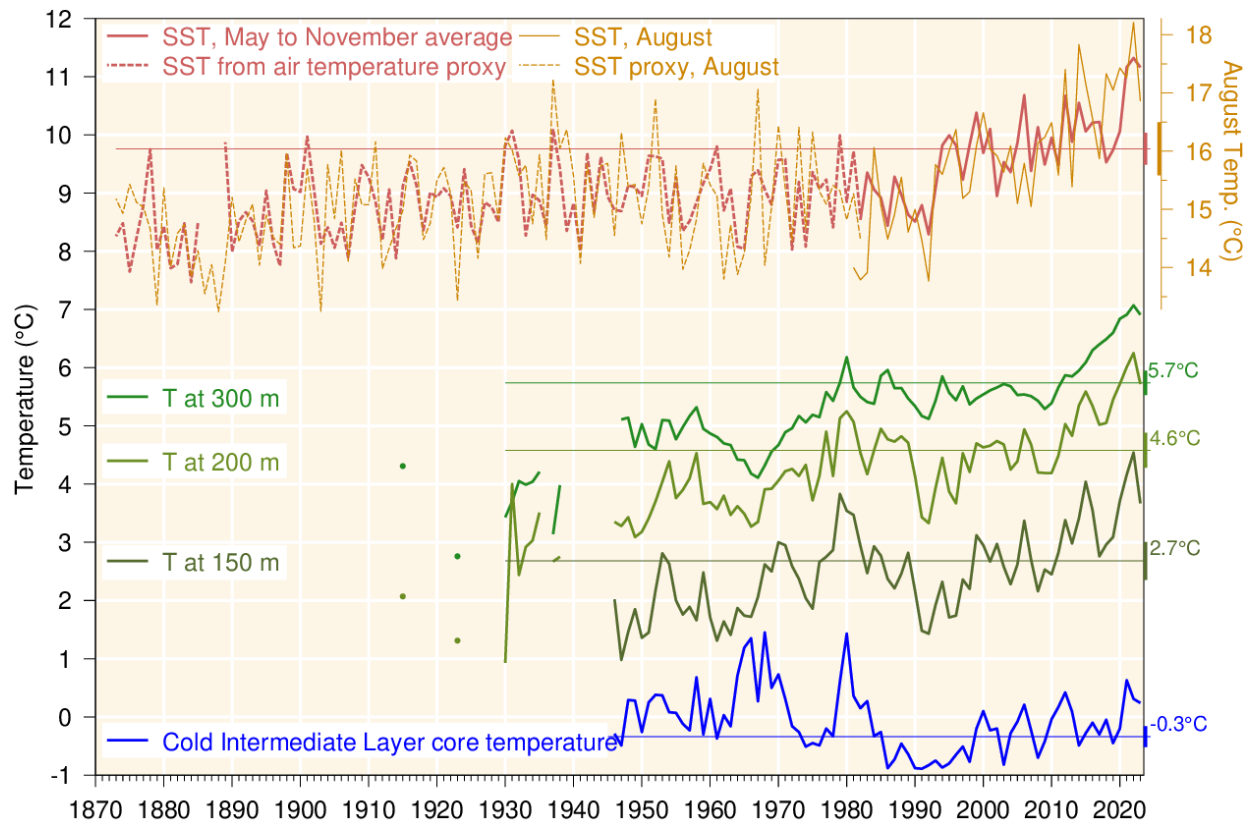
Fig. 68. Water temperatures in the Gulf of St. Lawrence. May–November SST averaged over the Gulf excluding the Estuary (1982–2023, red line), completed by a proxy based on April–November air temperature (1873–1982, red dashed line; average of all Adjusted and Homogenized Canadian Climate Data [AHCCD] stations in Fig. 4 but excluding Estuary stations at Baie Comeau and Mont-Joli). August SST is shown using temperature scale offset by 6.3 °C; its proxy is based on the average air temperature in July and August. Layer-averaged temperatures for the Gulf of St. Lawrence at 150 m, 200 m and 300 m (green lines). Cold intermediate layer minimum temperature index in the Gulf of St. Lawrence (blue line). SST air temperature proxy is similar to that of Galbraith et al. (2012). Climatological averages based on the 1991–2020 period are indicated by thin lines labelled on the right side, and half the standard deviation is shown by vertical bars on the right side. Figure adapted from Benoît et al. (2012).
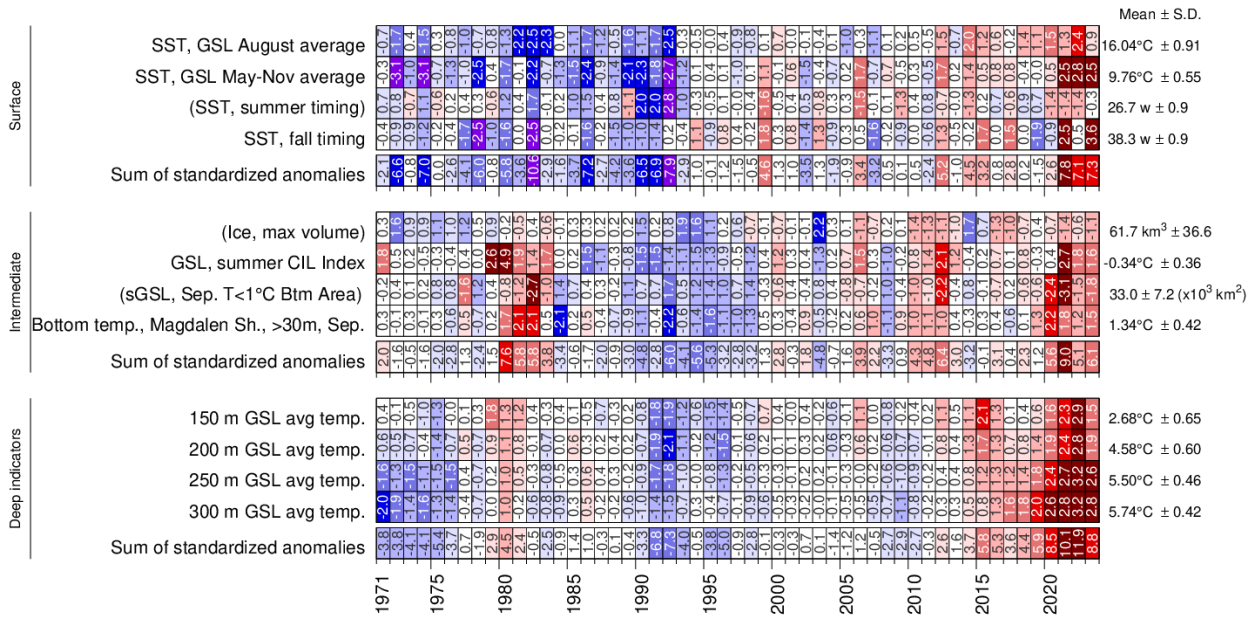
Fig. 69. Surface, intermediate (and sea-ice) and deep indicators used in the composite climate index (Fig. 70). The SST summer and fall timing are for 12 °C.
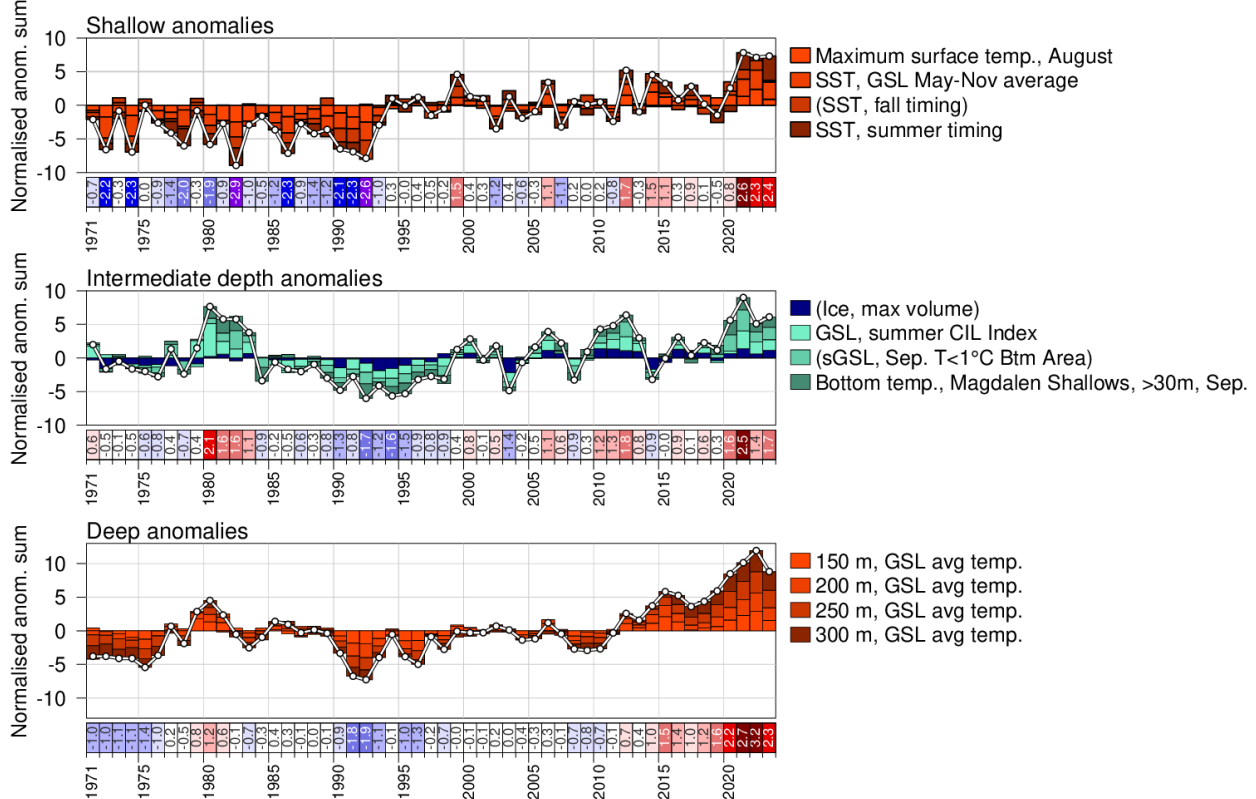

Fig. 70. Composite climate indices (white lines and dots) derived by summing various normalized anomalies from different parts of the environment (coloured boxes stacked above the abscissa are positive anomalies, and below are negative). Top panel sums anomalies representing shallow temperature anomalies, middle panel sums intermediate depth temperature anomalies and sea-ice (all related to winter formation), and bottom panel sums deep temperature anomalies. Each index is a sum of four normalized anomalies, and that time series is shown renormalized again at the bottom of each panel.
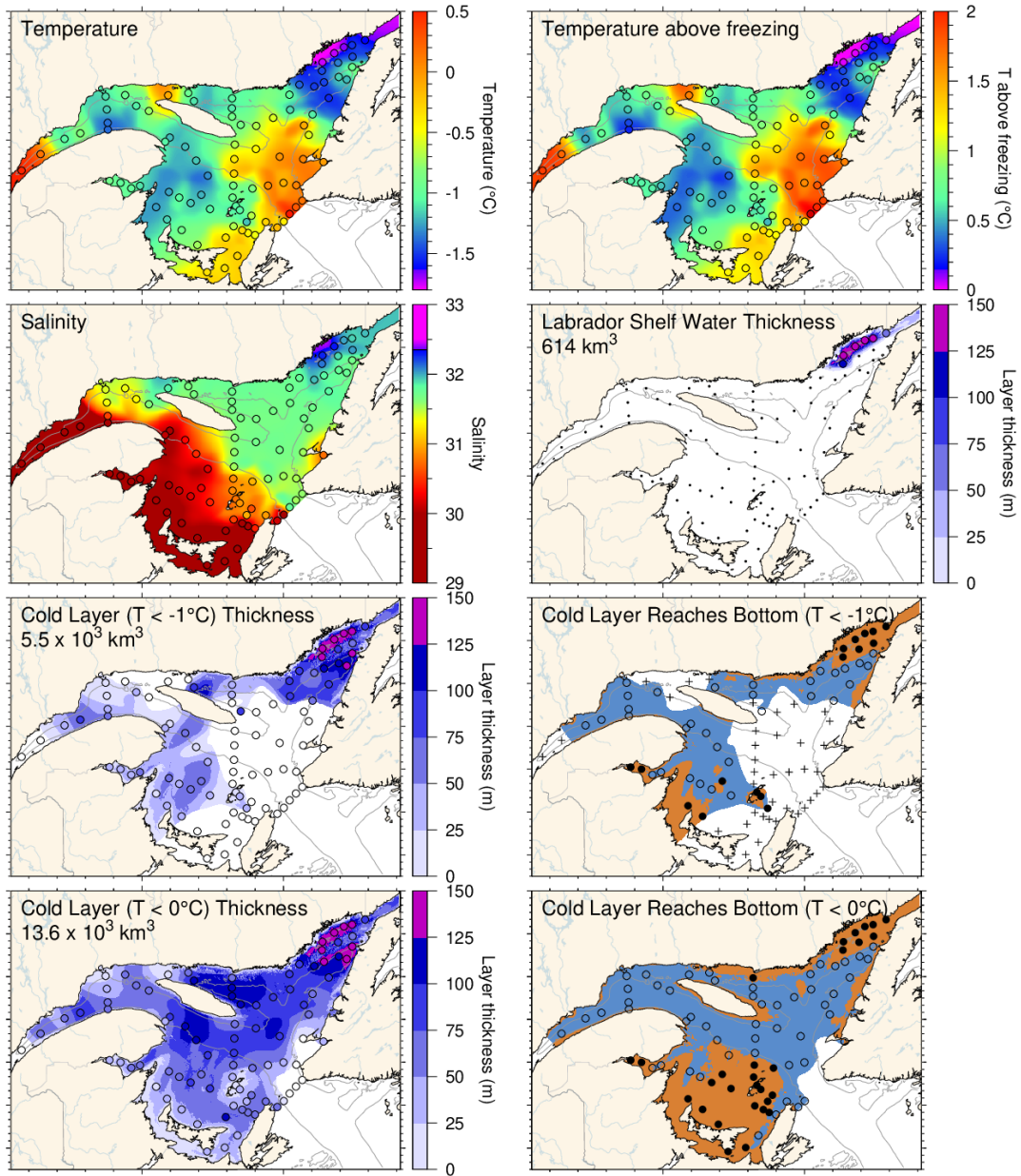
Fig. 71. March 2024 surface cold layer characteristics: surface water temperature (upper left), temperature difference with the freezing point (upper right), salinity (second row left), estimate of the thickness of the Labrador Shelf water intrusion (second row right), and cold layer (T < -1 °C and < 0 °C) thicknesses and where they reach bottom. The symbols are coloured according to the value observed at the station, using the same colour palette as the interpolated image. A good match is seen between the interpolation and the station observations where the station colours blend into the background.